Energy, Mines and Resources Canada
Énergie, Mines et Ressources Canada

CANMET

Canada Centre for Mineral and Energy Technology
Centre canadien de la technologie des minéraux et de l'énergie

Mining Research Laboratories
Laboratoires de recherche minière

THE POST-FAILURE BEHAVIOUR OF THE LAC DU BONNET PINK GRANITE

J.S.O. Lau and B. Gorski

November 1991

Divisional Report MRL 91-103(TR)

Canada

THE POST-FAILURE BEHAVIOUR OF THE LAC DU BONNET PINK GRANITE

J.S.O. Lau and B. Gorski November 1991

Divisional Report MRL 91-103(TR)

80pp

92-02360/

THE POST-FAILURE BEHAVIOUR OF THE LAC DU BONNET PINK GRANITE

by

J.S.O. Lau[1] and B. Gorski[2]

ABSTRACT

A laboratory testing program was carried out to study the post-failure behaviour of the Lac du Bonnet pink granite obtained from the 130 Level of the URL. The rock was found to exhibit class II behaviour. The development of cracks in the specimens appeared to start at a stress level in the range of 45 - 70% of the peak strength. The onset of dilation appeared to occur at a stress level equivalent to approximately 70 - 80% of the peak strength.

The peak strength increased with confining pressure. The predicted uniaxial compressive strength, σ_c, and the material constant, m, in the Hoek and Brown failure criterion for the pink granite were found to be 199 MPa and 31.77 respectively. For the residual strength envelope, using the same value of σ_c, the value of m_r was found to be 2.41.

Under the unconfined condition, cracks and axial fractures developed in the specimens, while single or conjugate shear fractures formed under the confined conditions. The inclination of the fracture plane, angle β, increased slightly with increasing confining pressure as predicted.

Confining pressure appeared to have little effect on the tangent Young's modulus. An increase in Poisson's ratio was observed only when the confining pressure was raised from 0 to 30 MPa.

Keywords: post-failure, uniaxial, triaxial, stress-strain, peak strength, failure criterion, angle β, tangent Young's modulus, Poisson's ratio

---

[1]Geotechnical Engineer, AECL Research, on attachment to Canadian Mine Technology Laboratory, Mining Research Laboratories, CANMET, Energy, Mines and Resources Canada, Ottawa, Ontario.

[2]Physical Scientist, Canadian Mine Technology Laboratory, Mining Research Laboratories, CANMET, Energy, Mines and Resources Canada, Ottawa, Ontario.

COMPORTEMENT POSTRUPTURE DU GRANITE ROSE DU LAC DU BONNET

par

J.S.O. Lau[1] et B. Gorski[2]

RÉSUMÉ

Un programme d'essai en laboratorie a été réalisé pour étudier le comportement postrupture du granite rose du lac du Bonnet prélevé au niveau 130 du Laboratorie de recherches souterraines. Les essais indiquent que le comportement de la roche est de classe II. La formation de fissures dans les échantillons a débuté à un niveau de contrainte variant entre 45 et 70% de la résistance maximale. La dilatation s'est amorcée à un niveau de contrainte équivalant à environ 70 - 80% de la résistance maximale.

Le résistance maximale a augmenté en appliquant une pression de confinement. La résistance à la compression uniaxiale, σ_c, et la constante du matériau, m, prévues selon le critère de rupture de Hoek et Brown pour le granite rose, ont atteint 199 MPa et 31.77, respectivement. En utilisant pour l'enveloppe de résistance résiduelle la même valeur de σ_c, on a obtenu 2.41 pour m_r.

Dans les conditions non confinées, des fissures et des fractures axiales se sont formées dans les échantillons alors que ce sont des fractures de cisaillement individuelles ou combinées qui se sont formées dans les conditions confinées. Conformément aux prévisions, l'angle d'inclinaison du plan de fracture, β, a légèrement augmenté lorsque la pression de confinement a été accrue.

La pression de confinement semble avoir peu d'effets sur le module de Young tangent. Le coefficient de Poisson n'a augmenté que lorsque la pression de confinement est passée de 0 à 30 MPa.

Mots clés: postrupture, uniaxiale, triaxiale, constrainte-déformation, résistance maximale, critère de rupture, angle β, module de Young tangent, coefficient de Poisson,

---

[1]Ingénieur en géotechnique, EACL Recherche, affecté au Laboratoire canadien de technologie minière, Laboratories de recherche minière, CANMET, Énergie, Mines et Ressources Canada, Ottawa, Ontario.

[2]Chercheur en sciences physique, Laboratoire canadien de technologie minière, Laboratoires de recherche minière, CANMET, Énergie, Mines et Ressources Canada, Ottawa, Ontario.

CONTENTS

	Page
ABSTRACT	i
RÉSUMÉ	iii
INTRODUCTION	1
ROCK TYPE AND SPECIMEN PREPARATION	1
TEST APPARATUS AND PROCEDURE	2
TEST PROGRAM AND RESULTS	3
DISCUSSION	4
Stress-Strain Observations	4
Strength and Failure Criterion	6
Failure Mode	7
Tangent Young's Modulus	8
Poisson's Ratio	8
CONCLUSIONS	9
RECOMMENDATIONS	10
ACKNOWLEDGEMENTS	10
REFERENCES	10
APPENDIX A	41

TABLES

No.		
1.	Dimensions, densities and p-wave velocities of rock specimens.	12
2.	Results of post-failure uniaxial and triaxial compression tests.	13
3.	Failure characteristics of rock specimens.	14

FIGURES

1. Stress-strain curves for specimen 101-004-HG2-36.053 ($\sigma_3 = 0$). 15
2. Stress-strain curves for specimen 101-004-HG2-40.742 ($\sigma_3 = 0$). 16
3. Stress-strain curves for specimen 101-004-HG2-43.520 ($\sigma_3 = 0$). 17
4. Stress-strain curves (strain gauges) for specimen 101-004-HG2-43.520 ($\sigma_3 = 0$). 18
5. Stress-strain curves for specimen 101-004-HG2-43.650 ($\sigma_3 = 0$). 19
6. Stress-strain curves (strain gauges) for specimen 101-004-HG2-43.650 ($\sigma_3 = 0$). 20
7. Stress-strain curves for specimen 101-004-HG2-36.170 ($\sigma_3 = 2$ MPa). . 21
8. Stress-strain curves for specimen 101-004-HG2-36.290 ($\sigma_3 = 4$ MPa). . 22
9. Stress-strain curves for specimen 101-004-HG2-36.418 ($\sigma_3 = 6$ MPa). . 23
10. Stress-strain curves for specimen 101-004-HG2-36.532 ($\sigma_3 = 8$ MPa). . 24
11. Stress-strain curves for specimen 101-004-HG2-40.621 ($\sigma_3 = 8$ MPa). . 25
12. Stress-strain curves for specimen 101-004-HG2-37.216 ($\sigma_3 = 10$ MPa). . 26
13. Stress-strain curves for specimen 101-004-HG2-37.335 ($\sigma_3 = 15$ MPa). . 27
14. Stress-strain curves for specimen 101-004-HG2-37.492 ($\sigma_3 = 20$ MPa). . 28
15. Stress-strain curves for specimen 101-004-HG2-37.613 ($\sigma_3 = 30$ MPa). . 29
16. Stress-strain curves for specimen 101-004-HG2-40.862 ($\sigma_3 = 30$ MPa). . 30
17. Stress-strain curves for specimen 101-004-HG2-40.381 ($\sigma_3 = 40$ MPa). . 31
18. Stress-strain curves for specimen 101-004-HG2-40.500 ($\sigma_3 = 60$ MPa). . 32
19. Stress-strain curves for specimen 101-004-HG2-43.390 ($\sigma_3 = 60$ MPa). . 33
20. Stress versus axial strain curves of pink granite in uniaxial and triaxial compression. 34
21. Volumetric strain versus axial strain curves of pink granite in uniaxial and triaxial compression 35
22. The Hoek and Brown failure envelope. 36
23. The residual strength envelope. 37
24. Plot of angle β versus confining pressure. 38
25. Plot of tangent Young's modulus E versus confining pressure. 39
26. Plot of Poisson's ratio ν versus confining pressure. 40

INTRODUCTION

AECL Research is assessing the concept of disposal of high-level nuclear fuel wastes in a vault located 500-1000 m deep in plutonic rock. As part of its waste management program, AECL Research has constructed the Underground Research Laboratory (URL) in the Lac du Bonnet Batholith, near Pinawa, Manitoba, for conducting large-scale geotechnical and hydrogeological investigations. In support of these activities, the Canada Centre for Mineral and Energy Technology (CANMET), in conjunction with AECL Research, has conducted laboratory-scale studies of samples from the URL and surrounding rock.

As part of the URL characterization program, studies between 1980 and 1990 focused on determining the mechanical properties in the pre-failure and peak strength regions of the various rock types found at the URL (Annor and Jackson, 1987; Jackson et al., 1989; Lau et al., 1991). More recently, as part of the URL Mine-by experiment, extensive post-failure testing has been carried out on three rock types: grey granite, granodiorite and pink granite. Results of post-failure testing on grey granite and granodiorite have been reported in CANMET division reports MRL 91-079(TR) (Lau and Gorski, 1991a) and MRL 91-098(TR) (Lau and Gorski, 1991b) respectively. This report presents and discusses the results of the post-failure uniaxial and triaxial tests on the Lac du Bonnet pink granite.

ROCK TYPE AND SPECIMEN PREPARATION

Samples used in these tests were NQ rock cores obtained from borehole 101-004-HG2 at the 130 Level of the URL. The rock type is a pink medium- to coarse-grained granite.

Specimens were prepared in accordance with the procedure described in the Pit Slope Manual Supplement 3-5 (Gyenge and Ladanyi, 1977) and the method suggested by the International Society for Rock Mechanics (Brown, 1981). The end surfaces of each of the specimens were ground flat to 0.025 mm to ensure that they were parallel to each other and perpendicular to the axis of the specimen.

The dimensions and bulk densities of the specimens are listed in Table 1. It should be noted that in Table 1, the last number in the specimen identification represents the downhole depth of the specimen in metres. The mean bulk density of the pink granite specimens was found to be 2.63 Mg/m^3. Specimen lengths and diameters varied from

112.85 to 118.09 mm and 44.89 to 44.99 mm respectively, with length to diameter ratios ranging from 2.51 to 2.63. Table 1 also shows the zero-pressure p-wave velocities measured on the specimens prior to testing. The mean p-wave velocity of the pink granite was found to be 5.275 km/s, which is considerably higher than the mean zero-pressure p-wave velocities of the grey granite specimens obtained from the 240 and 420 Levels of the URL (Lau et al., 1991), indicating the presence of fewer stress-induced microcracks in these pink granite specimens. This is not unexpected because the pink granite samples were obtained from the 130 Level of the URL where the in situ stress is lower.

Strain gauges were applied on two specimens (101-004-HG2-43.520 and 101-004-HG2-43.650) for uniaxial testing. Two diametrically opposed axial strain gauges were mounted and connected in series to form a single active gauge at midheight of each the specimens. Similarly, two circumferential strain gauges were mounted and connected at 90° to the axial gauges.

TEST APPARATUS AND PROCEDURE

The post-failure uniaxial and triaxial compression tests were conducted using the MTS 815 Rock Mechanics Test System, which is a computer-controlled, servo-hydraulic compression machine, consisting of a 2.22 MN rated load cell, load frame, hydraulic power supply, triaxial cell, confining pressure subsystem, test controller, test processor and DEC micro PDP 11/73 computer. The triaxial cell is equipped with three linear variable differential transducers (LVDTs) for the measurement of axial deformations and an extensometer with circumferential kit attachment (bicycle chain) for the measurement of circumferential deformation. Strain gauges were connected to the MTS system through B & K type 1526 strain indicators. A real time plot of load versus axial displacement could be obtained using a Kipp & Zonen pen recorder wired to the test controller. For a detailed description of the MTS system and its operation, the reader is referred to the MTS Operation Manual (MTS Systems Corp., 1986) and CANMET Division Report MRL 87-33(INT) (Gorski, 1987).

The procedures to conduct the post-failure uniaxial and triaxial compression tests were similar, except that in the triaxial test, the confining pressure and the axial stress were first increased simultaneously from zero, at a rate of 0.75 MPa/s, to the desired value of confining (equilibrium) pressure. All tests began under load control. The axial stress was increased at a rate of 0.75 MPa/s until the axial load exceeded the equilibrium load by 60 kN. The control mode was then switched over to an axial strain

rate approximating an axial stress rate of 0.75 MPa/s. The test continued under the axial strain control mode. As the peak strength of the specimen was approached, special care was taken to prevent rapid failure and enable testing to continue into the post-failure region. The MTS system was programmed to unload immediately when a drop in the axial load (initial failure) was detected, reducing the axial strain by 20%. The system then started to reload again, in axial strain control mode, until another drop in the axial load was detected. It should be noted that the unloading path could be interrupted (shortened) by the operator during the test in order to speed up the test. The process was repeated until the residual strength of the specimen was attained or the uncontrolled failure of the specimen occurred. A plateau in the real time plot of load versus axial displacement was taken as the residual strength. At this point, the strain rate was raised to 0.0714 mm/s, and the test continued for 70 seconds at this strain rate. During the first 10 seconds, the confining pressure was maintained at the test level. After that, the confining pressure was reduced linearly to zero in 60 seconds, and the test terminated. As the confining pressure decreased, the axial stress also decreased, and a set of residual stress data (σ_{1r} and σ_{3r}) were obtained for the development of the residual strength envelope which will be discussed later in this report.

Cyclic loading was also performed in three uniaxial tests and two triaxial tests at the confining pressures of 30 and 60 MPa. In these tests, each unloading sequence consisted of reducing the axial stress to a value slightly above the confining pressure. Unloading and reloading cycles were performed at 40-MPa increments of axial stress until the axial stress reached approximately 75% of the estimated peak strength. Above that stress level, unloading and reloading cycles were performed at 0.063-mm increments of circumferential deformation. It should be noted that loading remained under the axial strain control mode throughout the test.

During the test, analog signals from the load cell, LVDTs, extensometer, strain gauges (if applicable) and confining pressure subsystem were scanned every 3 seconds, and the data were stored on hard disk in the PDP 11/73 computer. After the test was terminated, the data were transferred from the PDP 11/73 computer to the VAX 750 computer for data storage and analysis. Plots of axial stress versus axial strain and axial stress versus circumferential strain (loading and unloading curves) were obtained from a DEC LVP16 pen plotter connected to the PDP 11/73 computer.

TEST PROGRAM AND RESULTS

Testing for this study took place in March and April, 1991 at Canadian Mine Technology Laboratory, Mining Research Laboratories, CANMET, Energy, Mines and

Resources Canada in Ottawa. The program consisted of four uniaxial tests and thirteen triaxial tests conducted at confining pressures of 2, 4, 6, 8, 10, 15, 20, 30, 40 and 60 MPa. The loading and unloading curves for each test are presented in Appendix A. The envelopes to these loading and unloading curves were plotted in Figures 1 to 19. These envelopes will be referred to as stress-strain curves in this report. Plots of stress versus volumetric strain are also shown in those figures. Volumetric strain was computed by using the following equation:

$$\varepsilon_v = \varepsilon_a + 2\varepsilon_c \tag{1}$$

where ε_v = volumetric strain
ε_a = axial strain
ε_c = circumferential strain

For each test, the deviator stress $(\sigma_1 - \sigma_3)_p$, axial strain ε_{ap} and volumetric strain ε_{vp} at peak load, and the deviator stress $(\sigma_1 - \sigma_3)_u$, axial strain ε_{au} and volumetric strain ε_{vu} at the termination of the test were recorded and are given in Table 2.

DISCUSSION

STRESS-STRAIN OBSERVATIONS

Figures 1 to 19 show the stress-strain characteristics for the pink granite specimens under uniaxial compression and triaxial compression. It should be noted that specimens 101-004-HG2-43.520 and 101-004-HG2-43.650 were equipped with strain gauges, and the stress-strain curves using strain gauge results are also presented (Figs. 4 and 6). In general, the pre-failure stress-strain (axial strain) curve may be divided into three regions. The bottom one is characterized by a steadily increasing slope, indicating the closure of microcracks in the specimen. This region reduces as the confining presuure increases and completely disappears at confining pressures above 10 MPa. The middle region is nearly linear, approximating linear elastic behaviour. In the top region, the slope decreases, indicating crack formation, crack growth and sliding on existing crack interfaces. The peak of the stress-strain curve was taken as the failure point. The post-failure behaviour of the pink granite is marked by regions of abrupt decreases and regions of more gentle decreases in stress, indicating the formation of larger cracks and steeply inclined shear fractures in the specimen. Abrupt decreases are characterized

by positive slopes, showing class II rock behaviour. Failure for class II rock behaviour is self-sustaining (Wawersik and Fairhurst, 1970), indicating the elastic strain energy stored in the specimen at peak load is sufficient to maintain fracture propagation until the specimen has lost its load-carrying ability.

The stress-strain curves for the circumferential strain, measured using the bicycle chain, are nearly linear from initial loading to stress levels equivalent to approximately 45% (at high confining pressure) to 70% (under unconfined condition) of the peak deviator stresses. The curves then start to deviate from linear behaviour, indicating the development of cracks in the specimens. The slopes of the curves decrease steadily and the peaks of the curves were taken as the failure points. It should be noted that by using the strain gauge results (Figs. 4 and 6), under the unconfined condition, deviation from linear behaviour occurs at a stress level equal to only approximately 45 to 50% of the peak deviator stress. This suggests that the 70% recorded by using the bicycle chain might be a result of utilising a less sensitive measuring device rather than a property of the rock. In the post-failure regions, the circumferential strains increase rapidly, due to the formation of small fractures and possibly spalling in the specimens. However, a decrease in the circumferential strain with increasing confining pressure can be observed.

Failure development and the eventual disintegration of the specimens can be illustrated, using the plots of stress versus volumetric strain (Figs. 1-19). In general, the slopes of the curves increase from initial loading to stress levels equal to approximately 70 - 80% of the peak deviator stresses, where the volumetric strains reach their maximum values. After that, the slopes of the curves become negative, suggesting the formation and growth of cracks in the specimens and the onset of dilation. The maximum rate of cracking occurs at the peak of each curve. In the post-failure regions, the volumetric strains increase rapidly as the stresses decrease, due to the disintegration of the specimens.

The stress-strain (axial strain) curve and the volumetric strain versus axial strain curve for each of the confining pressures are plotted in Figures 20 and 21 respectively to study the effect of the confining pressure on the stress-strain curves. From these figures, it is evident that the compressive strength increases with confining pressure, and there is a progressive increase in the post-failure axial strain and reduction in the post-failure volumetric strain (dilation) with increasing confining pressure. It can also be seen that there is a progressive slight flattening of the stress-strain curves with increasing confining pressure.

STRENGTH AND FAILURE CRITERION

As mentioned earlier, the failure of a specimen was taken to occur at its peak strength. The peak strengths of the pink granite specimens are the maximum compressive strengths recorded in the tests, and are given as peak deviator stresses in Table 2. It should be noted that the peak strength of specimen 101-004-HG2-36.532, tested at the confining pressure of 8 MPa, was quite low due to the presence of a large feldspar inclusion.

The peak strengths were used to estimate the rock mass strength of the pink granite, using the Hoek and Brown failure criterion (Hoek and Brown, 1980) which is defined by the following equation:

$$\sigma_1 = \sigma_3 + \sqrt{m\sigma_c\sigma_3 + s\sigma_c{}^2} \qquad (2)$$

where σ_1 = major principal stress at failure
σ_3 = minor principal stress applied to the rock sample
σ_c = uniaxial compressive strength of the intact rock material in the specimen
m and s are constants and for these intact rock specimens, $s = 1$

The predicted uniaxial compressive strength of the intact rock material, σ_c, and the material constant, m, for the pink granite were calculated by using the equations suggested by Hoek and Brown (1980) and found to be 199 MPa and 31.77 respectively. These values were used to develop the Hoek and Brown failure envelope shown in Figure 22. The pink granite was found to be stronger than the grey granite (σ_c = 157 MPa, m = 35.28), but weaker than the granodiorite (σ_c = 224 MPa, m = 26.27) used in previous post-failure testing programs (Lau and Gorski, 1991a; Lau and Gorski, 1991b).

A residual strength envelope was also developed using the Hoek and Brown failure criterion. The predicted intact strength (σ_c = 199 MPa) and the observed residual strengths (σ_{1r} and σ_{3r} respectively) were entered into Equation 3 (Hoek and Brown, 1980) for the computation of m_r, assuming $s_r = 0$. The value of m_r was found to be 2.41, and the residual strength envelope, developed by using these values of σ_c and m_r, is shown in Figure 23. Although all residual strength data were used in this analysis, it should be noted that specimens tested at lower confining pressures exhibited higher residual strengths.

$$m_r = \frac{\sum y_i}{\sigma_c \sum x_i} \tag{3}$$

where $x = \sigma_{3r}$

$y = (\sigma_{1r} - \sigma_{3r})^2$

FAILURE MODE

The failure characteristics of the specimens are shown in Table 3. Cracks and axial fractures developed in the specimens tested under the unconfined condition. With the application of confining pressure, even as low as 2 MPa, the failure characteristics changed. Cracks and single or conjugate shear fractures developed in the specimens. The inclination (angle β) of the fracture plane with the specimen axis was measured for each specimen. These angles are given in Table 3 and plotted against the confining pressure in Figure 24. It can be seen that the angles β are slightly greater for specimens tested at confining pressures ranging from 20 to 60 MPa than for those tested at lower confining pressures. Also plotted in Figure 24 as a solid line is the relationship between the fracture plane inclination and confining pressure, calculated by means of the following equations suggested by Hoek and Brown (Hoek and Brown, 1980), using $\sigma_c = 199$ MPa and $m = 31.77$:

$$\tau_m = \frac{1}{2}(\sigma_1 - \sigma_3) \tag{4}$$

$$\sigma = \sigma_3 + \frac{\tau_m^2}{\tau_m + m\sigma_c/8} \tag{5}$$

$$\tau = (\sigma - \sigma_3)\sqrt{1 + m\sigma_c/4\tau_m} \tag{6}$$

The angle β is defined by:

$$sin2\beta = \frac{\tau}{\tau_m} \tag{7}$$

There is a general agreement between the measured and predicted values of angle β. This suggests that Equation 7 can be used to give a rough guide to the inclination of shear fractures in the pink granite, should failure occur.

TANGENT YOUNG'S MODULUS

The tangent Young's modulus, E, for each of the specimens was computed from the stress-strain curve at the stress level equal to 50% of the peak deviator stress, $0.5(\sigma_1 - \sigma_3)_p$. A cubic spline fit was first performed on the stress-strain data in the pre-failure region, employing a third degree equation model of the form:

$$\sigma = a_0 + a_1\varepsilon + a_2\varepsilon^2 + a_3\varepsilon^3 \tag{8}$$

where σ = stress
ε = strain
and a_0, a_1, a_2 and a_3 are coefficients

The modulus value was then determined by substituting the axial strain value at the stress level of $0.5(\sigma_1 - \sigma_3)_p$ into the derivative of Equation 8 representing the stress-strain curve. The tangent Young's moduli are given in Table 2 and are plotted against confining pressure in Figure 25.

Figure 25 reveals that the confining pressure had little effect on the tangent modulus. The increase of modulus with confining pressure at low confining pressures, which was commonly observed in compression tests on the Lac du Bonnet grey granite, was not observed in these tests on the pink granite. This suggests that the effect of confining pressure on the modulus of the grey granite might be the effect of sample disturbance due to the presence of stress-induced microcracks, rather than a property of the rock.

POISSON'S RATIO

The Poisson's ratio, ν, for each of the specimens was determined from the ratio of the circumferential to the axial tangent moduli obtained from the stress-strain curves at the stress level equivalent to $0.5(\sigma_1 - \sigma_3)_p$. The circumferential tangent modulus was determined in the same manner as the axial tangent modulus, E. The Poisson's ratios are presented in Table 2 and plotted versus confining pressure in Figure 26.

Figure 26 shows that the Poisson's ratio rose gradually when the confining pressure was raised from 0 to 30 MPa, indicating that, although present in small amount, there were stress-induced microcracks in these specimens. Above 30 MPa, the confining pressure appeared to have no effect on the Poisson's ratio.

CONCLUSIONS

These tests have provided some stress and strain data in the pre-failure, peak strength and post-failure regions for the Lac du Bonnet pink granite. The results have also provided some insight into the post-failure behaviour of the rock. The pink granite exhibited class II rock behaviour. This implies that if the behaviour of the pink granite in the laboratory can be applied directly to its behaviour in the field, in situ fracturing in the rock could proceed unstably with the release of considerable amount of strain energy and violent failure might occur, should the peak strength be exceeded. From the results, the following conclusions can be made.

The stress-strain (axial) curves from initial loading to peak strength are marked progressively by regions of increasing slope, approximate linear elasticity and decreasing slope. However, the bottom region diminishes with increasing confining pressure and disappears at confining pressures above 10 MPa. The development of cracks in the specimens appeared to start at stress levels equal to approximately 45% (at high confining pressure) to 70% (under unconfined condition) of the peak strengths. The high 70% might be a result of using a less sensitive measuring device rather than a property of the rock. The onset of dilation appeared to occur at stress levels equivalent to approximately 70 - 80% of the peak strength. The post-failure regions are characterized by series of abrupt and gentle drops in stress. The circumferential and volumetric strains increased rapidly in the post-failure regions, indicating the disintegration of the specimens. Confining pressure was found to have some effect on the stress-strain behaviour of the rock. The axial strain increased but the circumferential strain and volumetric strain (dilation) decreased with increasing confining pressure.

The peak strength of the pink granite increased with increasing confining pressure. A failure envelope was developed by using the Hoek and Brown failure criterion. The predicted uniaxial compressive strength, σ_c and the material constant, m, in the failure criterion were calculated and found to be 199 MPa and 31.77 respectively.

A residual strength envelope was also developed for the pink granite, and the value of the material constant, m_r, was found to be 2.41.

Cracks and axial fractures developed in the specimens in the uniaxial tests. Whereas, under the confined conditions, cracks and single or conjugate shear fractures formed. The fracture plane inclination (angle β) increased slightly with increasing confining pressure, and there is a general agreement between the measured and predicted values of angle β.

With the presence of only a small amount of stress-induced microcracks in these specimens, the confining pressure appeared to have little effect on the pink granite. The Poisson's ratio increased when the confining pressure was raised from 0 to 30 MPa. Above that, the confining pressure appeared to have no effect on the Poisson's ratio.

RECOMMENDATIONS

Experimentally identifying the pre-failure, peak strength and post-failure behaviours of the host rock is one of the main rock mechanics issues related to the construction and operation of the URL. This post-failure testing program has addressed the issue and is recommended for the URL characterization program and the Mine-by experiment, and for any future site selection and repository design programs if the disposal concept is deemed acceptable.

As suggested in CANMET Division Report MRL 91-098(TR), class II behaviour observed in laboratory testing of rock may be a scale effect rather than a property of the rock. It is therefore strongly recommended to conduct a study on the scale effect in post-failure testing for the Lac du Bonnet granite.

ACKNOWLEDGEMENTS

The authors wish to express their thanks to R. Jackson of CANMET for reviewing this report and making several helpful suggestions. Gratitude is expressed to J. Folta of CANMET for the preparation of specimens and for carrying out the compression wave velocity measurements on the specimens.

REFERENCES

Annor, A. and Jackson, R. (1987), "Mechanical, thermomechanical and joint properties of rock samples from the Lac du Bonnet Batholith, Manitoba" in Geotechnical studies at

Whiteshell Research Area (RA-3) (edited by Katsube, T.J. and Hume, J.P.), Divisional Report MRL 87-52(TR), CANMET, Energy, Mines and Resources Canada, p. 49-110.

Brown, E.T. (1981), "Rock characterization testing and monitoring, ISRM suggested methods", International Society for Rock Mechanics, the Commission on Testing Methods, Pergamon, 211 p.

Gorski, B. (1987), "Post-failure uniaxial strength determinations using a servo-hydraulic test system", Division Report MRL 87-33(INT), CANMET, Energy, Mines and Resources Canada, 77 p.

Gyenge, M. and Ladanyi, B. (1977), "Pit slope manual supplement 3-5 - sampling and specimen preparation", CANMET, Report 77-29, 30 p.

Hoek, E. and Brown, E.T. (1980), "Underground excavations in rock", The Institution of Mining and Metallurgy, London, 527 p.

Jackson, R., Lau, J.S.O. and Annor, A. (1989), "Mechanical, thermo-mechanical and joint properties of rock samples from the site of AECL's Underground Research Laboratory, Lac du Bonnet, Manitoba", in Proceedings of the 42nd Canadian Geotechnical Conference, Winnipeg, Manitoba, October 23-25, 1989, p. 41-49.

Lau, J.S.O., Jackson, R. and Gorski, B. (1991), "The effects of temperature and pressure on the mechanical properties of Lac du Bonnet grey granite", in Proceedings of the 32nd U.S. Symposium on Rock Mechanics, Norman, Oklahoma, July 10-12, 1991, p. 313-323.

Lau, J.S.O. and Gorski, B. (1991a), "The post-failure behaviour of the Lac du Bonnet grey granite", Divisional Report MRL 91-079(TR), CANMET, Energy, Mines and Resources Canada, 140 p.

Lau, J.S.O. and Gorski, B. (1991b), "The post-failure behaviour of the Lac du Bonnet granodiorite", Divisional Report MRL 91-098(TR), CANMET, Energy, Mines and Resources Canada, 54 p.

MTS Systems Corporation (1986), "Operation manual for 815 rock mechanics test systems", MTS Systems Corp., Minneapolis, Minnesota, U.S.A.

Wawersik, W.R. and Fairhurst, C. (1970), "A study of brittle rock fracture in laboratory compression experiments", Int. J. Rock Mech. Min. Sci., Vol. 7, p. 561-575.

Table 1. Dimensions, densities and p-wave velocities of rock specimens.

Specimen identification	Length (mm)	Diameter (mm)	Bulk density (Mg/m^3)	P-wave velocity (km/s)
101-004-HG2-36.053	114.70	44.99	2.63	5.360
101-004-HG2-36.170	116.70	44.90	2.63	5.187
101-004-HG2-36.290	117.29	44.95	2.63	5.133
101-004-HG2-36.418	115.00	44.95	2.63	5.157
101-004-HG2-36.532	114.69	44.95	2.67	5.285
101-004-HG2-37.216	115.44	44.97	2.64	5.283
101-004-HG2-37.335	116.53	44.97	2.64	5.261
101-004-HG2-37.492	115.18	44.97	2.63	5.177
101-004-HG2-37.613	114.70	44.97	2.63	5.261
101-004-HG2-40.381	112.85	44.90	2.64	5.261
101-004-HG2-40.500	113.64	44.89	2.64	5.304
101-004-HG2-40.621	114.96	44.90	2.64	5.286
101-004-HG2-40.742	113.24	44.90	2.63	5.392
101-004-HG2-40.862	114.64	44.90	2.60	5.223
101-004-HG2-43.390	116.39	44.94	2.63	5.267
101-004-HG2-43.520	118.09	44.95	2.63	5.331
101-004-HG2-43.650	116.80	44.94	2.64	5.509
Mean			2.63	5.275
Standard deviation			0.01	0.092

Table 2. Results of post-failure uniaxial and triaxial compression tests.

Specimen Identification	σ_3	Deviator Stress		Axial Strain		Volumetric Strain		Young's Modulus	Poisson's Ratio
		$(\sigma_1 - \sigma_3)_p$	$(\sigma_1 - \sigma_3)_u$	ε_{ap}	ε_{au}	ε_{vp}	ε_{vu}	E	ν
	(MPa)	(MPa)	(MPa)	(10^{-2})	(10^{-2})	(10^{-2})	(10^{-2})	(GPa)	
101-004-HG2-36.053	0	186	31	0.322	0.274	0.015	-4.509	66.90	0.19
101-004-HG2-40.742*	0	177	34	0.320	0.269	-0.149	-4.566	64.84	0.17
101-004-HG2-43.520*	0	175	47	0.304	0.302	0.030	-3.695	65.63	0.19
				0.277†		-0.117†		70.75†	0.31†
101-004-HG2-43.650*	0	206	73	0.350	0.308	0.018	-4.510	67.86	0.24
				0.303†		-0.055†		72.62†	0.34†
101-004-HG2-36.170	2	214	37	0.381	0.549	-0.172	-2.371	66.52	0.19
101-004-HG2-36.290	4	253	65	0.441	0.699	-0.177	-2.773	67.51	0.21
101-004-HG2-36.418	6	279	84	0.498	0.753	-0.478	-3.679	67.63	0.25
101-004-HG2-36.532	8	255	76	0.433	0.584	-0.004	-1.498	68.26	0.21
101-004-HG2-40.621	8	297	78	0.522	0.727	-0.269	-2.197	67.18	0.24
101-004-HG2-37.216	10	318	92	0.538	0.665	-0.320	-1.863	68.09	0.24
101-004-HG2-37.335	15	378	90	0.626	0.921	-0.127	-0.988	69.05	0.26
101-004-HG2-37.492	20	423	138	0.700	0.978	-0.223	-1.517	67.68	0.29
101-004-HG2-37.613	30	492	218	0.825	1.061	-0.150	-2.473	65.95	0.33
101-004-HG2-40.862*	30	487	303	0.810	0.736	-0.120	-0.760	66.13	0.33
101-004-HG2-40.381	40	546	139	0.903	1.400	-0.109		67.94	0.34
101-004-HG2-40.500	60	624	190	1.035	1.118	0.083	-0.855	65.33	0.32
101-004-HG2-43.390*	60	653	443	1.069	1.016	0.186	-0.253	64.03	0.32

*cyclic loading

†using strain gauges

Table 3. Failure Characteristics of rock specimens.

Specimen Identification	σ_3 (MPa)	β (degree)	Failure Characteristics
101-004-HG2-36.053	0		axial fractures, cracks
101-004-HG2-40.742	0		axial fractures, cracks
101-004-HG2-43.520	0		axial fractures, cracks
101-004-HG2-43.650	0		axial fractures, cracks
101-004-HG2-36.170	2	17	shear fracture, cracks
101-004-HG2-36.290	4	17	shear fracture, cracks
101-004-HG2-36.418	6	17	shear fracture, cracks
101-004-HG2-36.532	8	15	conjugate fractures, cracks
101-004-HG2-40.621	8	15	stepped shear fracture, cracks
101-004-HG2-37.216	10	15	conjugate fractures, cracks
101-004-HG2-37.335	15	15	shear fracture, cracks
101-004-HG2-37.492	20	20	shear fracture, cracks
101-004-HG2-37.613	30	25	stepped shear fracture, cracks
101-004-HG2-40.862	30	18	shear fracture
101-004-HG2-40.381	40	20	shear fracture, cracks
101-004-HG2-40.500	60	20	shear fracture, cracks
101-004-HG2-43.390	60	20	shear fracture, cracks

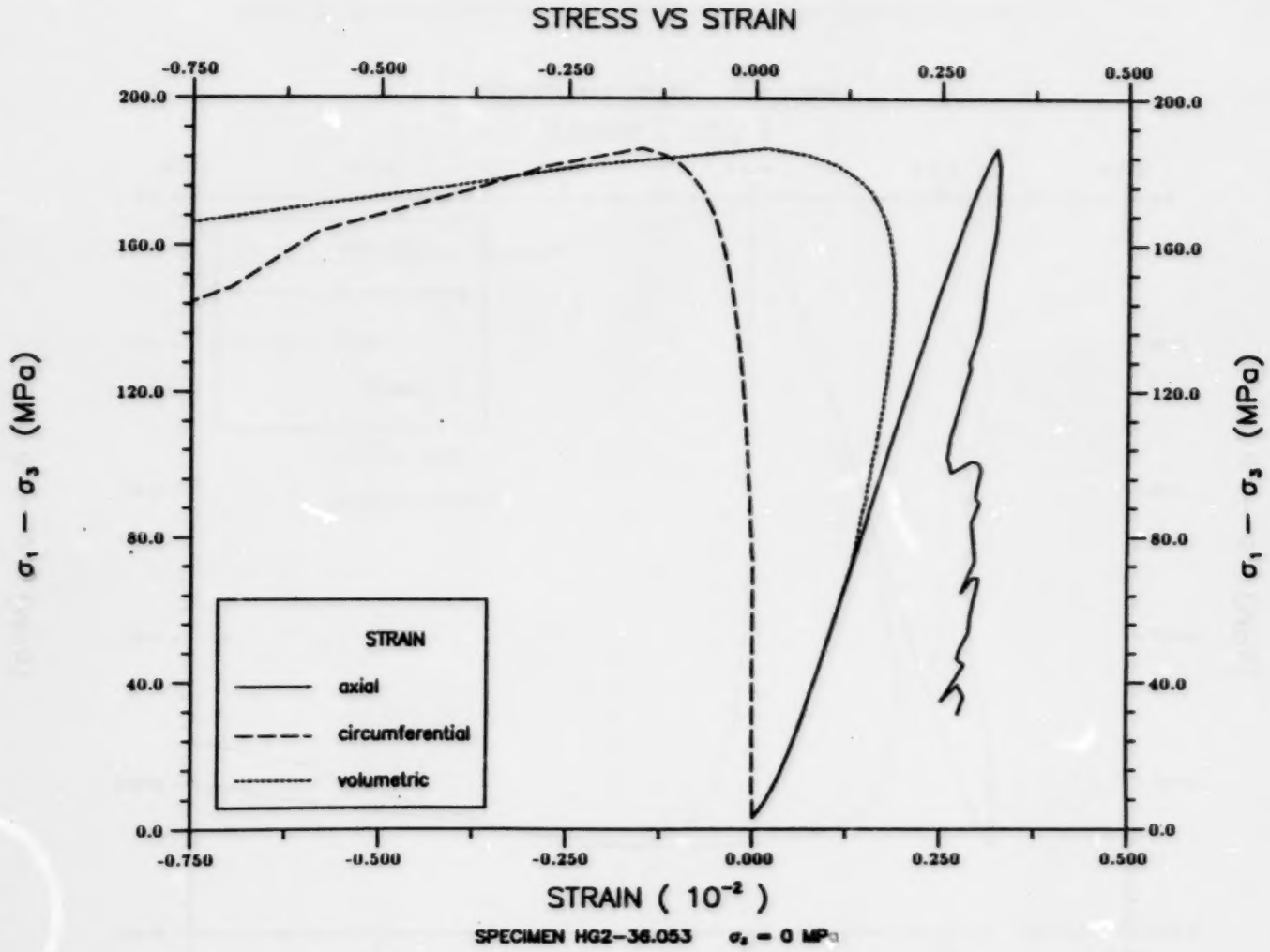

Figure 1. Stress-strain curves for specimen 101-004-HG2-36.053 ($\sigma_3 = 0$).

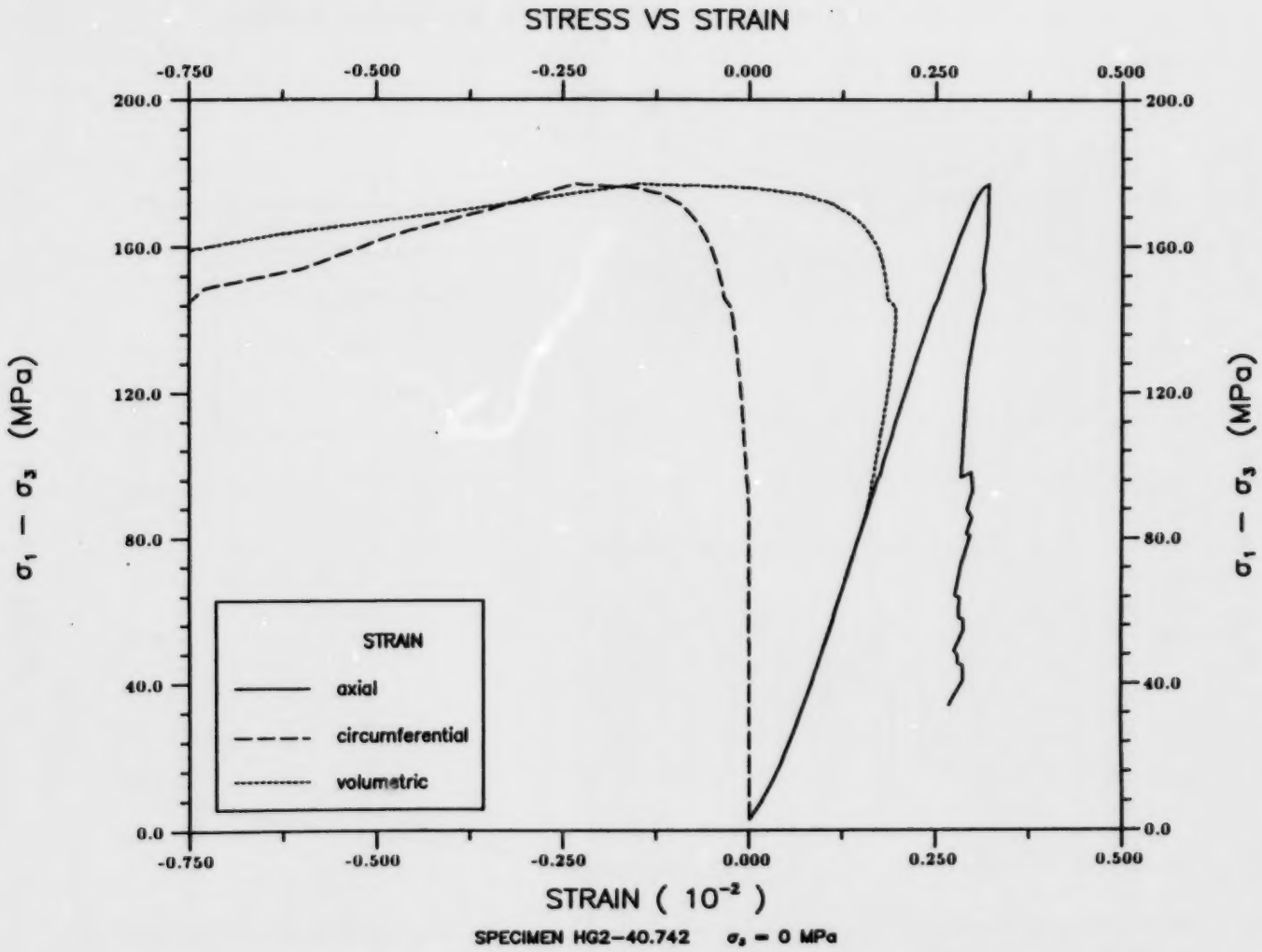

Figure 2. Stress-strain curves for specimen 101-004-HG2-40.742 ($\sigma_3 = 0$).

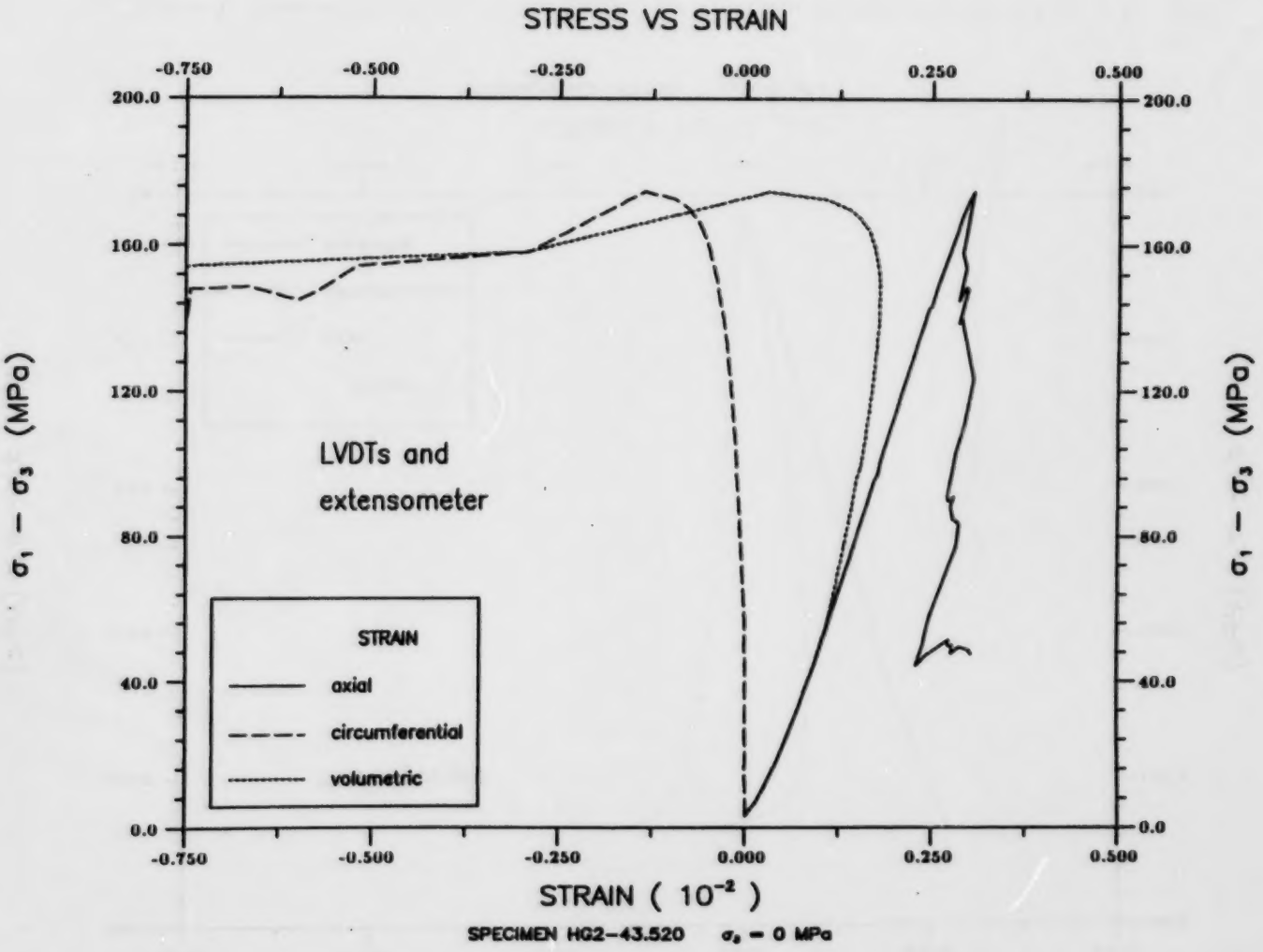

Figure 3. Stress-strain curves for specimen 101-004-HG2-43.520 ($\sigma_3 = 0$).

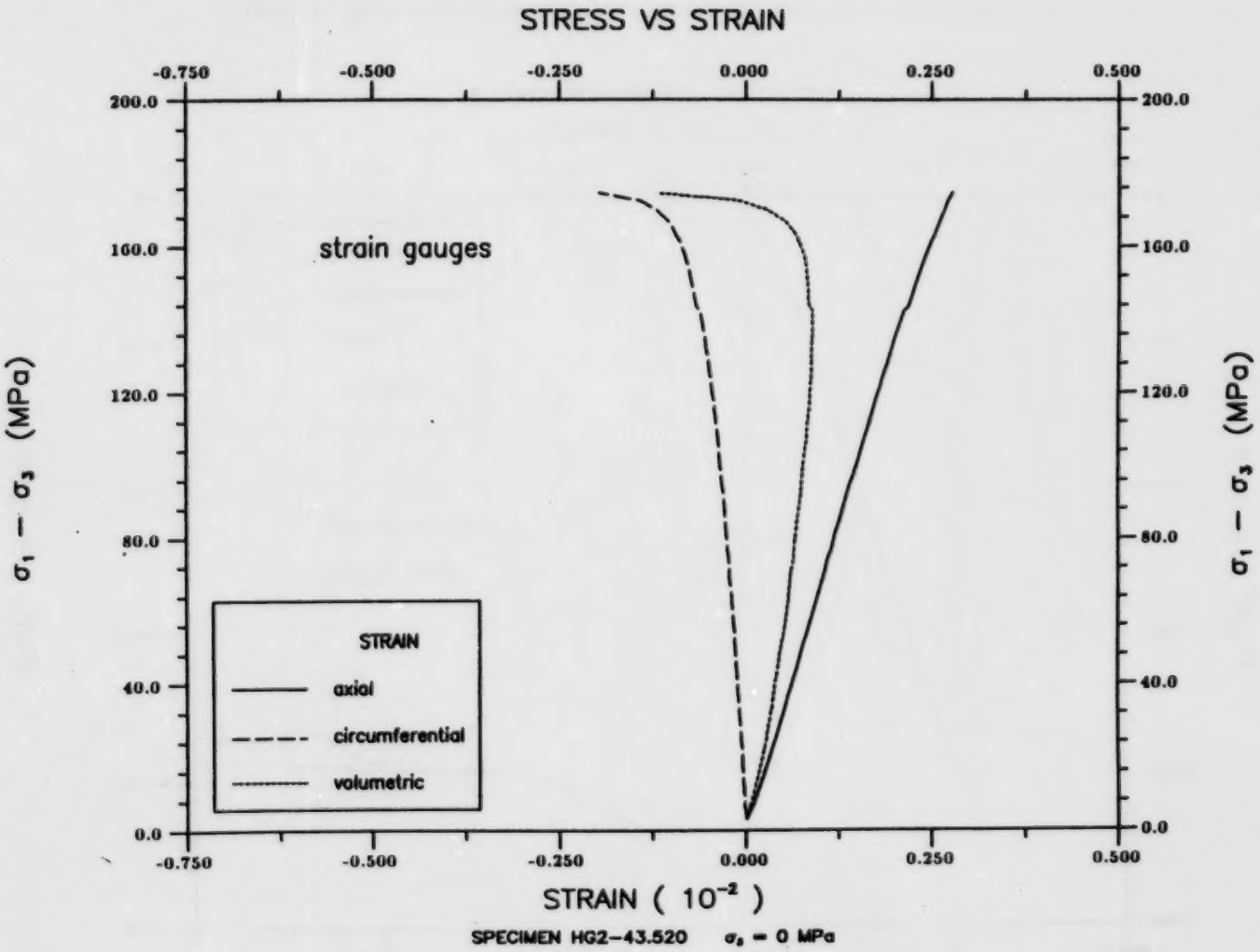

Figure 4. Stress-strain curves (strain gauges) for specimen 101-004-HG2-43.520 ($\sigma_3 = 0$).

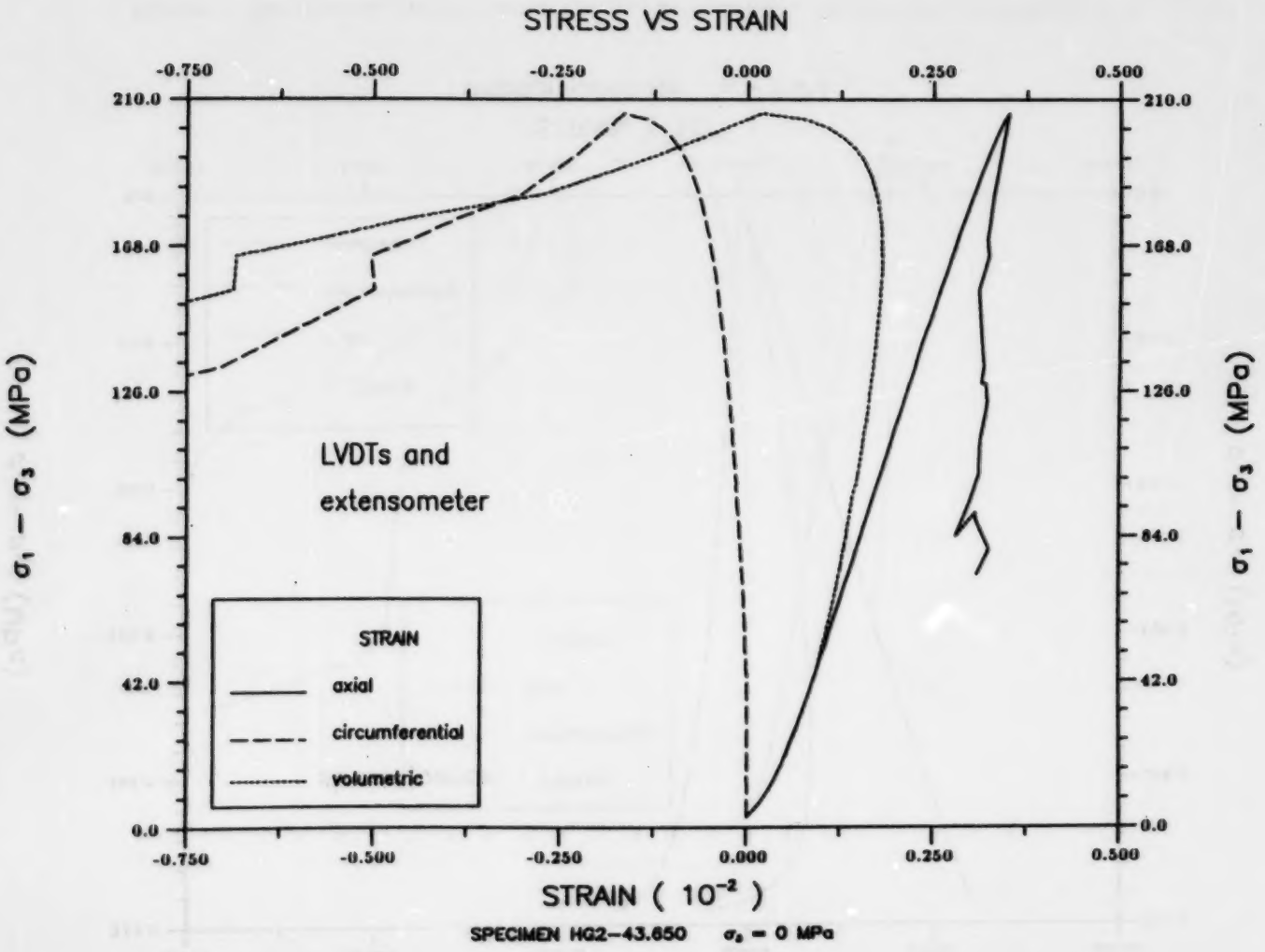

Figure 5. Stress-strain curves for specimen 101-004-HG2-43.650 ($\sigma_3 = 0$).

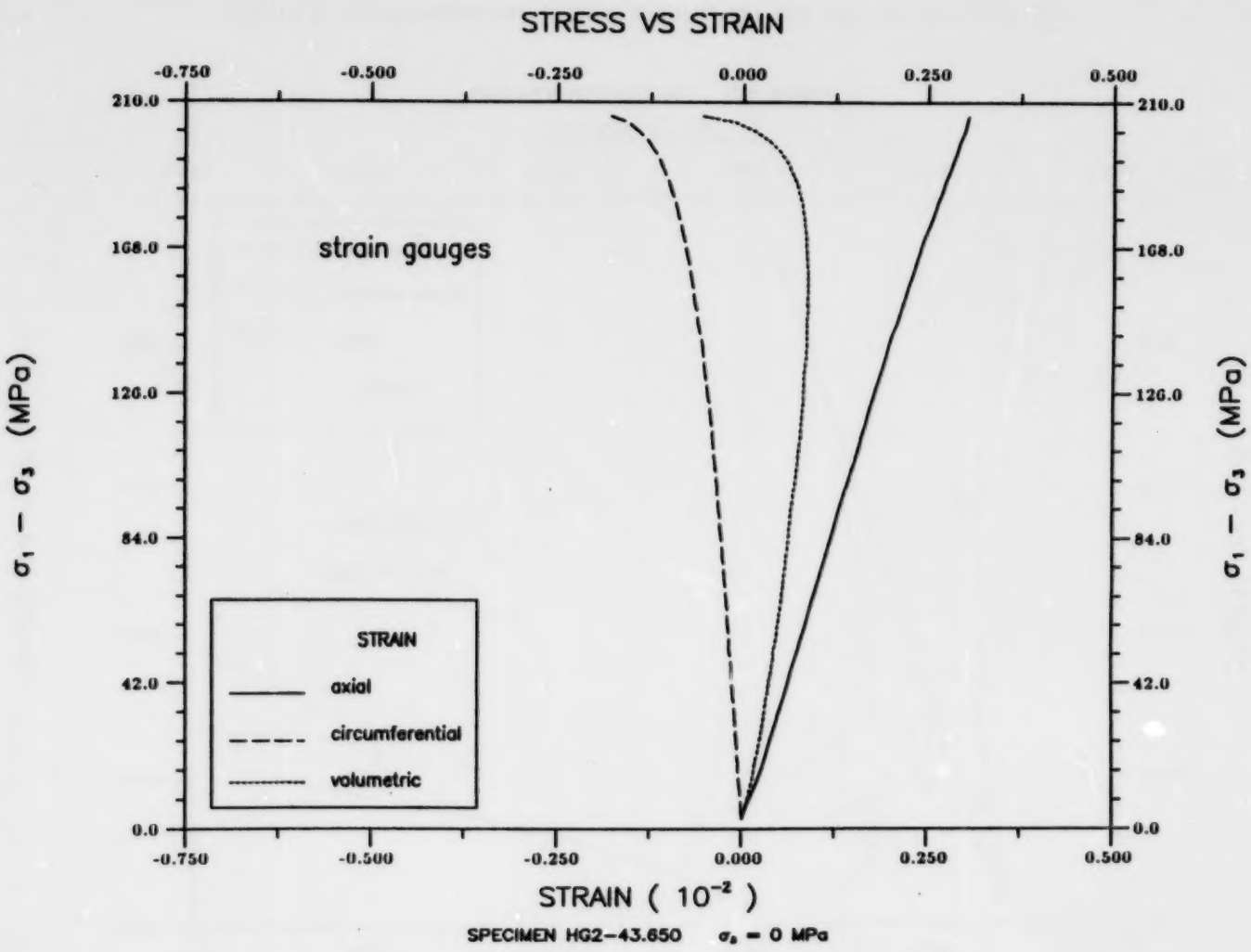

Figure 6. Stress-strain curves (strain gauges) for specimen 101-004-HG2-43.650 ($\sigma_3 = 0$).

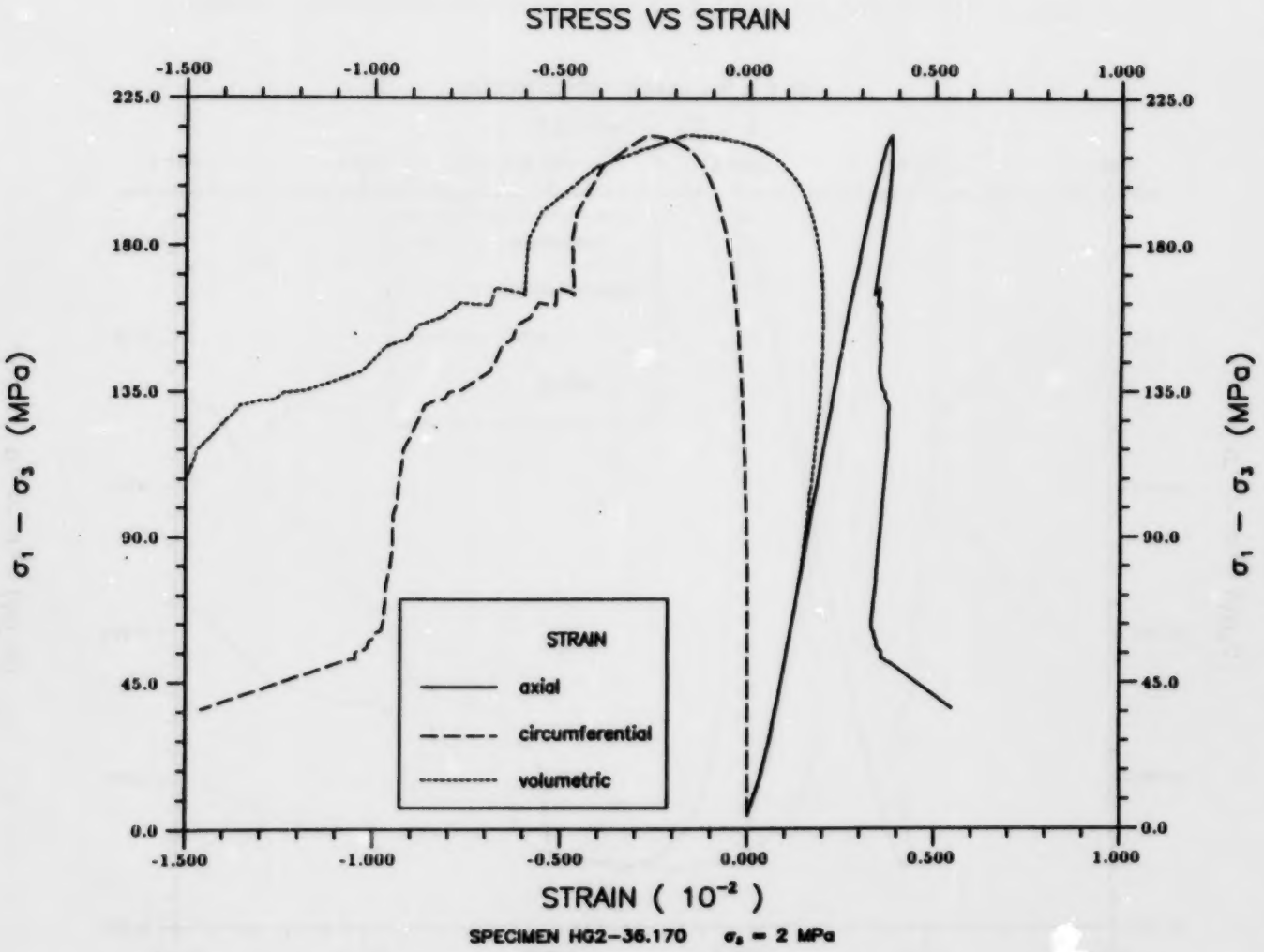

Figure 7. Stress-strain curves for specimen 101-004-HG2-36.170 ($\sigma_3 = 2$ MPa).

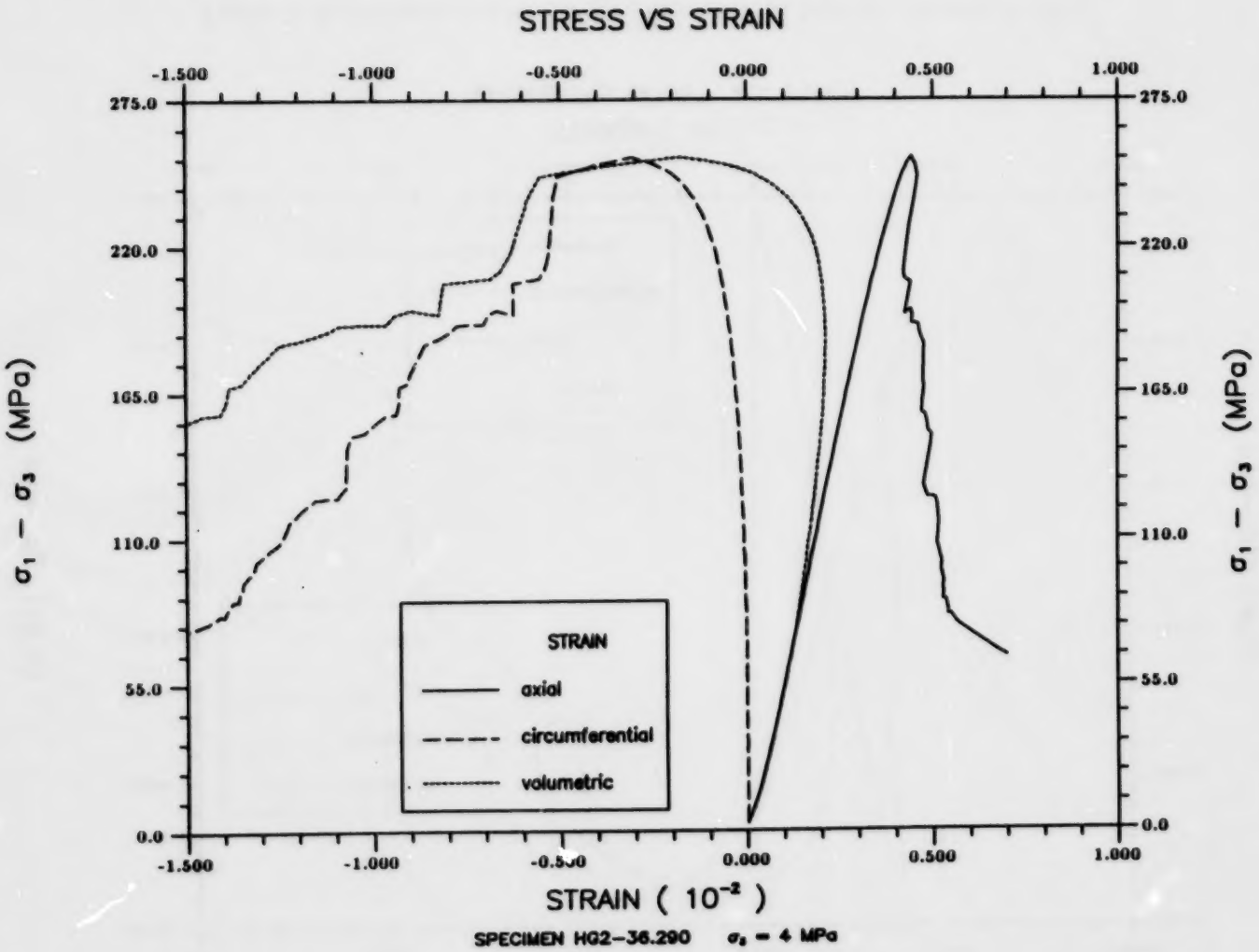

Figure 8. Stress-strain curves for specimen 101-004-HG2-36.290 ($\sigma_3 = 4$ MPa).

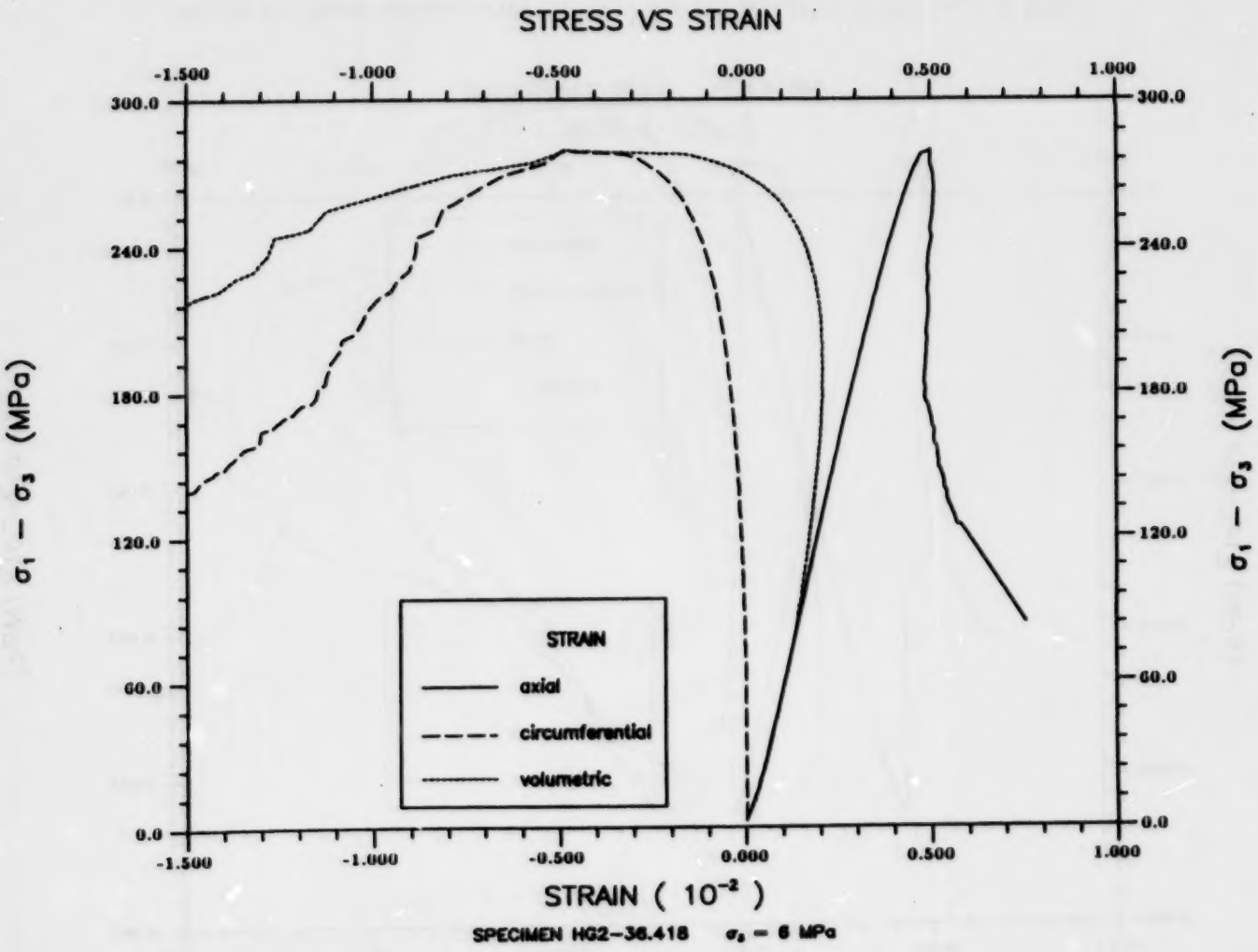

Figure 9. Stress-strain curves for specimen 101-004-HG2-36.418 ($\sigma_3 = 6$ MPa).

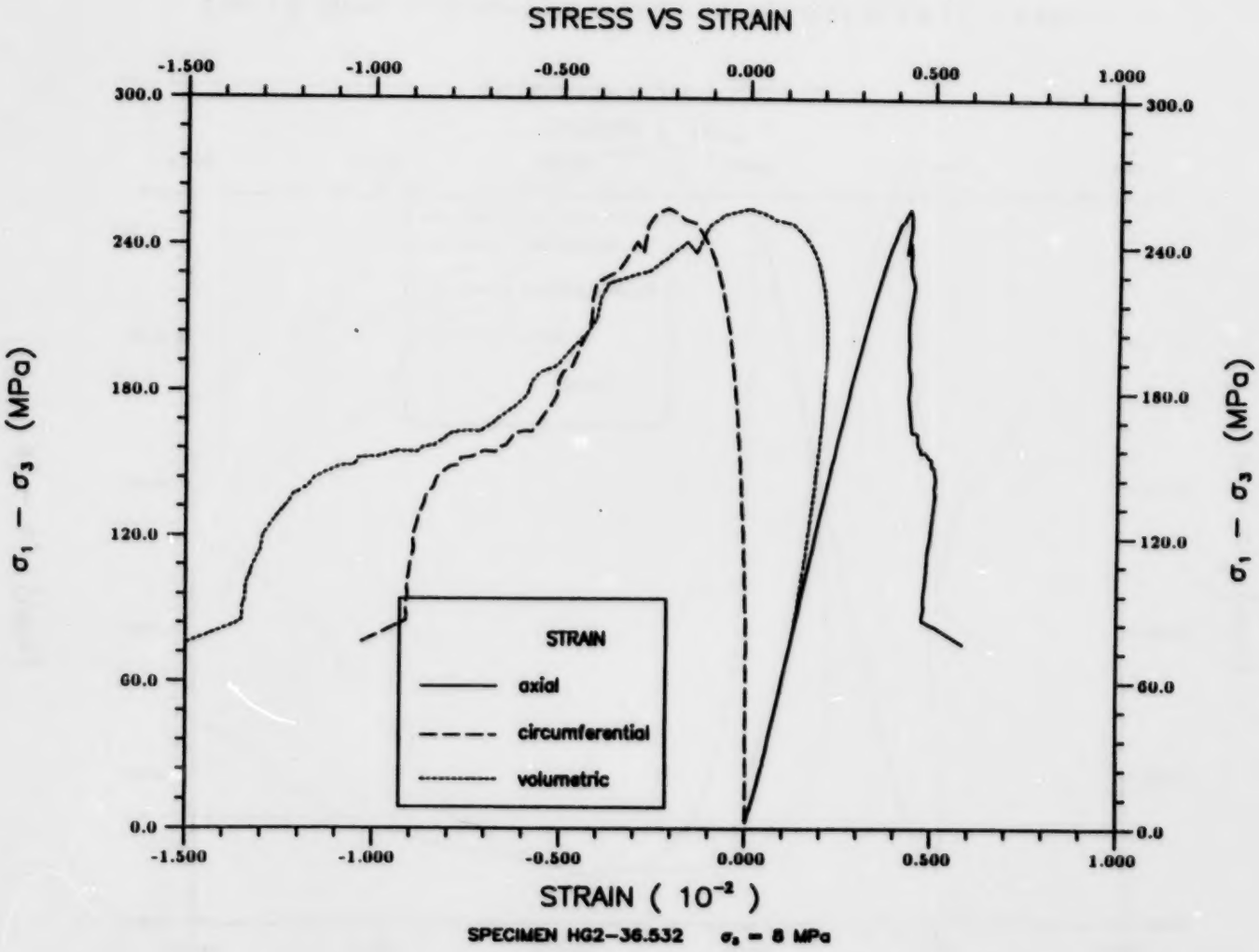

Figure 10. Stress-strain curves for specimen 101-004-HG2-36.532 ($\sigma_3 = 8$ MPa).

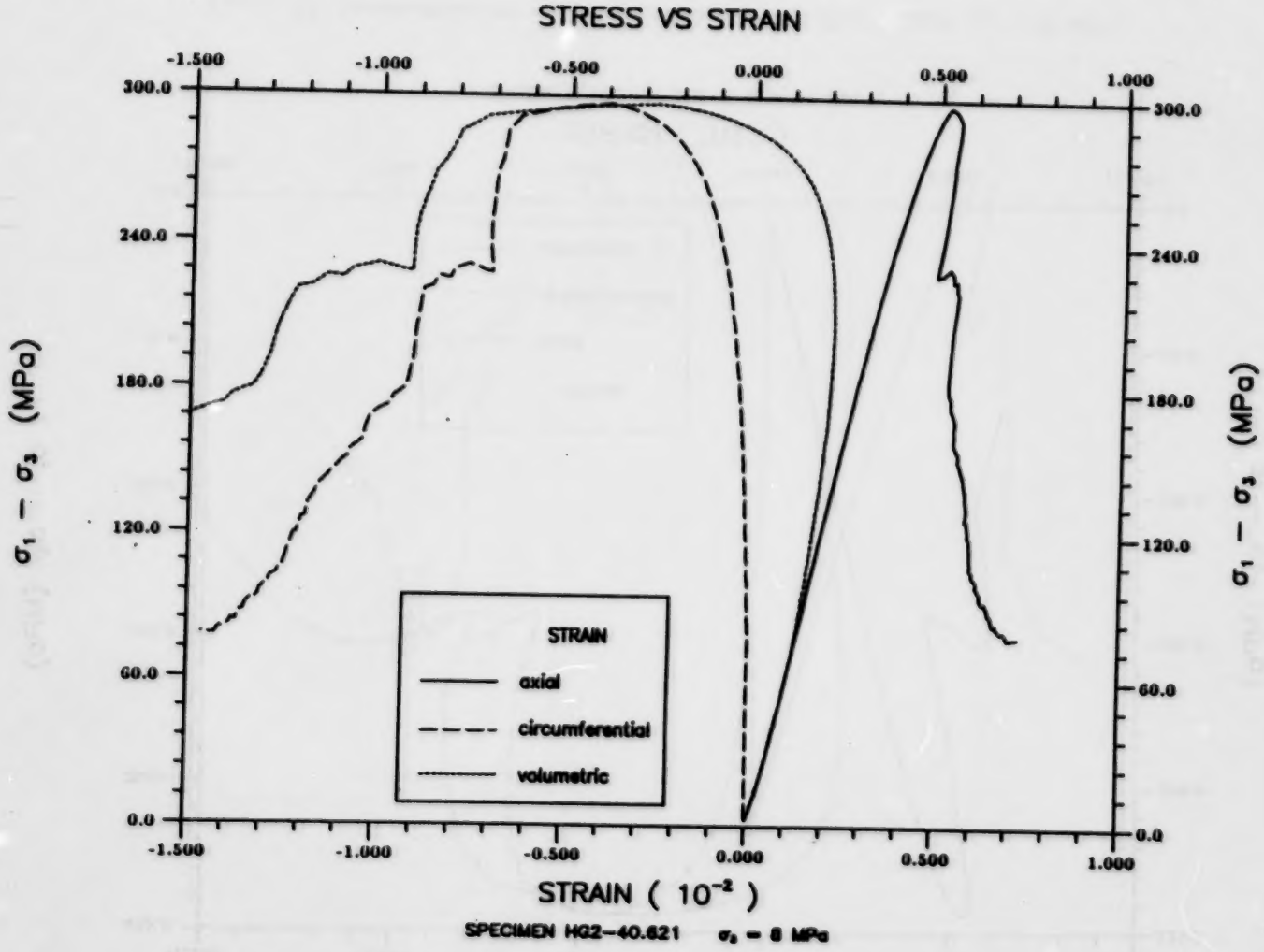

Figure 11. Stress-strain curves for specimen 101-004-HG2-40.621 ($\sigma_3 = 8$ MPa).

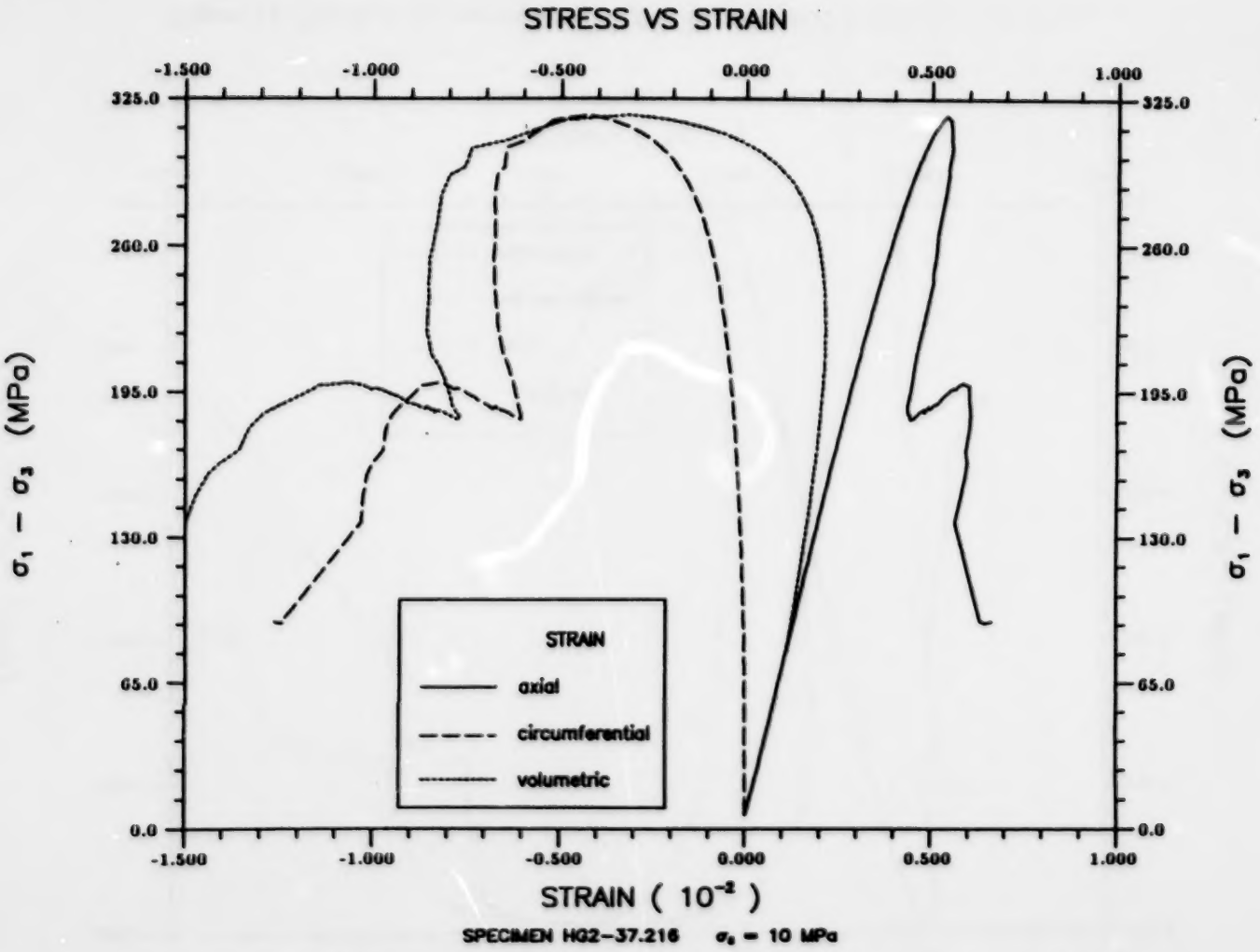

Figure 12. Stress-strain curves for specimen 101-004-HG2-37.216 ($\sigma_3 = 10$ MPa).

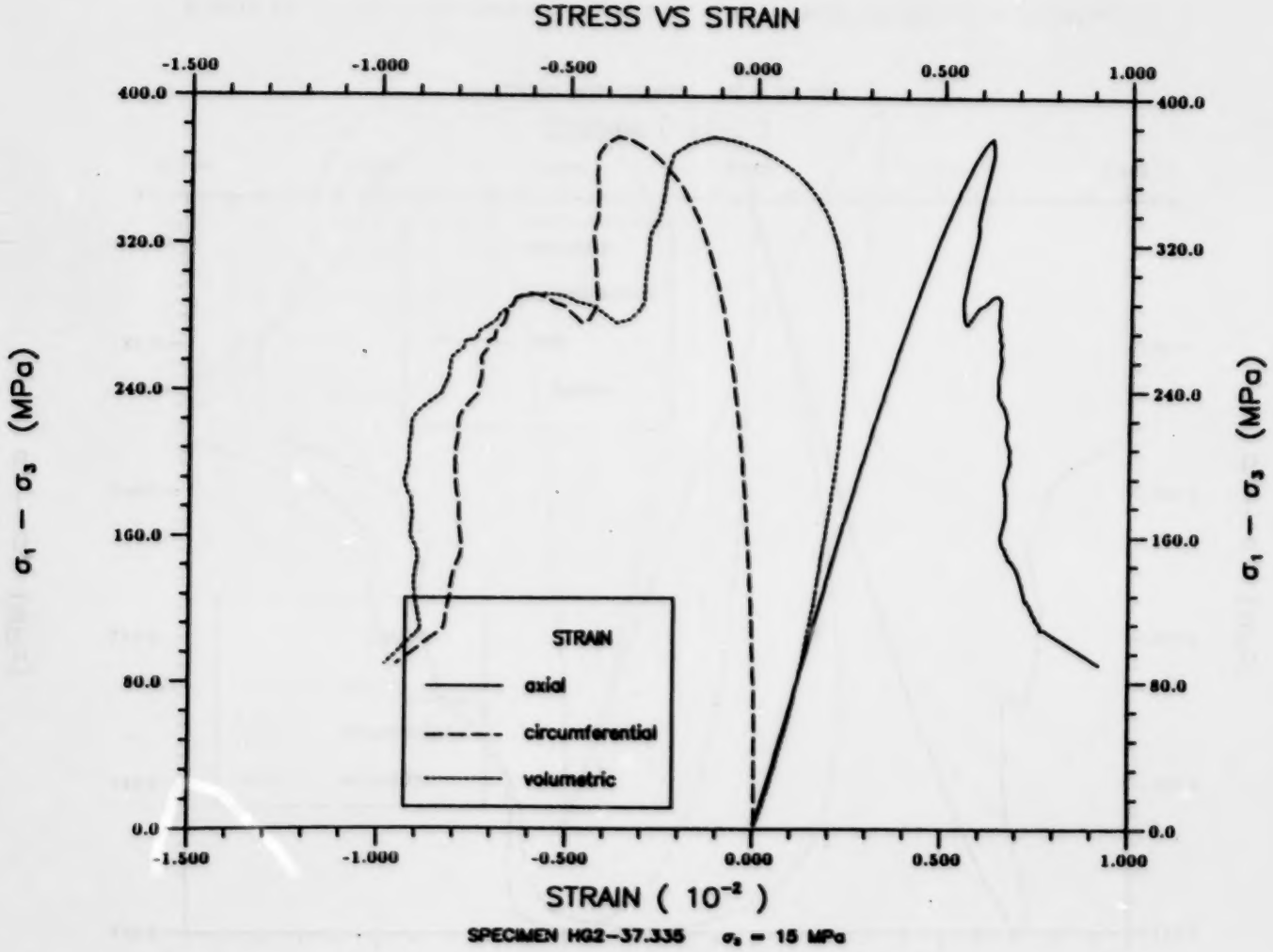

Figure 13. Stress-strain curves for specimen 101-004-HG2-37.335 ($\sigma_3 = 15$ MPa).

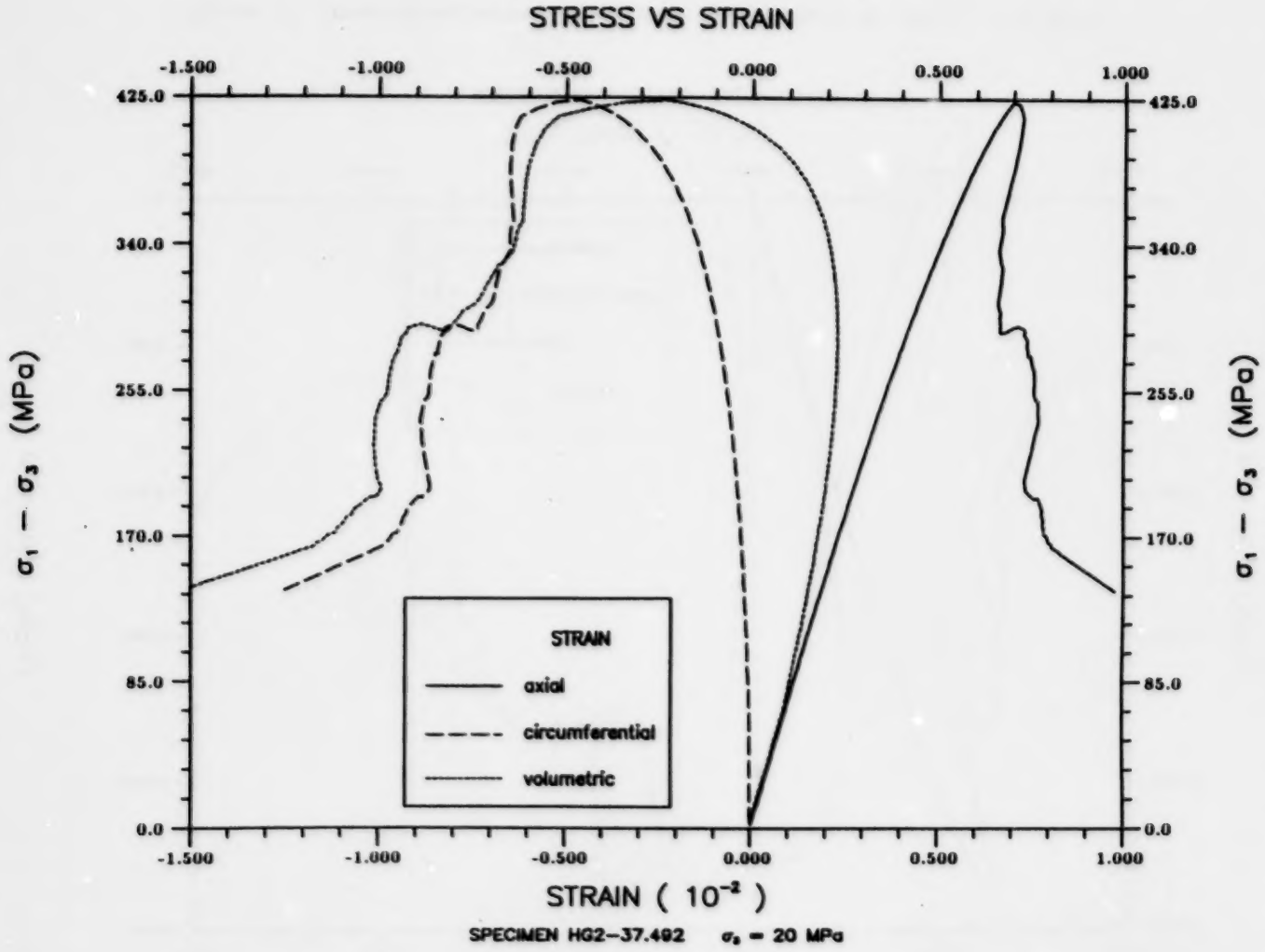

Figure 14. Stress-strain curves for specimen 101-004-HG2-37.492 ($\sigma_3 = 20$ MPa).

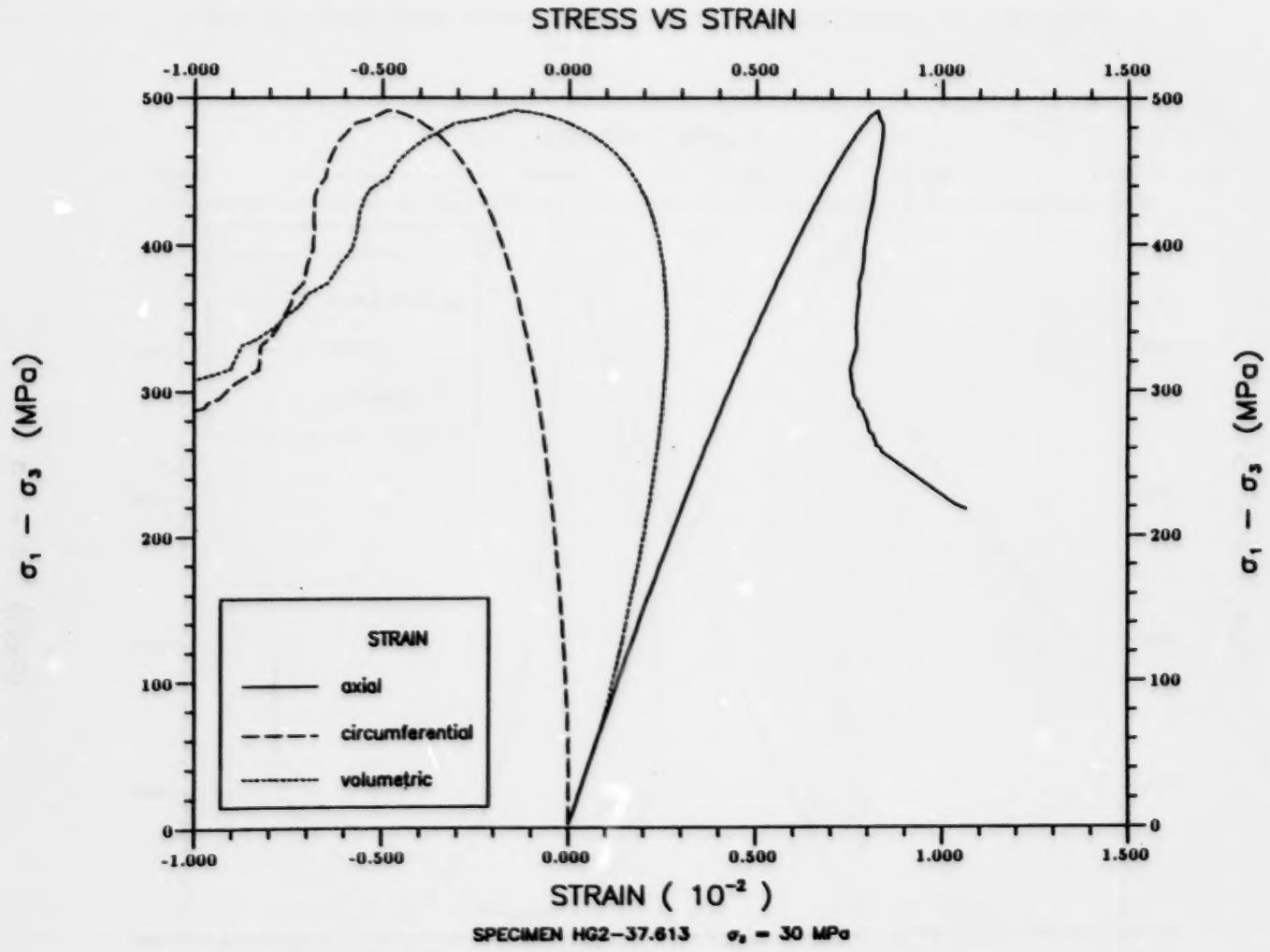

Figure 15. Stress-strain curves for specimen 101-004-HG2-37.613 ($\sigma_3 = 30$ MPa).

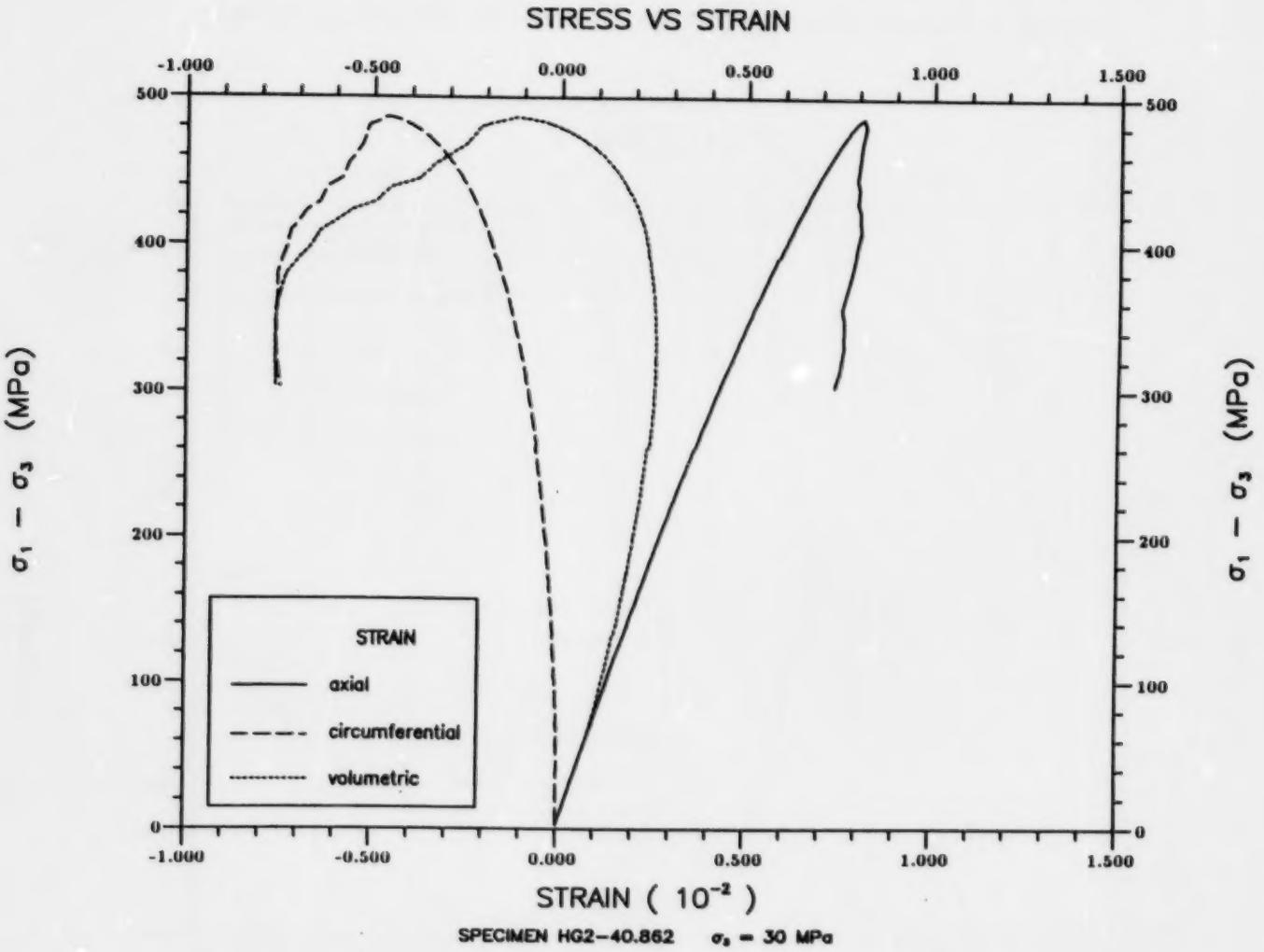

Figure 16. Stress-strain curves for specimen 101-004-HG2-40.862 ($\sigma_3 = 30$ MPa).

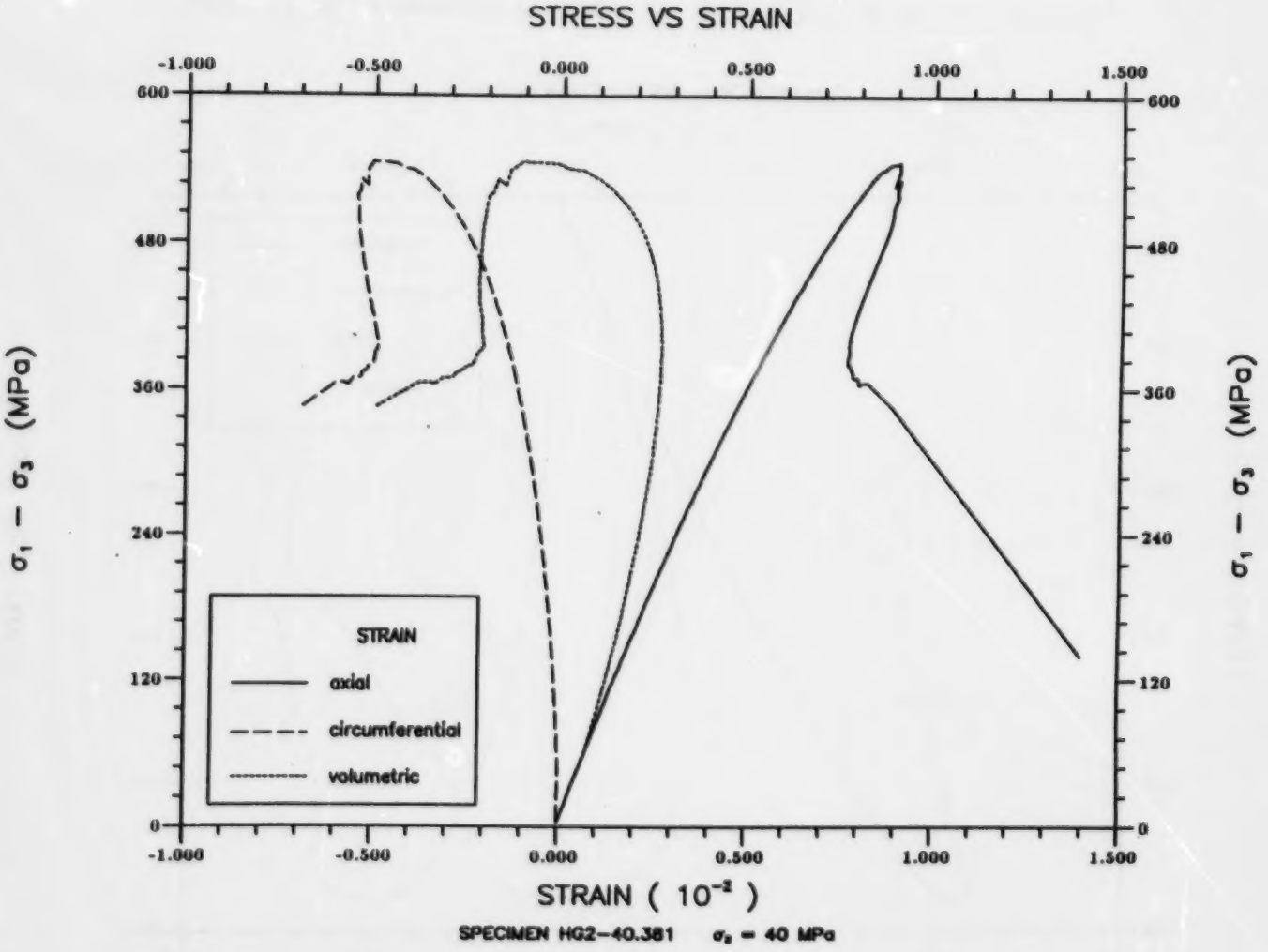

Figure 17. Stress-strain curves for specimen 101-004-HG2-40.381 ($\sigma_3 = 40$ MPa).

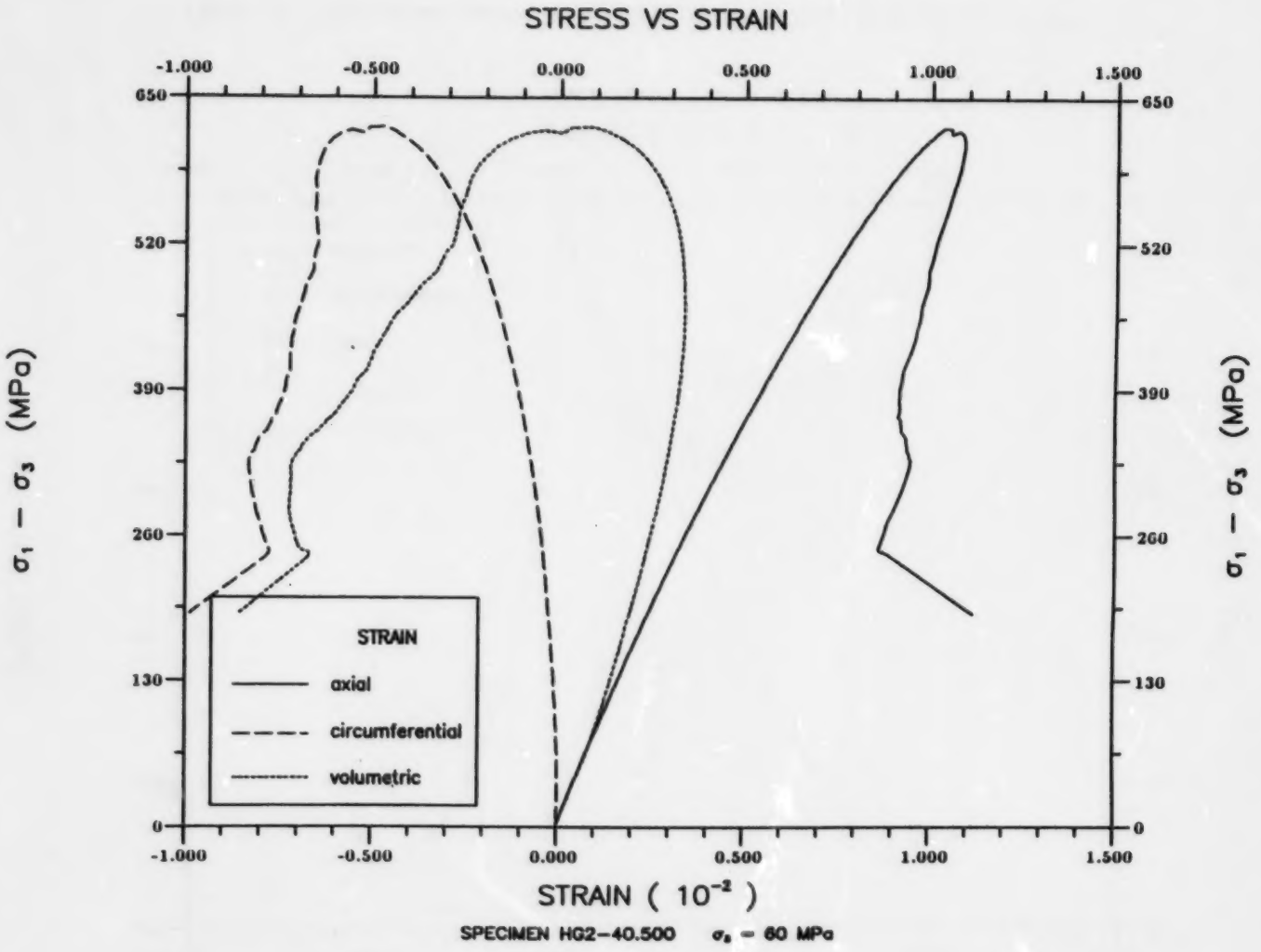

Figure 18. Stress-strain curves for specimen 101-004-HG2-40.500 ($\sigma_3 = 60$ MPa).

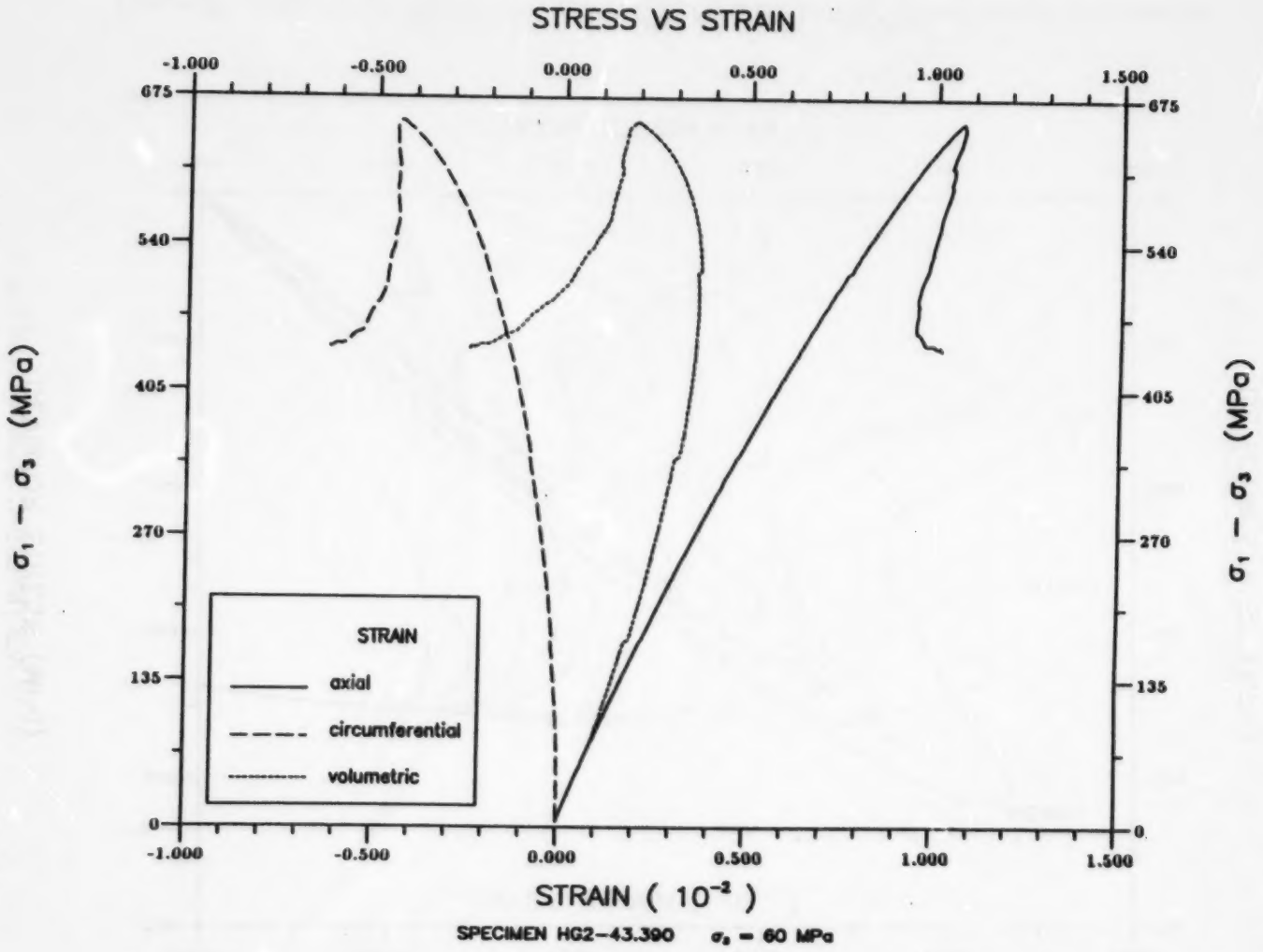

Figure 19. Stress-strain curves for specimen 101-004-HG2-43.390 ($\sigma_3 = 60$ MPa).

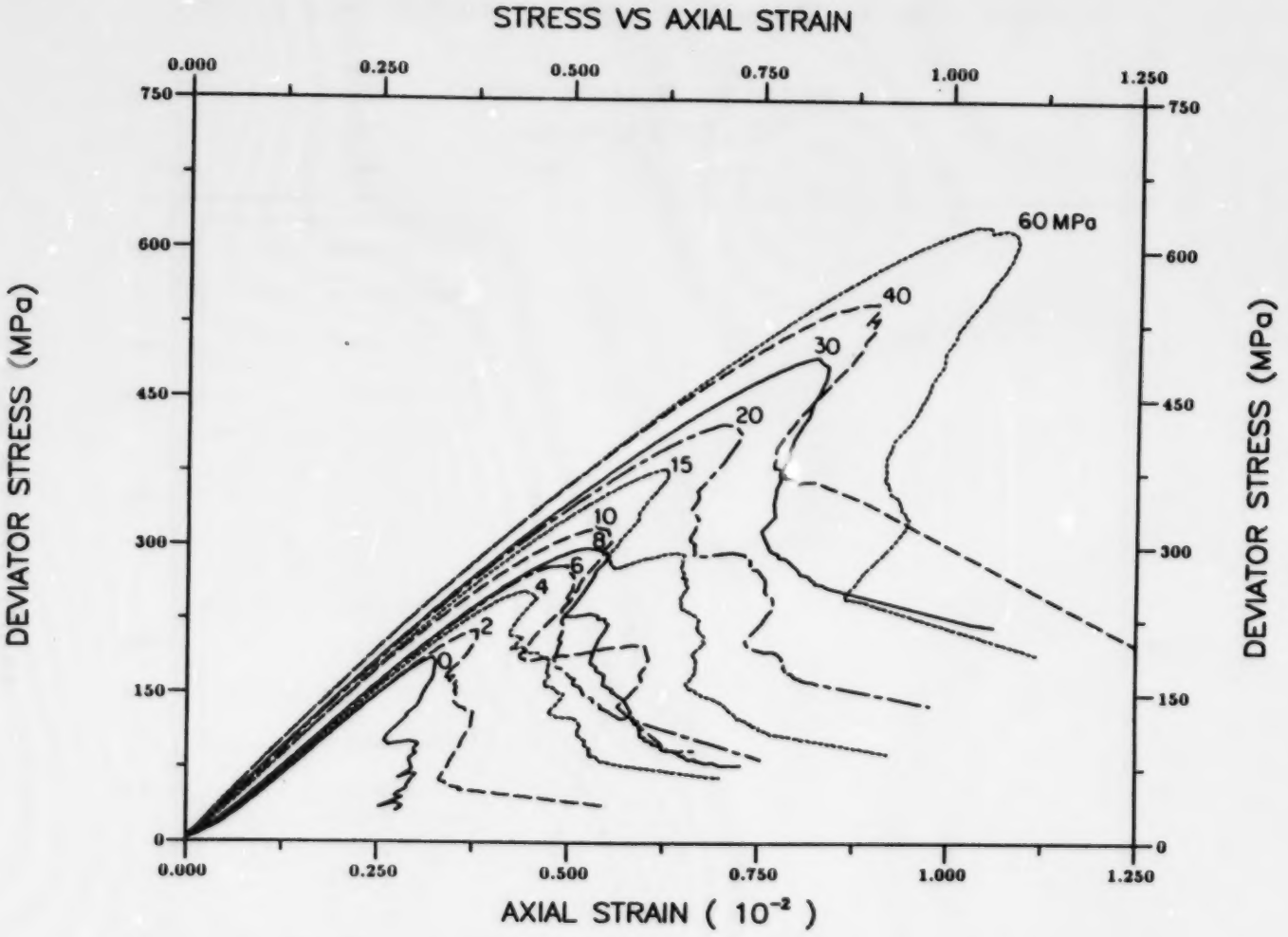

Figure 20. Stress versus axial strain curves of pink granite in uniaxial and triaxial compression.

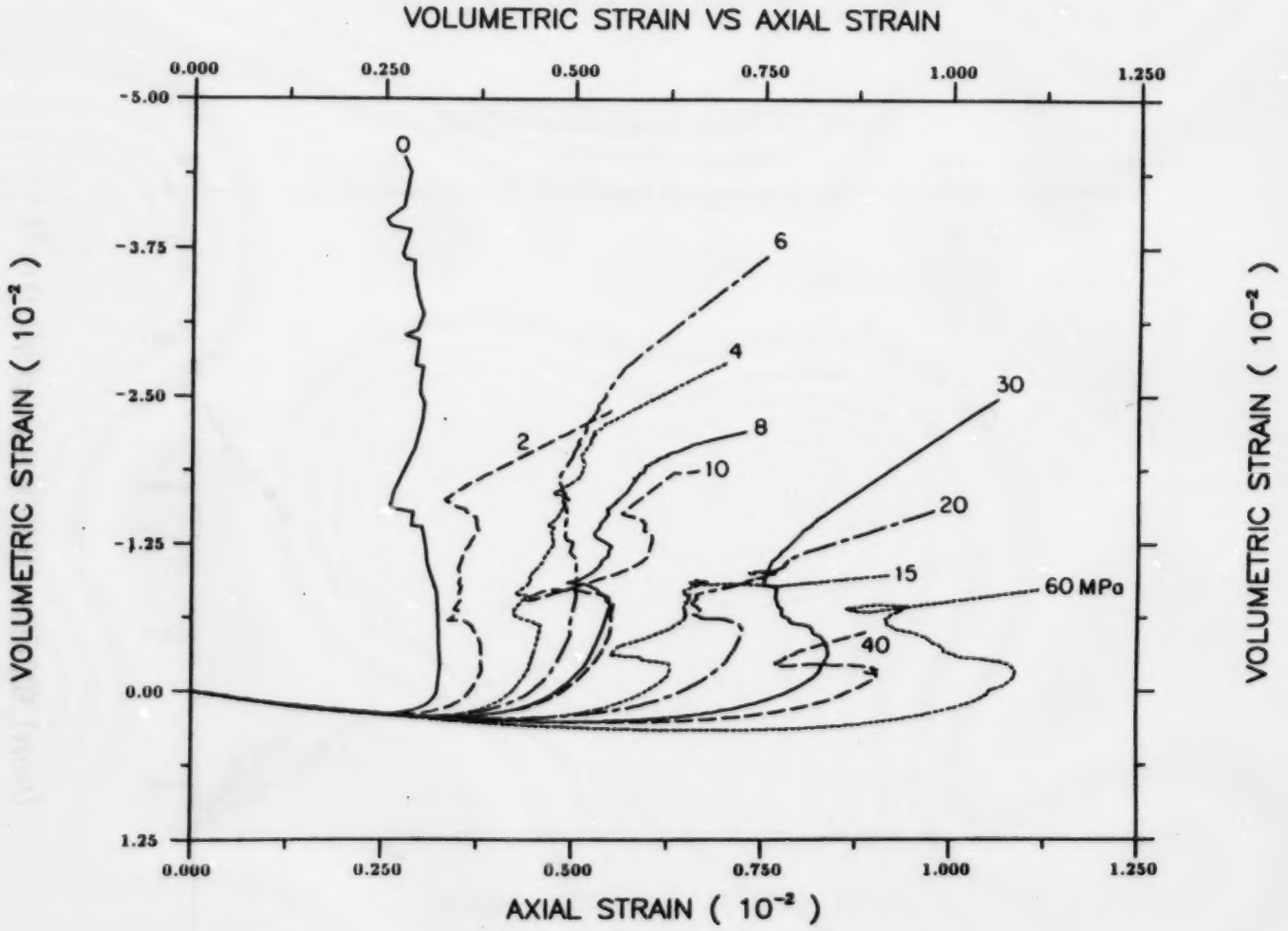

Figure 21. Volumetric strain versus axial strain curves of pink granite in uniaxial and triaxial compression.

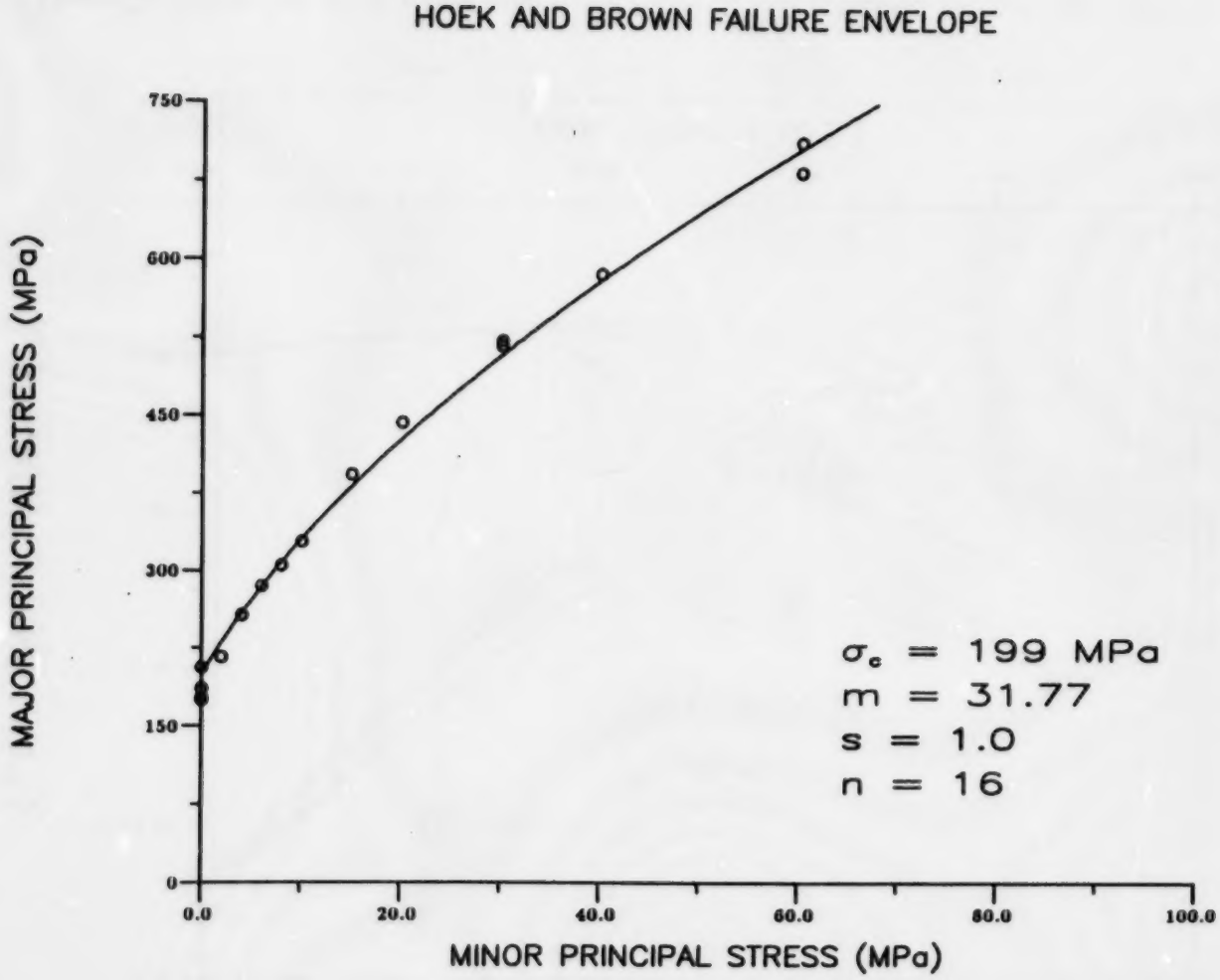

Figure 22. The Hoek and Brown failure envelope.

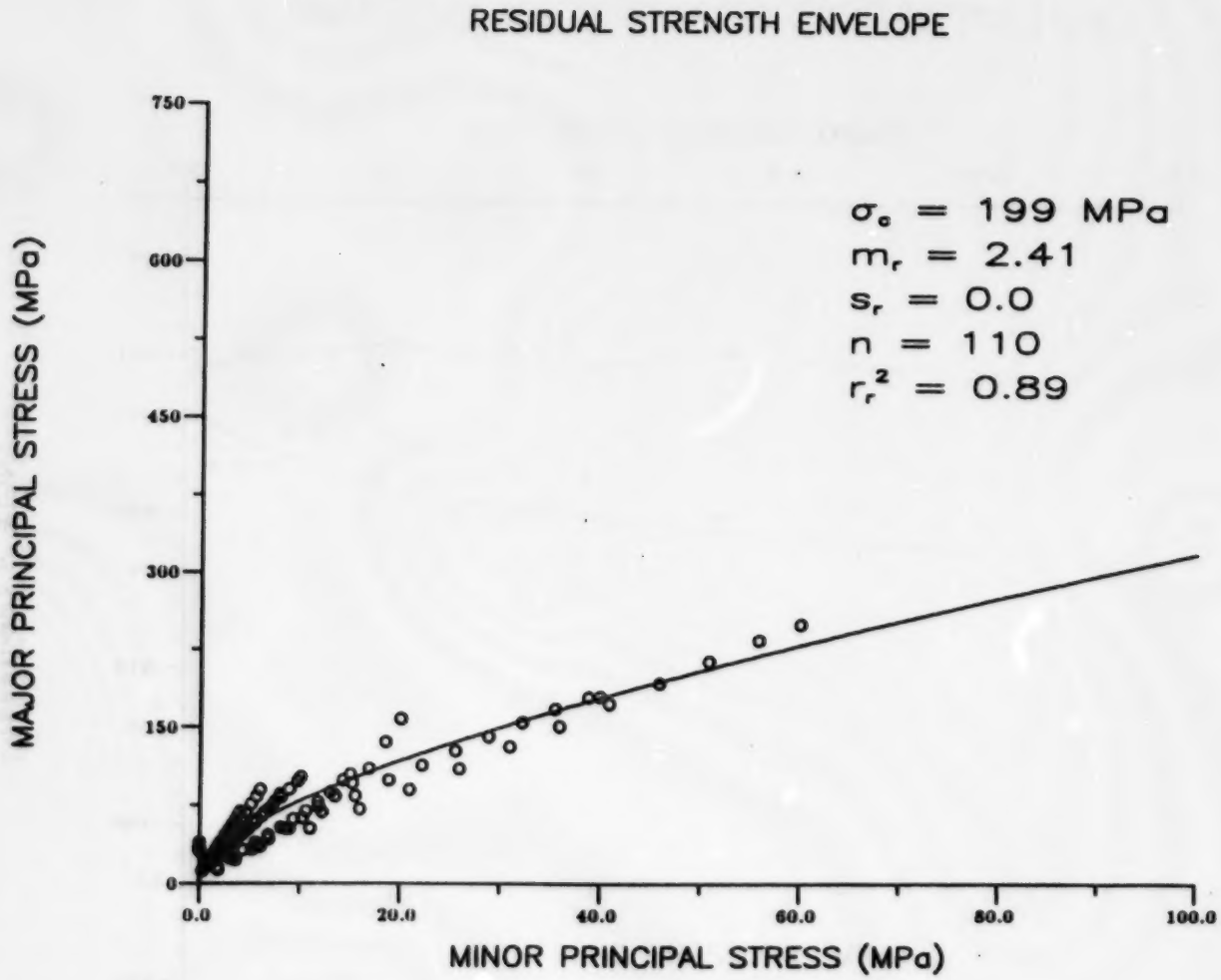

Figure 23. The residual strength envelope.

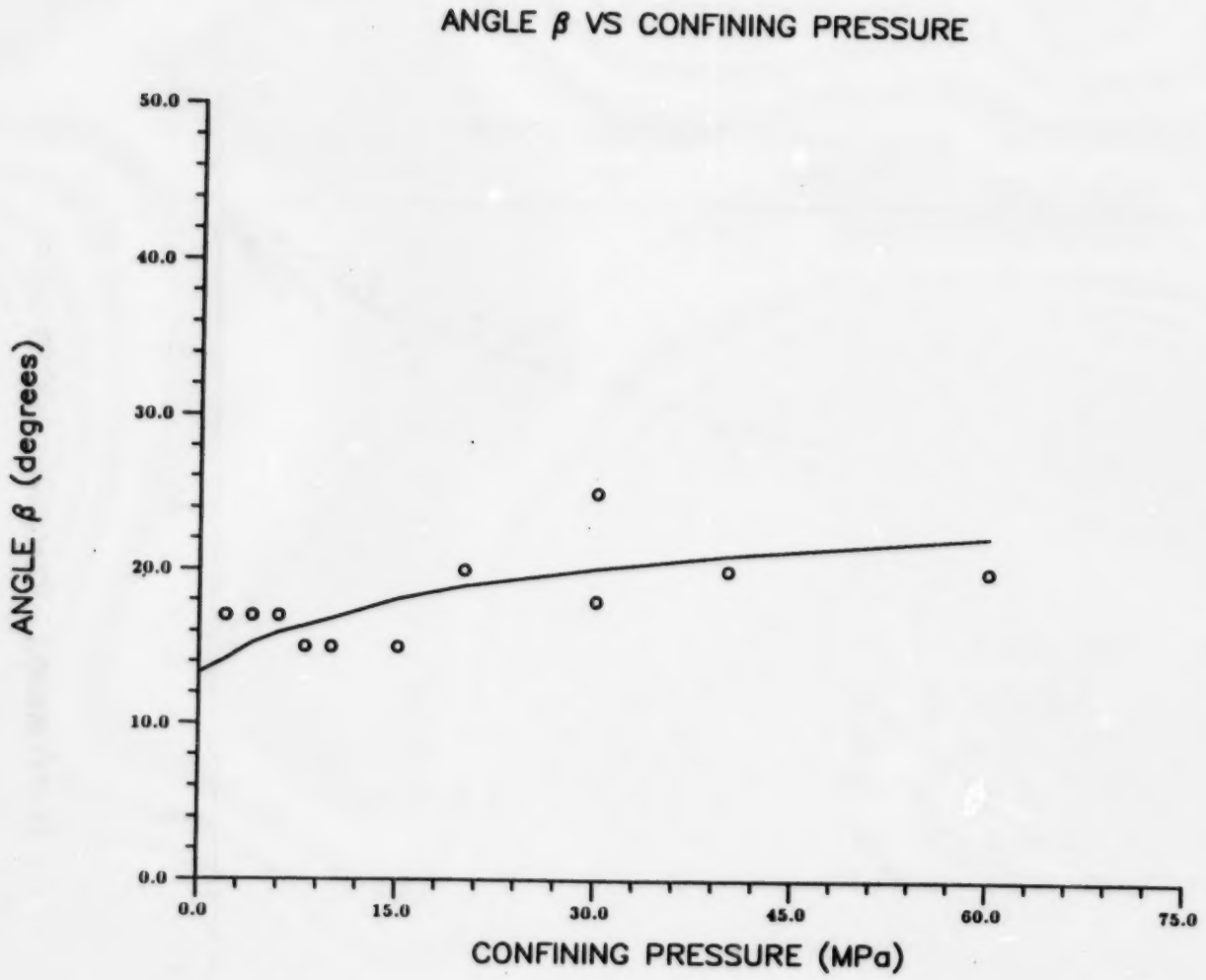

Figure 24. Plot of angle β versus confining pressure.

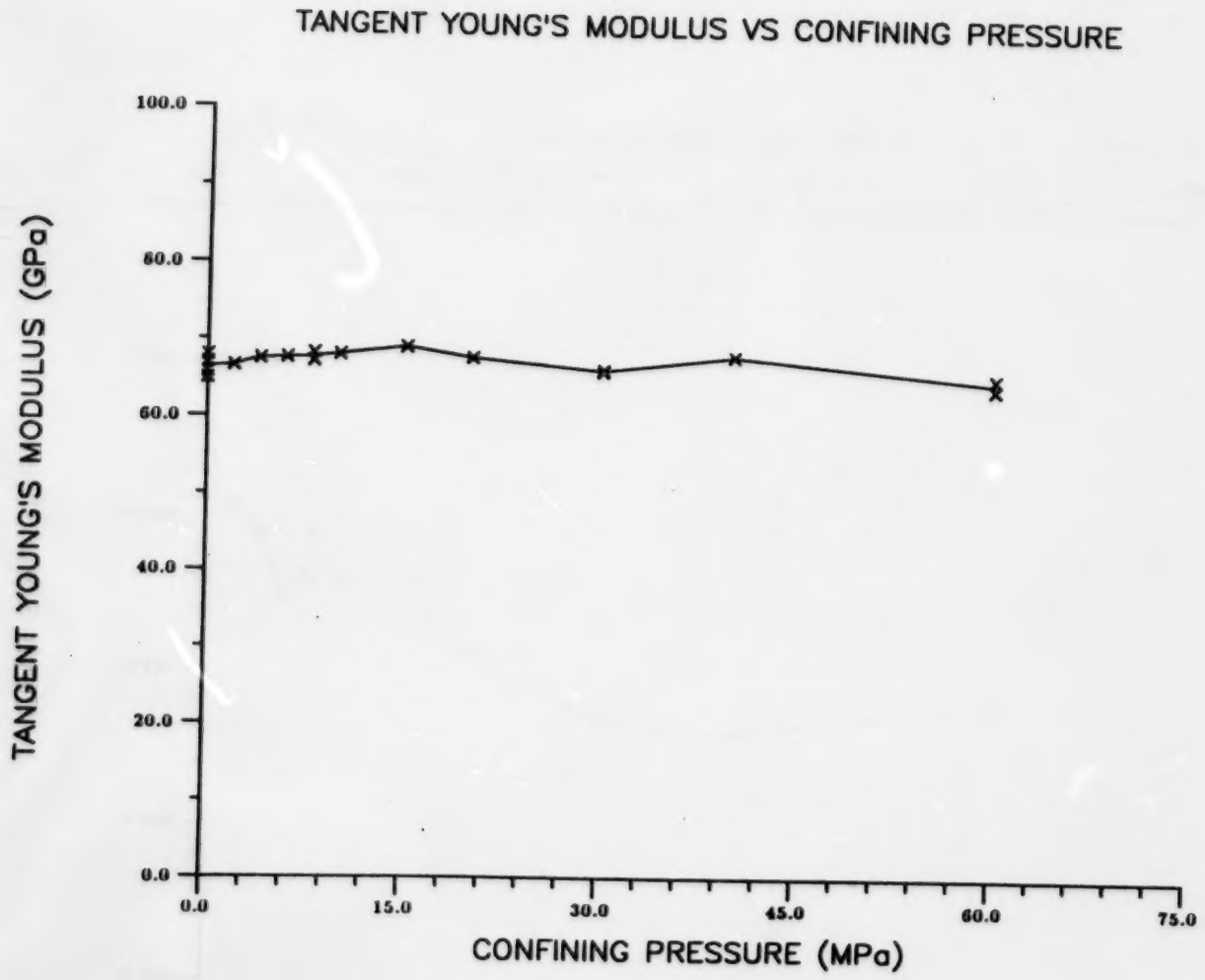

Figure 25. Plot of tangent Young's modulus **E** versus confining pressure.

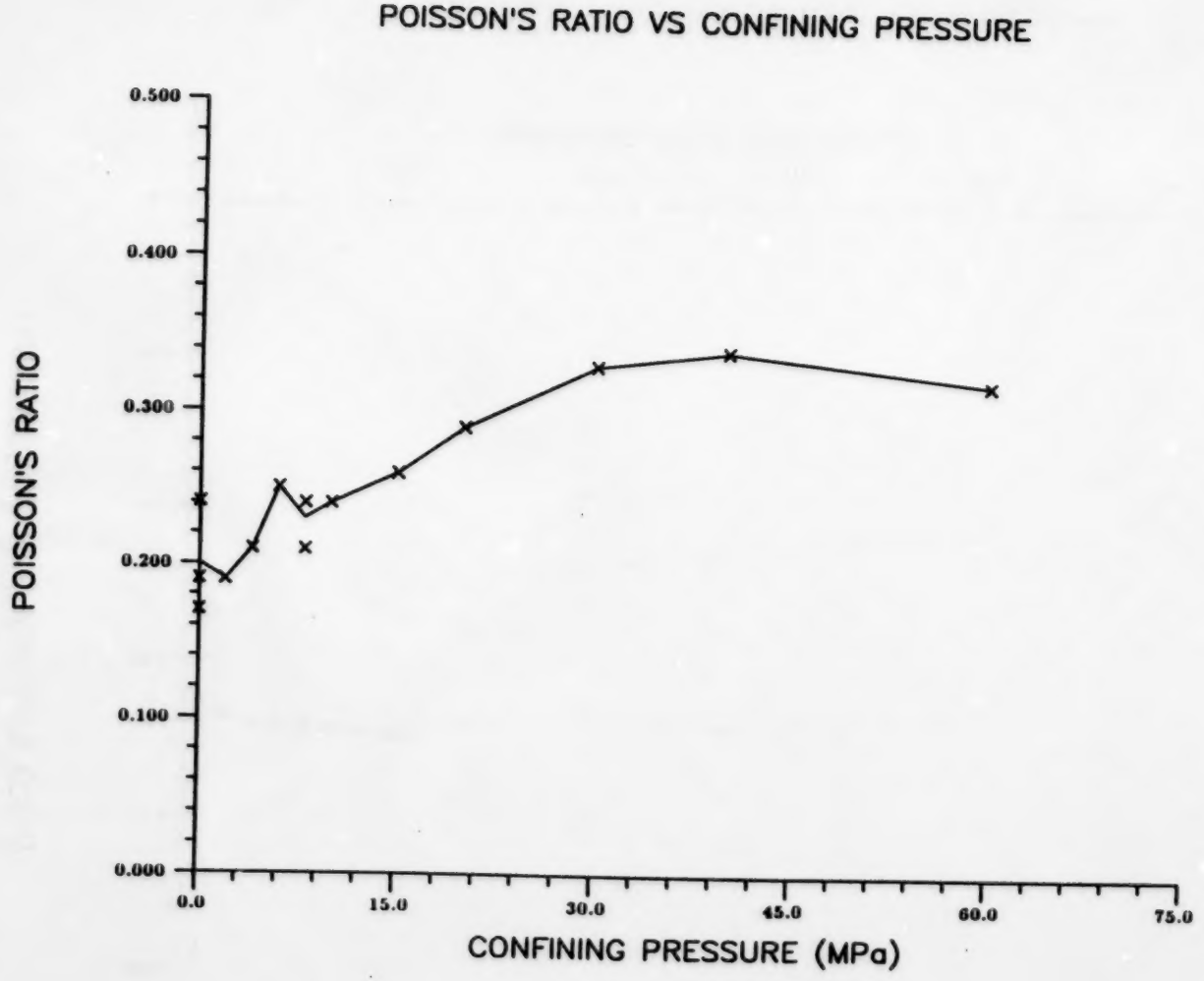

Figure 26. Plot of Poisson's ratio ν versus confining pressure.

APPENDIX A

Loading-unloading Curves

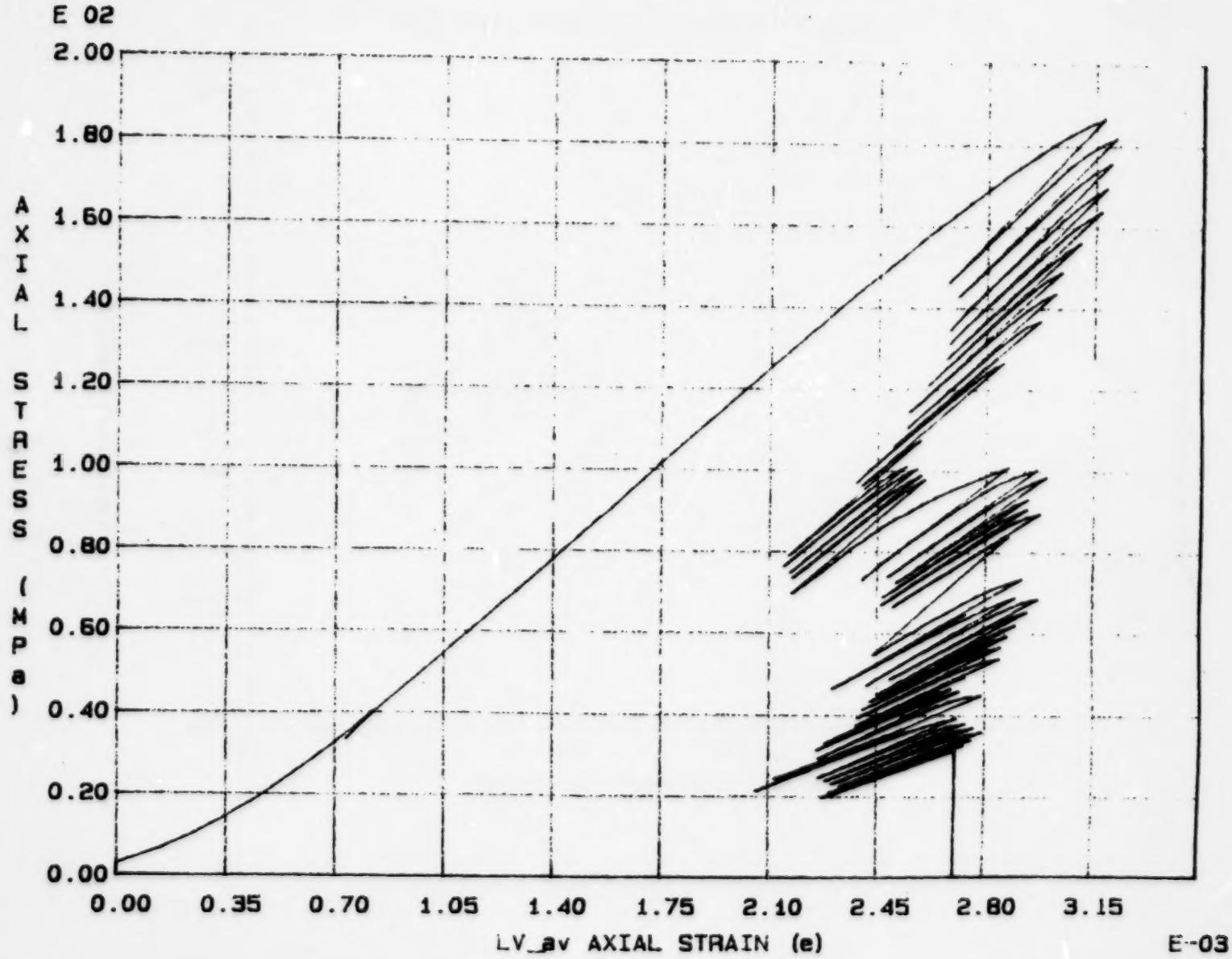

Figure A1. Loading and unloading curves (axial strain) for Specimen HG2-36.053.

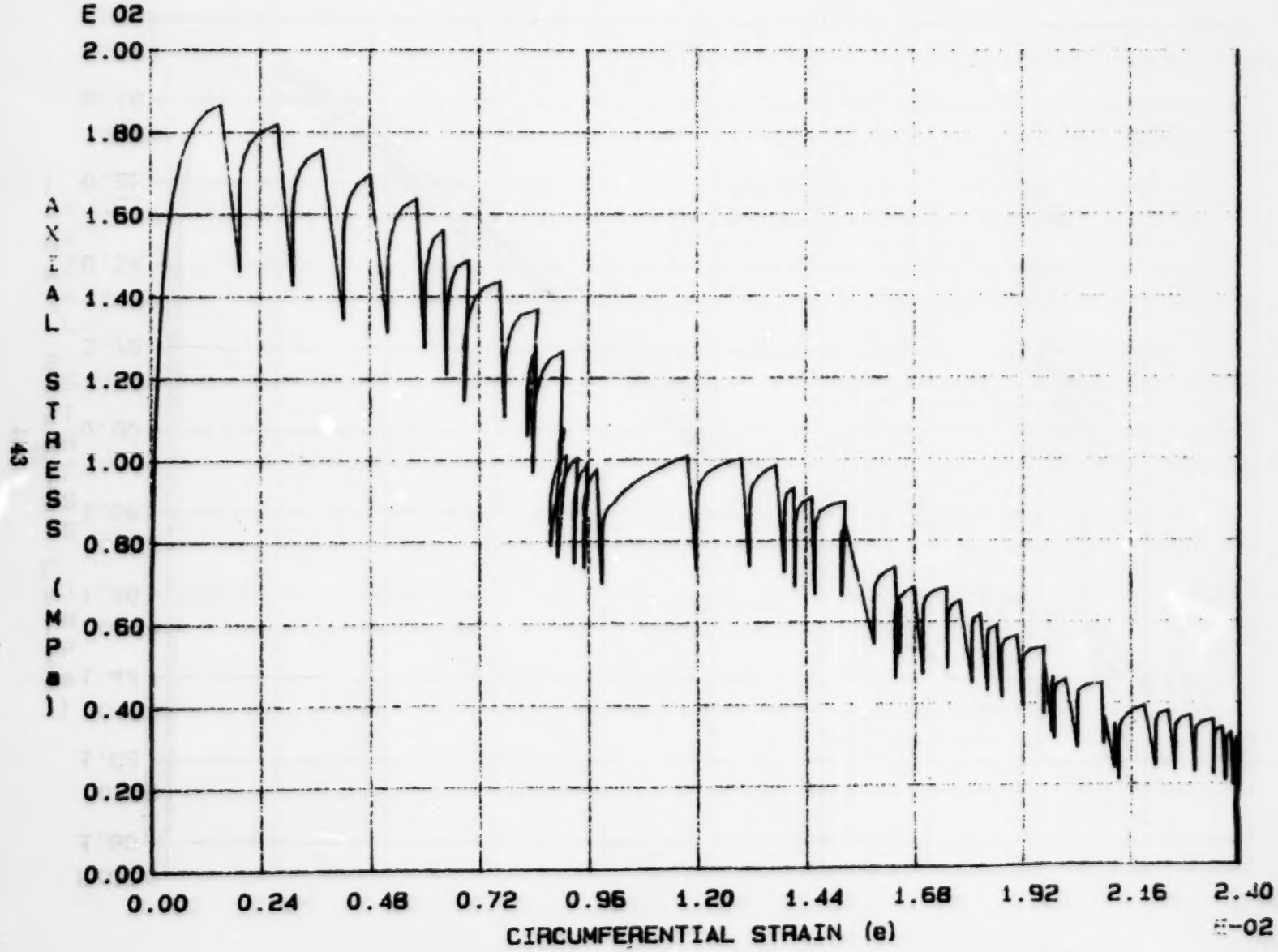

Figure A2. Loading and unloading curves (cir. strain) for Specimen HG2-36.053.

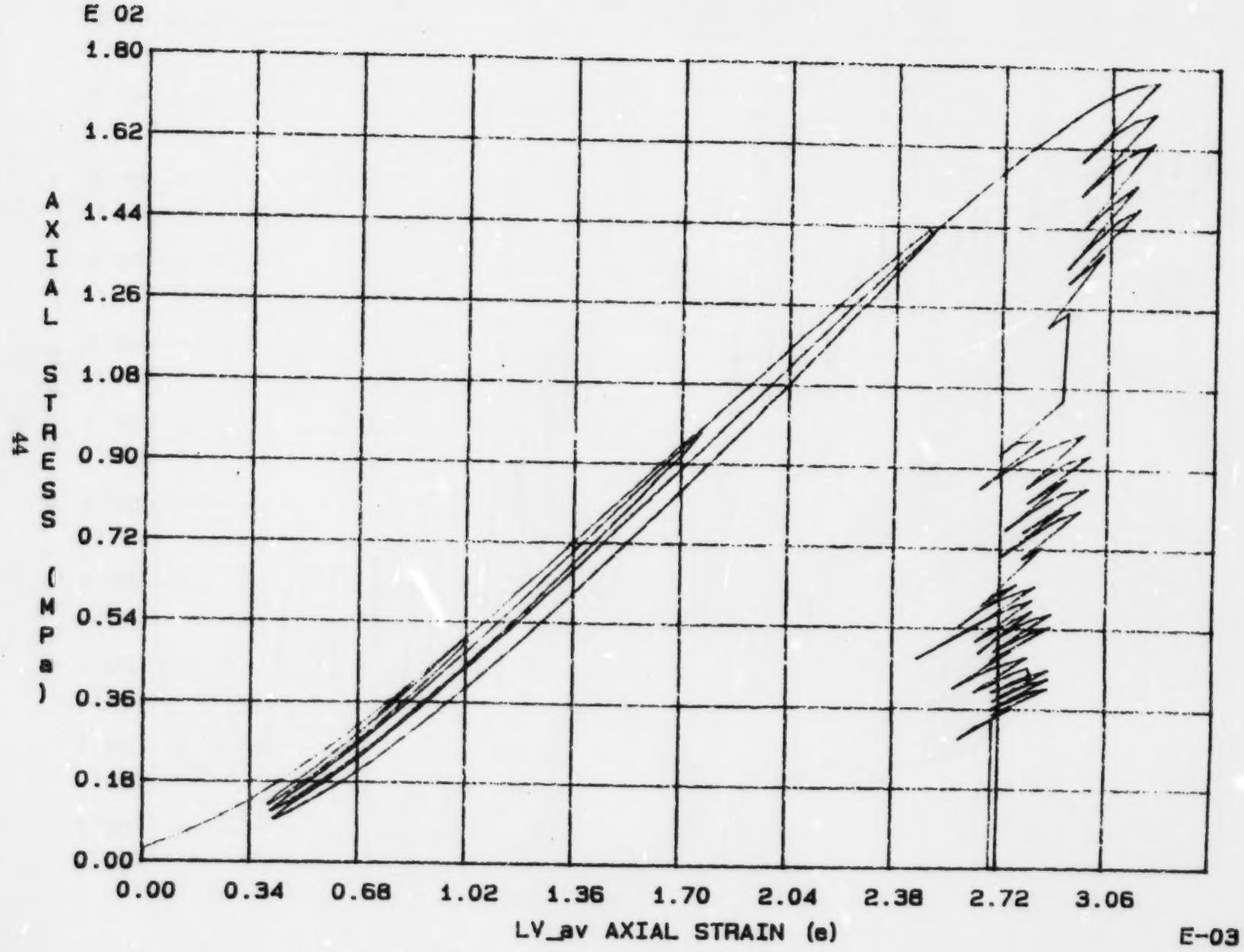

Figure A3. Loading and unloading curves (axial strain) for Specimen HG2-40.742.

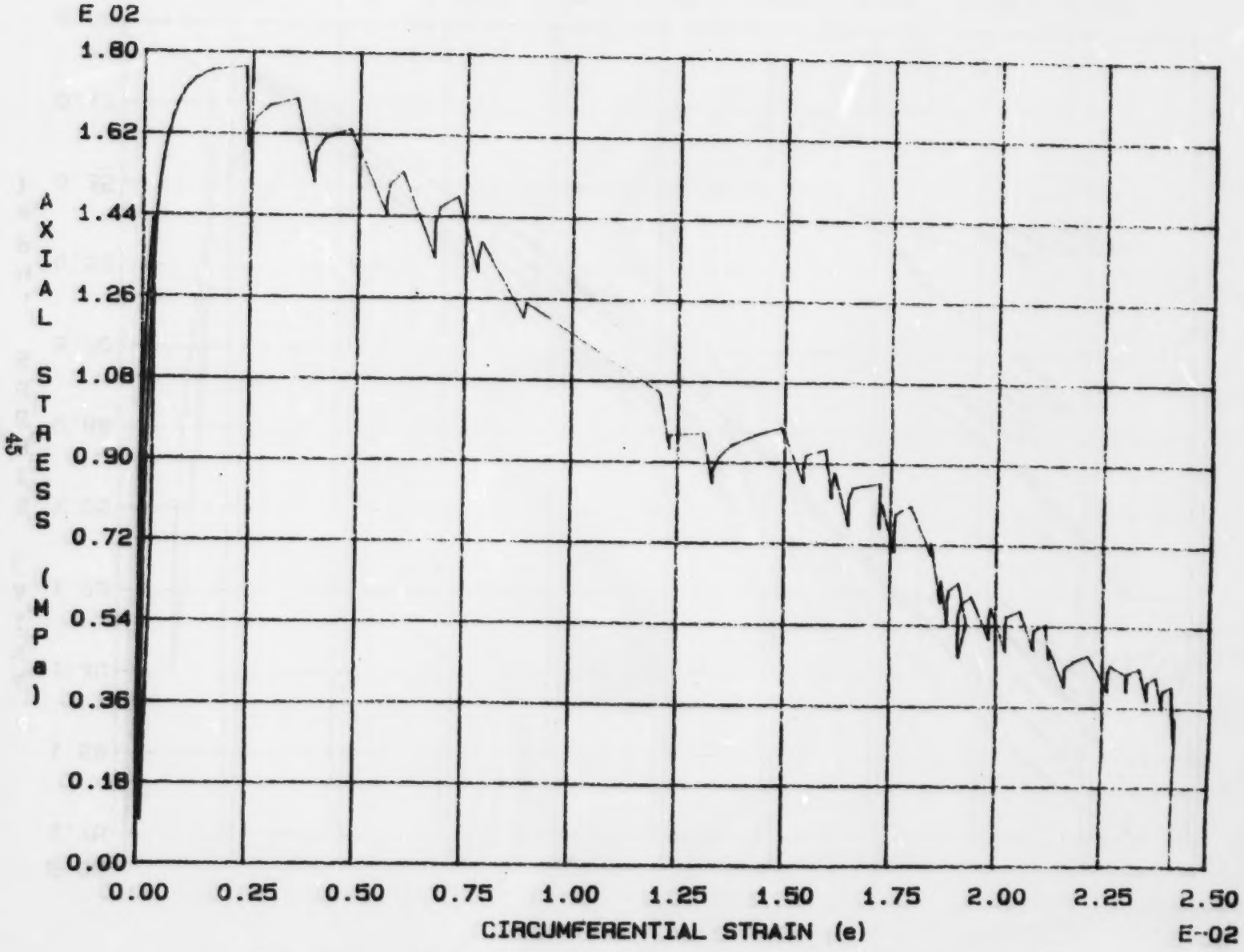

Figure A4. Loading and unloading curves (cir. strain) for Specimen HG2-40.742.

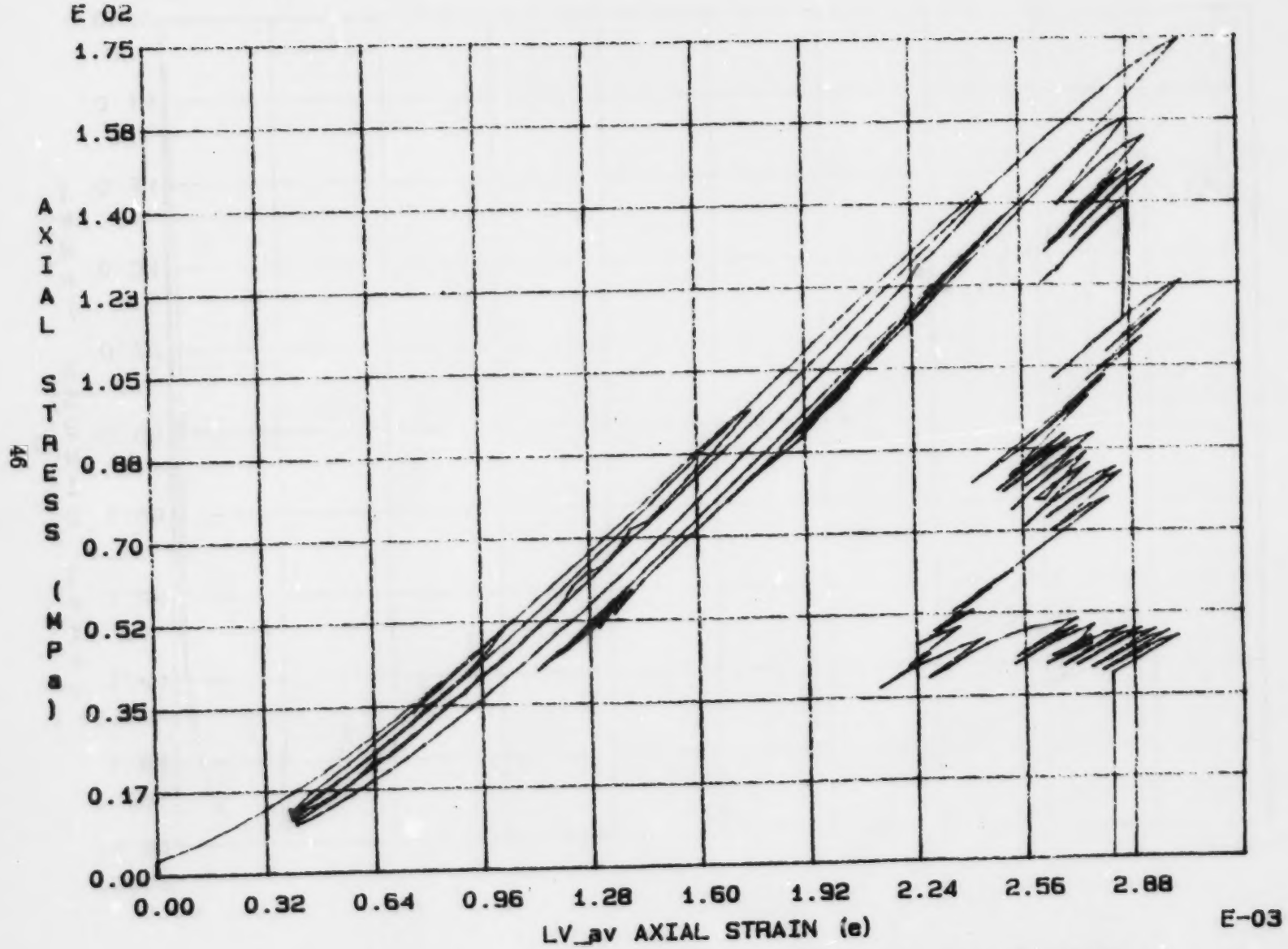

Figure A5. Loading and unloading curves (axial strain) for Specimen HG2-43.520.

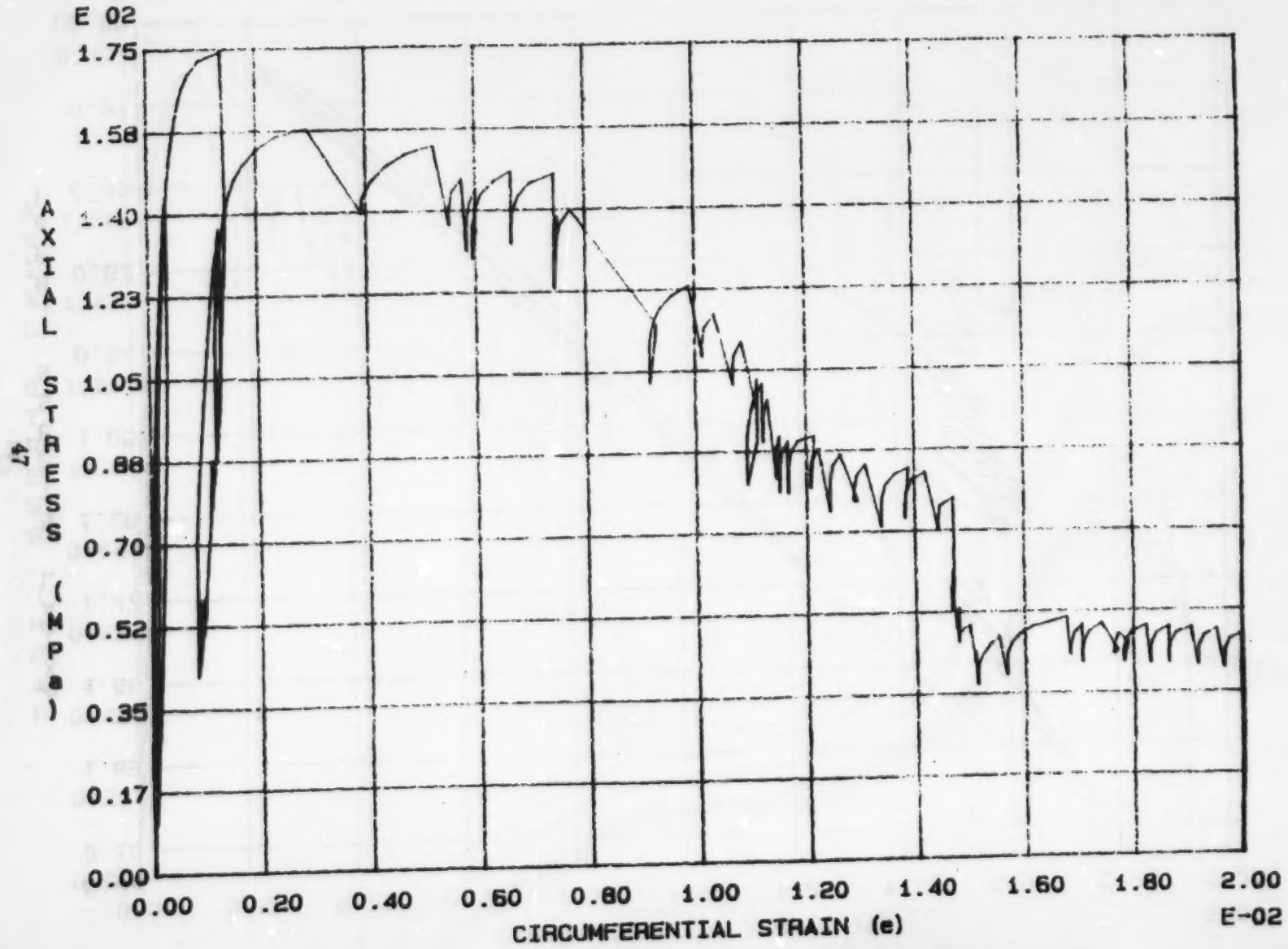

Figure A6. Loading and unloading curves (cir. strain) for Specimen HG2-43.520.

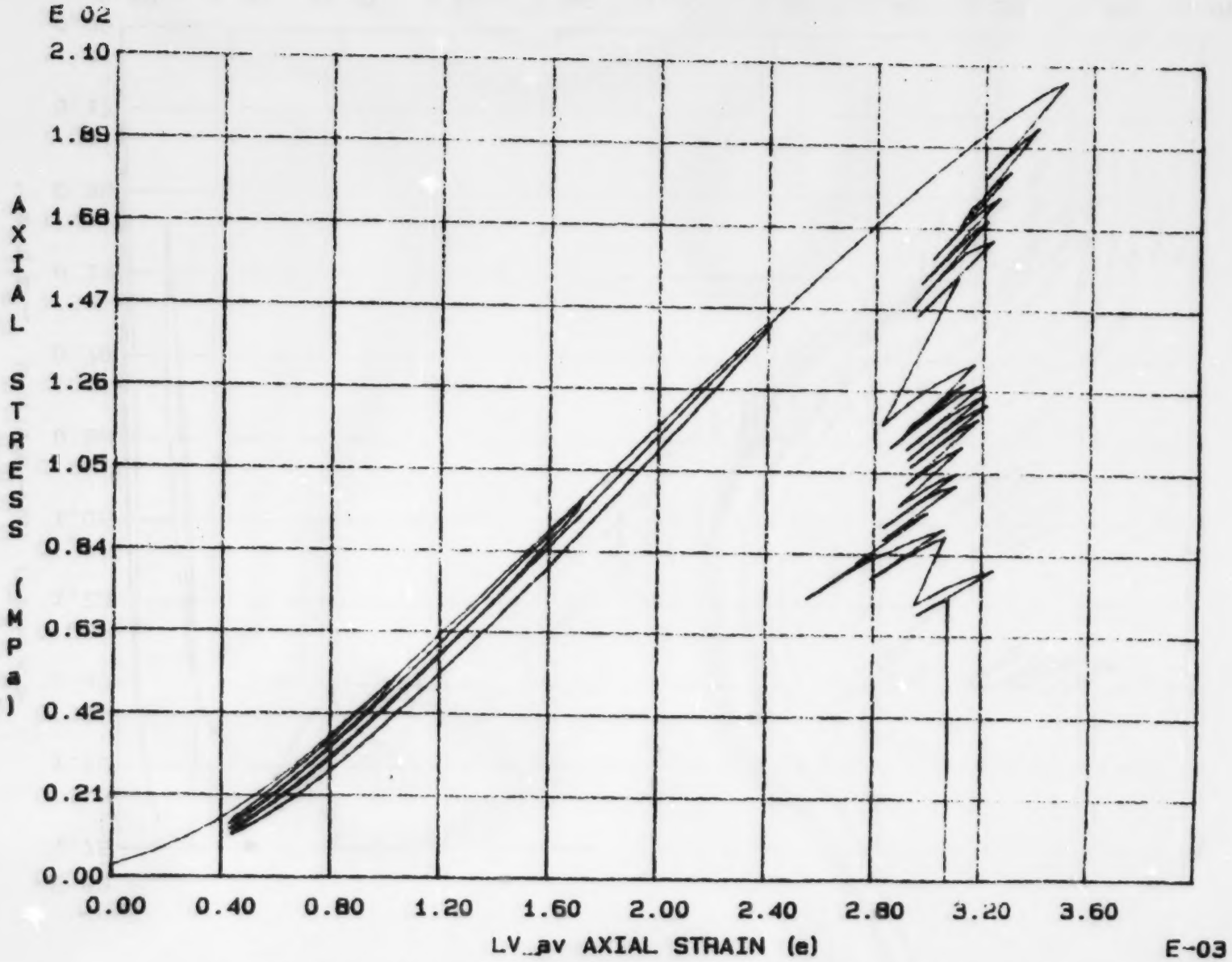

Figure A7. Loading and unloading curves (axial strain) for Specimen HG2-43.650.

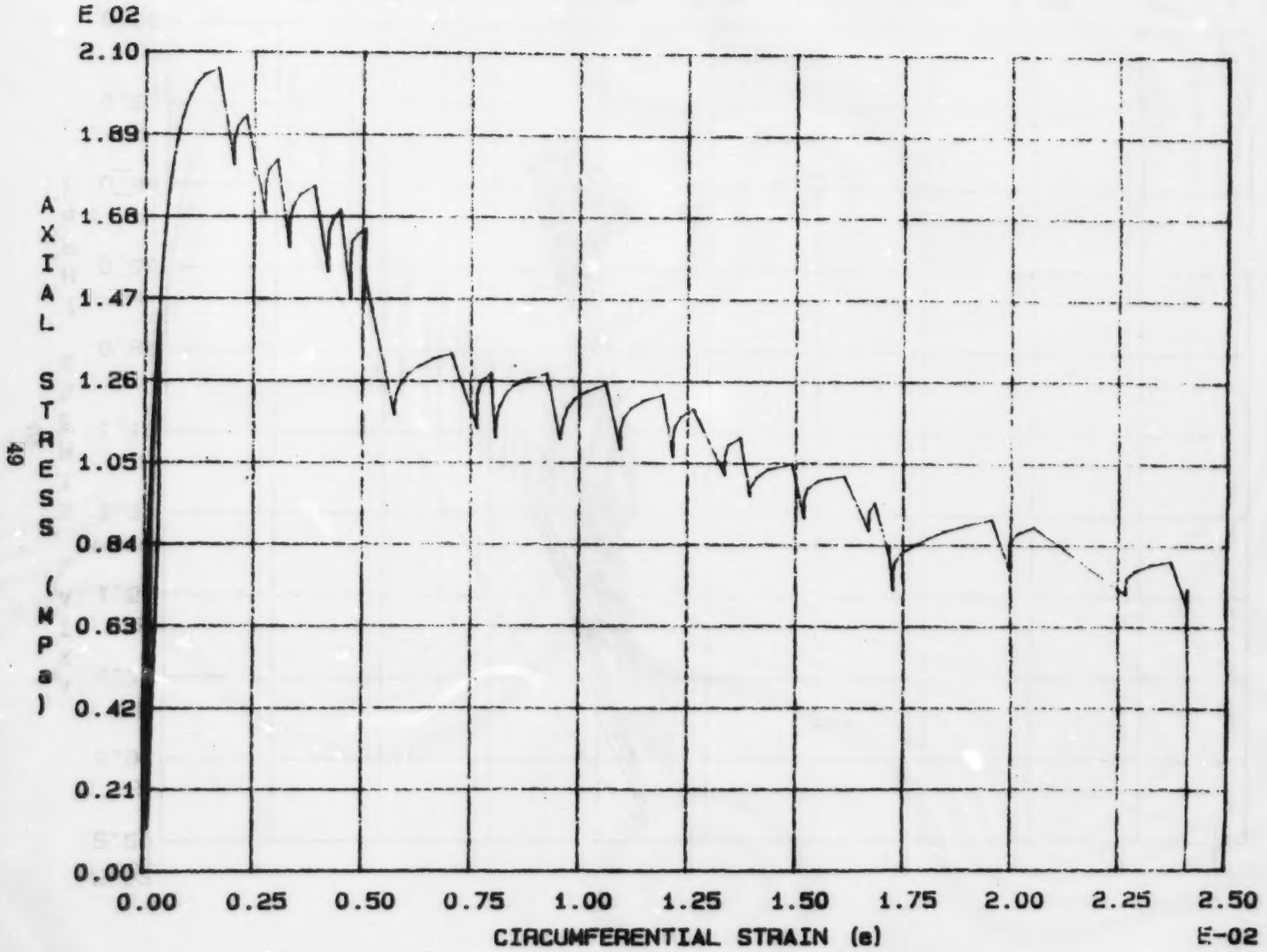

Figure A8. Loading and unloading curves (cir. strain) for Specimen HG2-43.650.

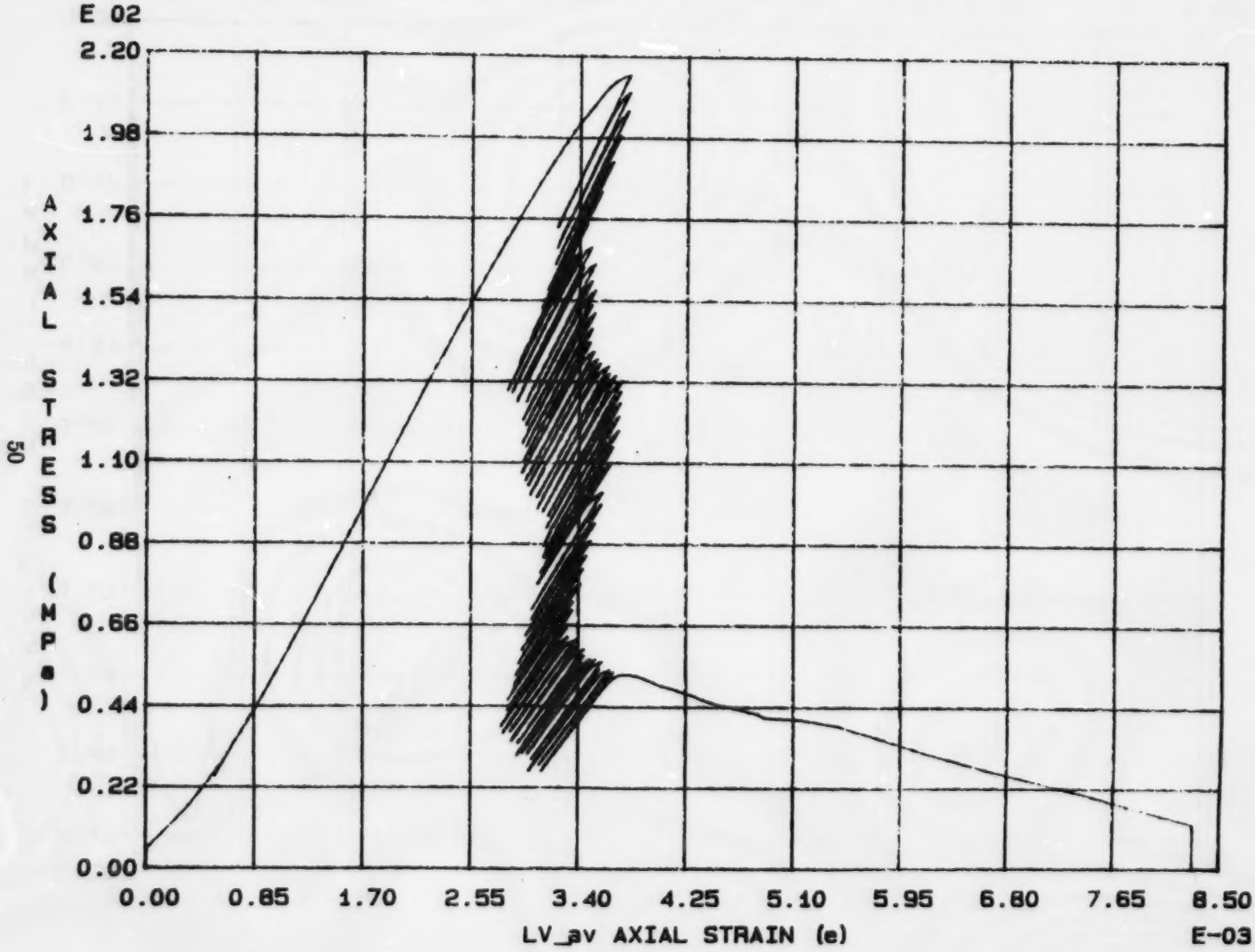

Figure A9. Loading and unloading curves (axial strain) for Specimen HG2-36.170.

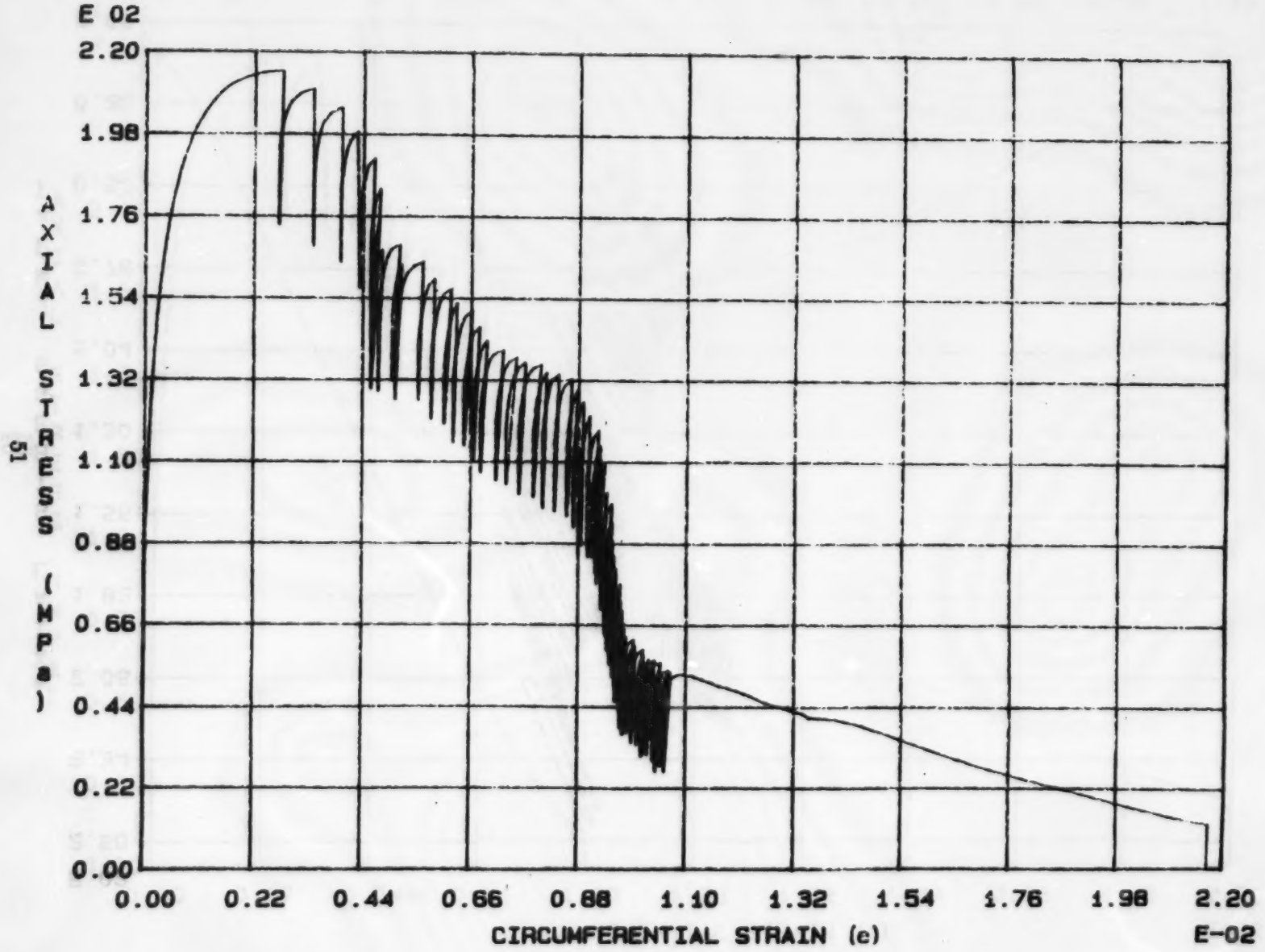

Figure A10. Loading and unloading curves (cir. strain) for Specimen HG2-36.170.

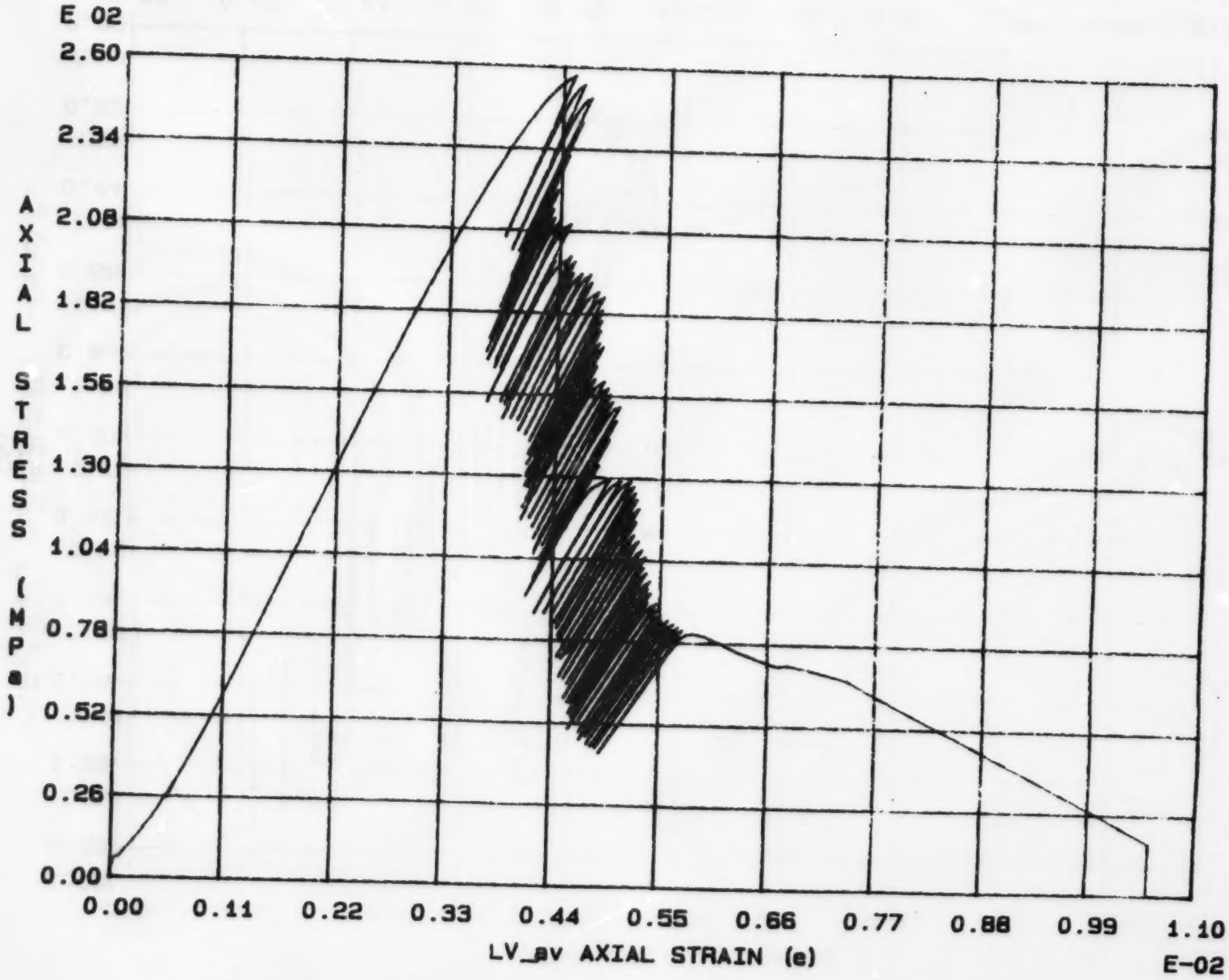

Figure A11. Loading and unloading curves (axial strain) for Specimen HG2-36.290.

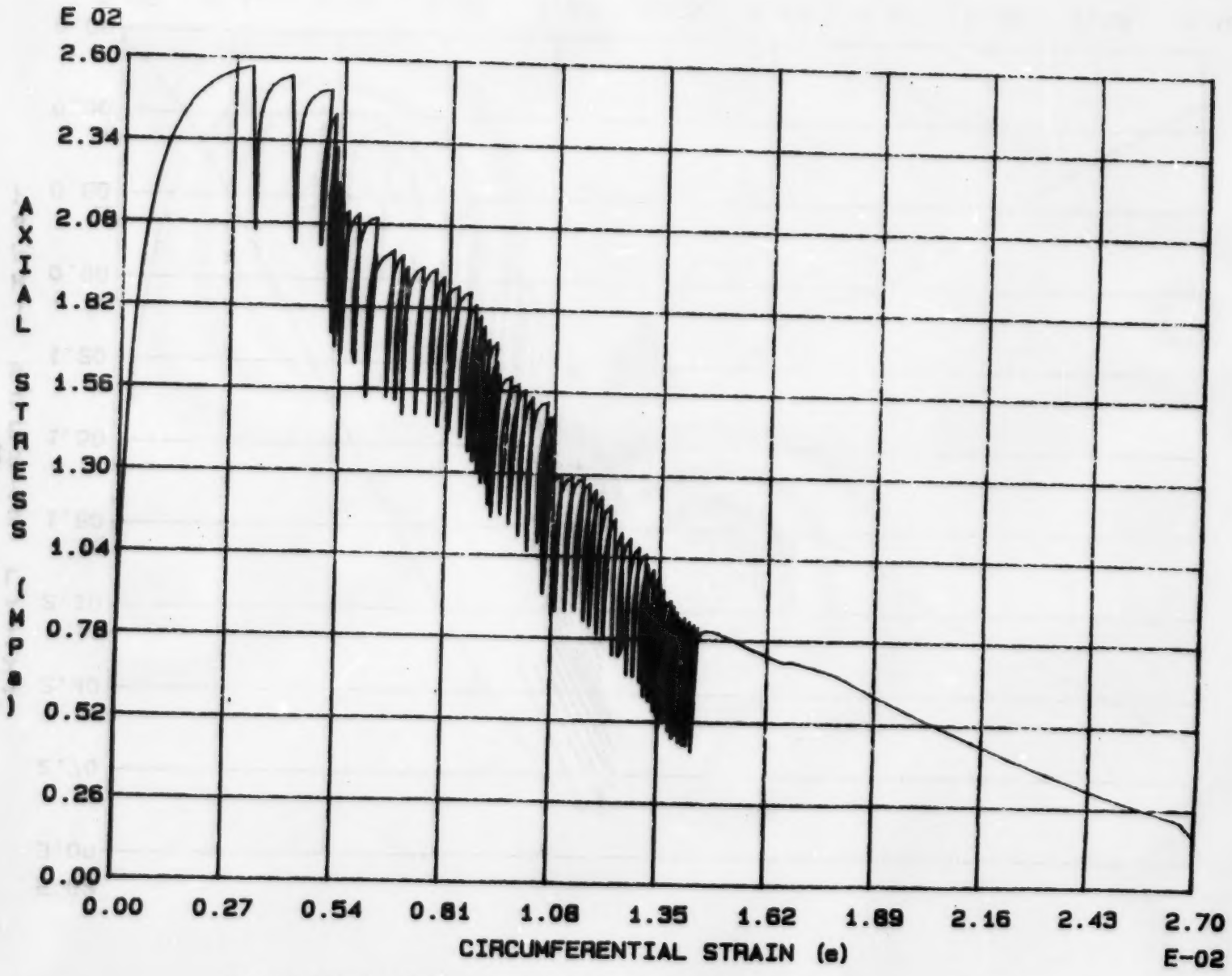

Figure A12. Loading and unloading curves (cir. strain) for Specimen HG2-36.290.

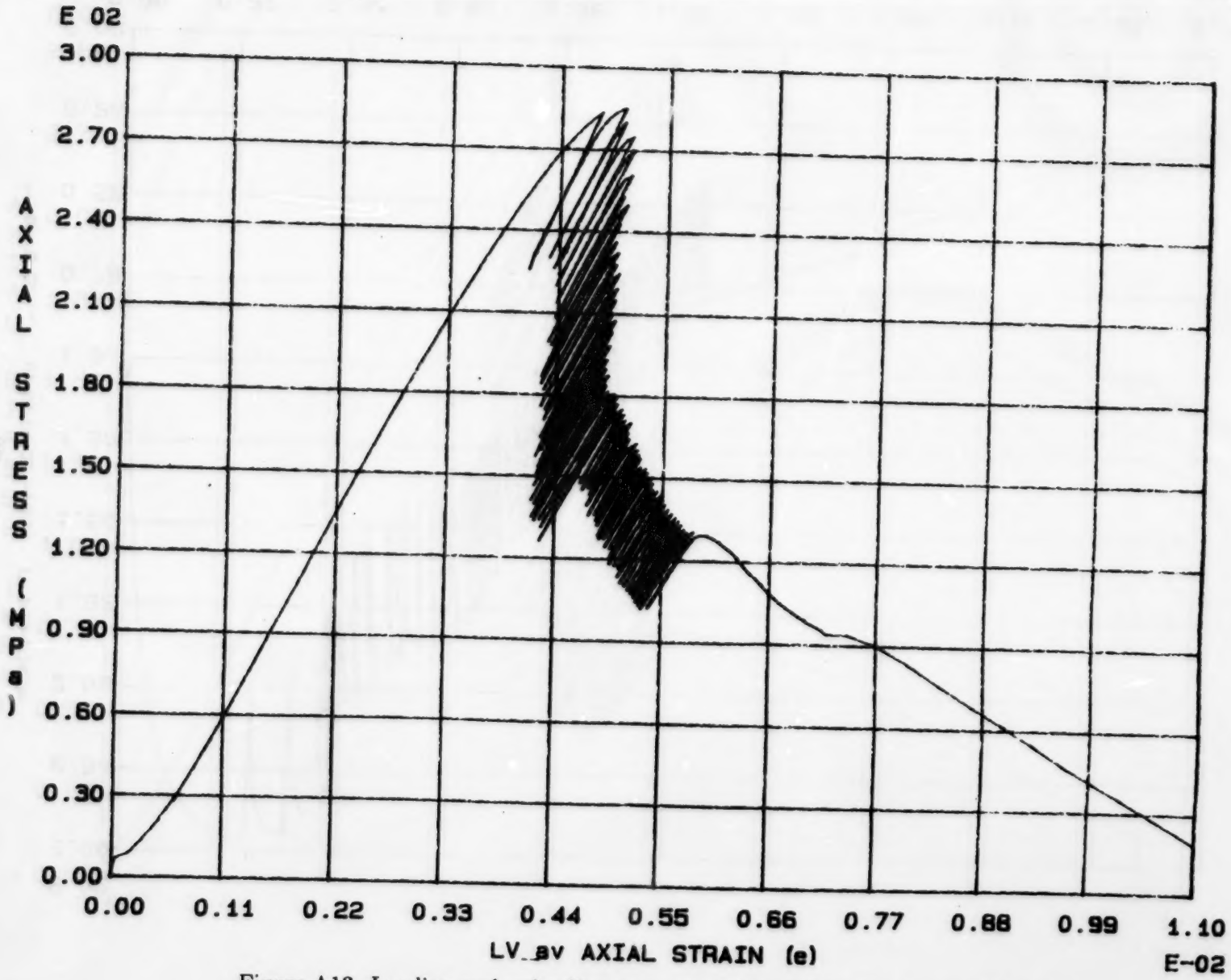

Figure A13. Loading and unloading curves (axial strain) for Specimen HG2-36.418.

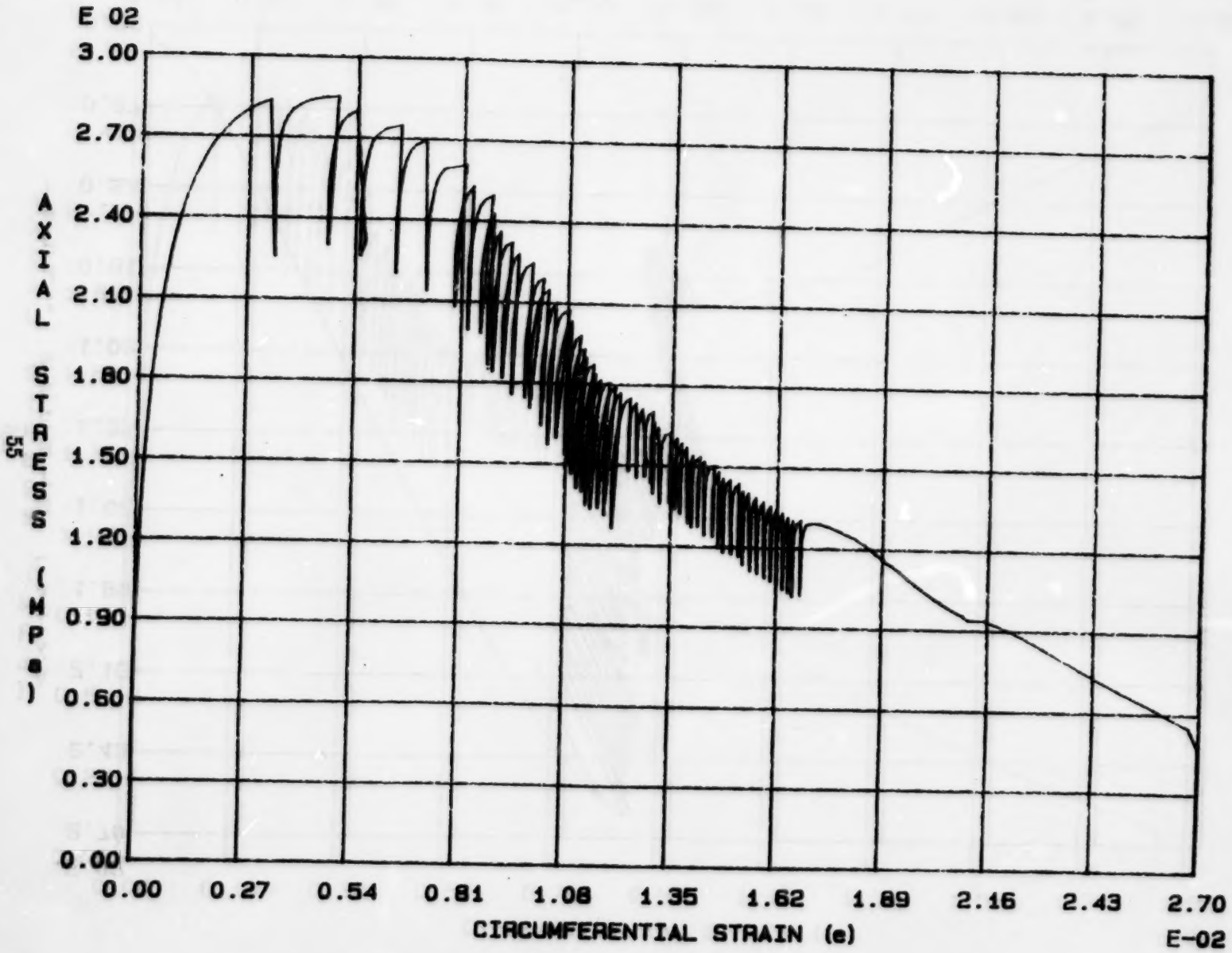

Figure A14. Loading and unloading curves (cir. strain) for Specimen HG2-36.418.

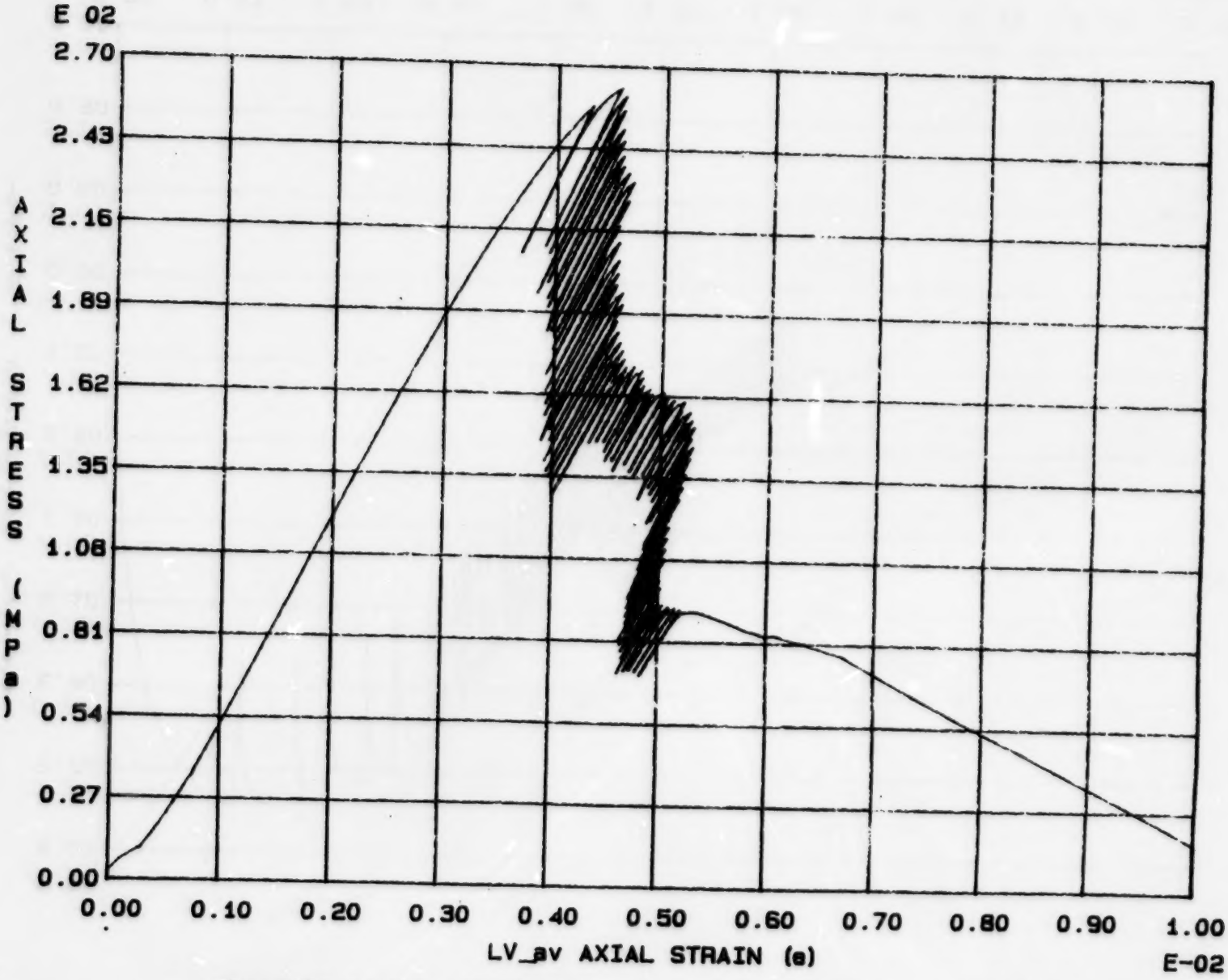

Figure A15. Loading and unloading curves (axial strain) for Specimen HG2-36.532.

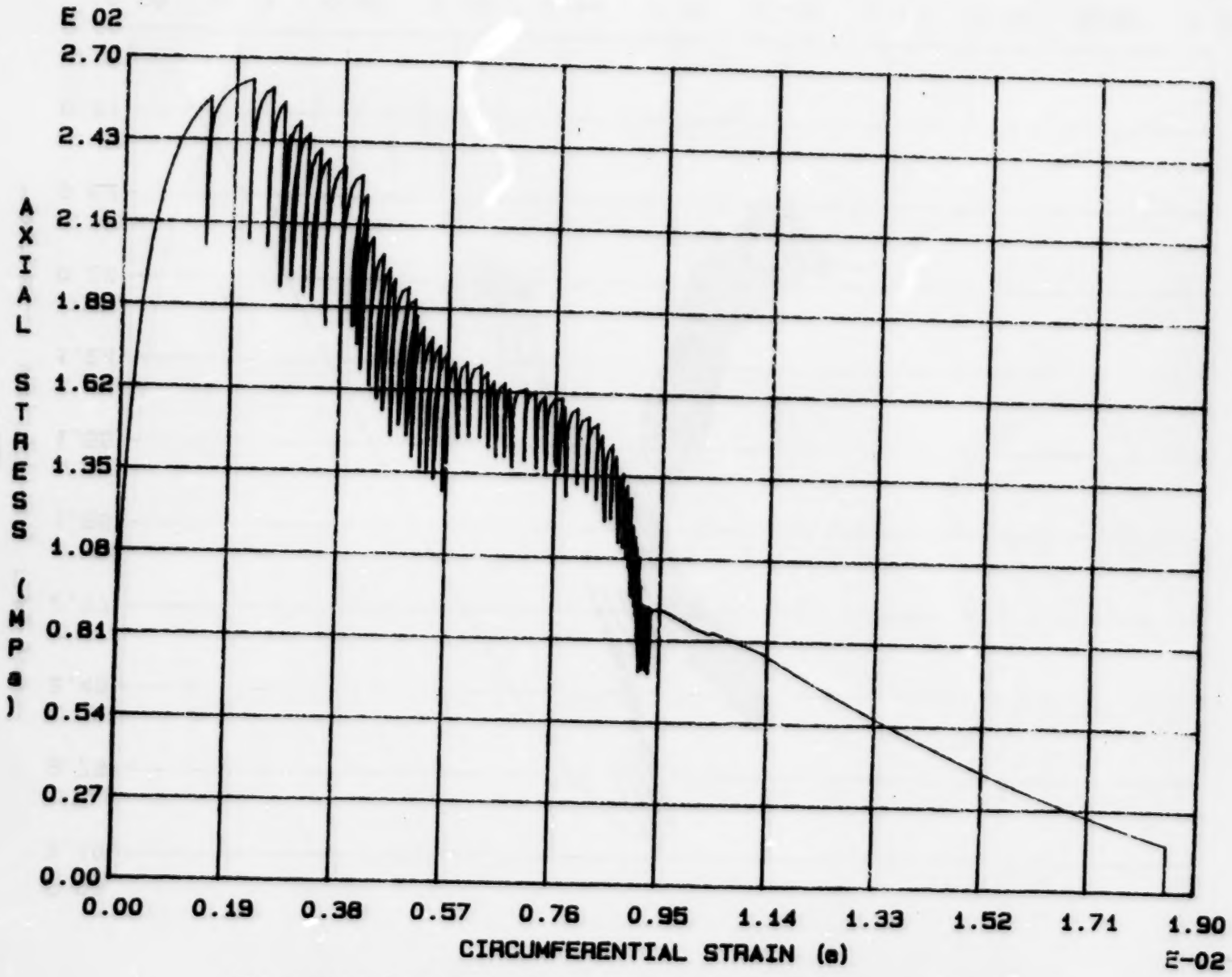

Figure A16. Loading and unloading curves (cir. strain) for Specimen HG2-36.532.

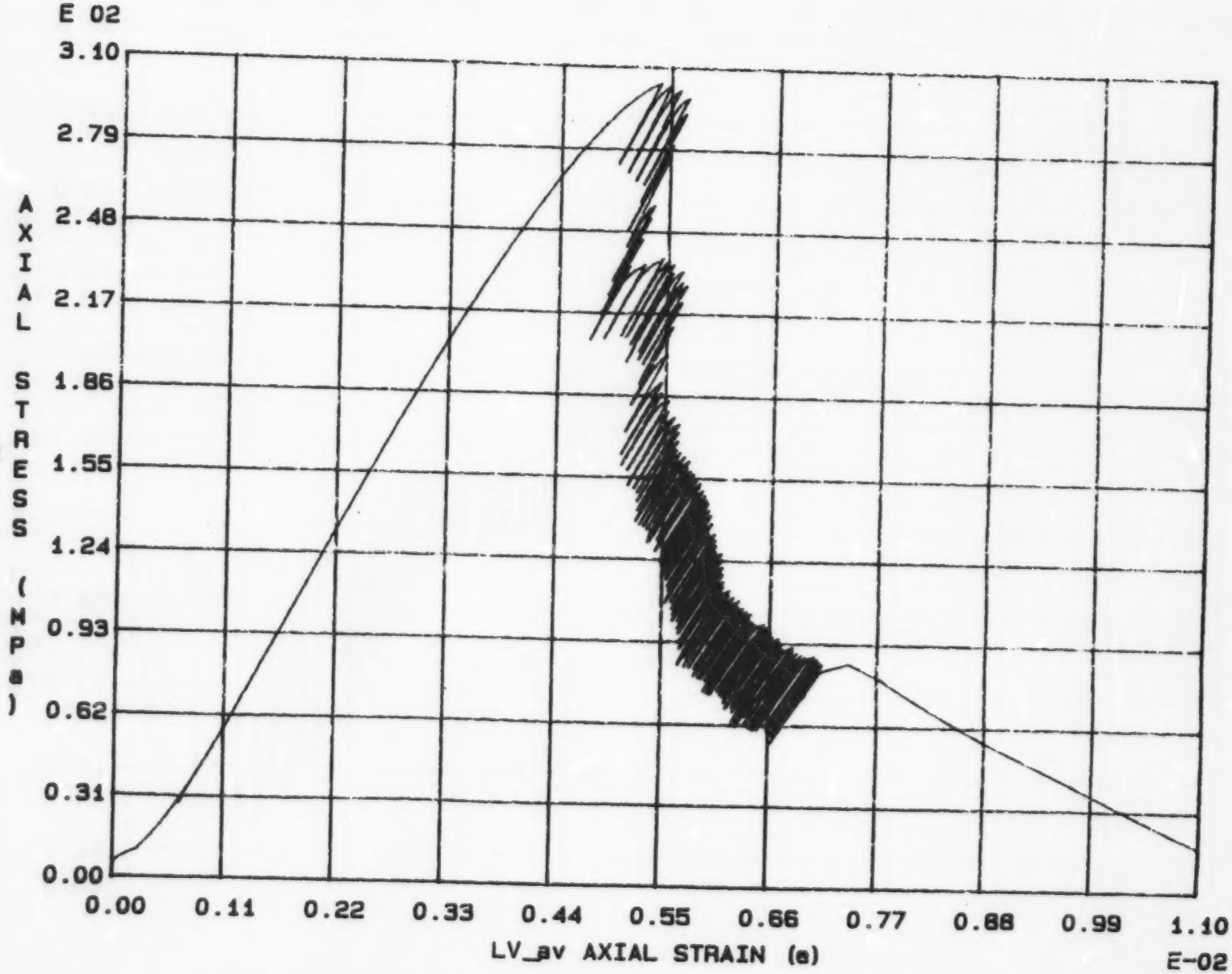

Figure A17. Loading and unloading curves (axial strain) for Specimen HG2-40.621.

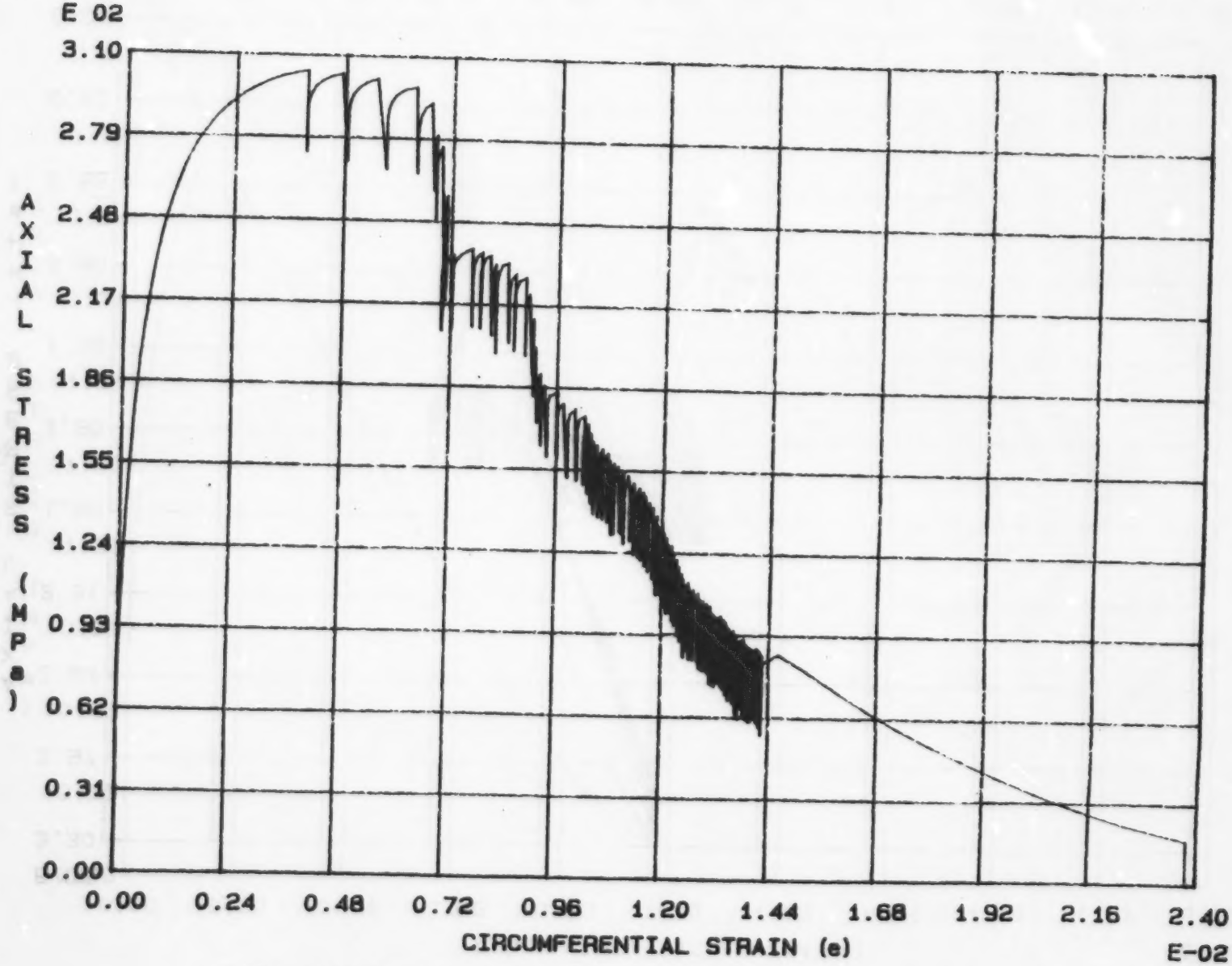

Figure A18. Loading and unloading curves (cir. strain) for Specimen HG2-40.621.

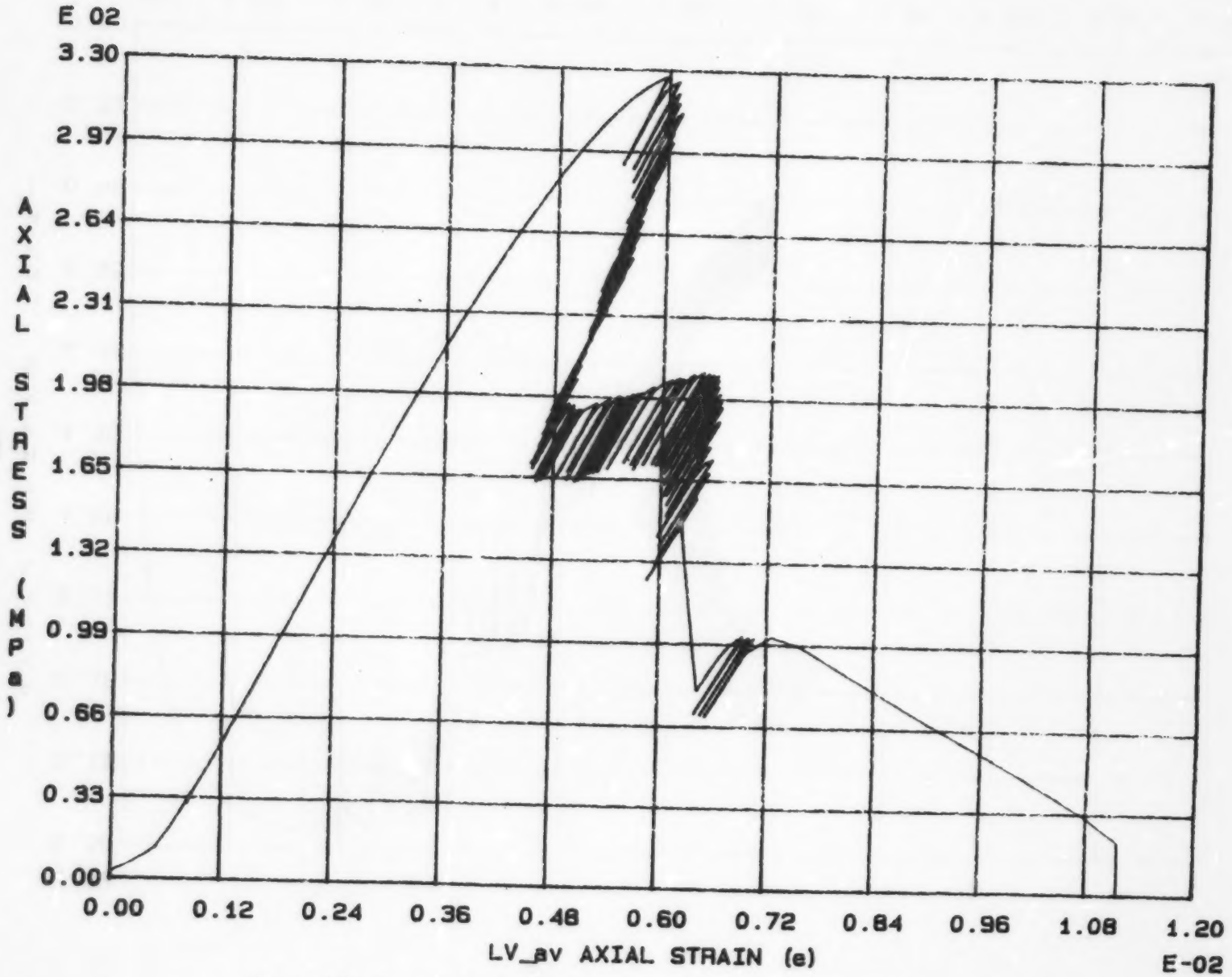

Figure A19. Loading and unloading curves (axial strain) for Specimen HG2-37.216.

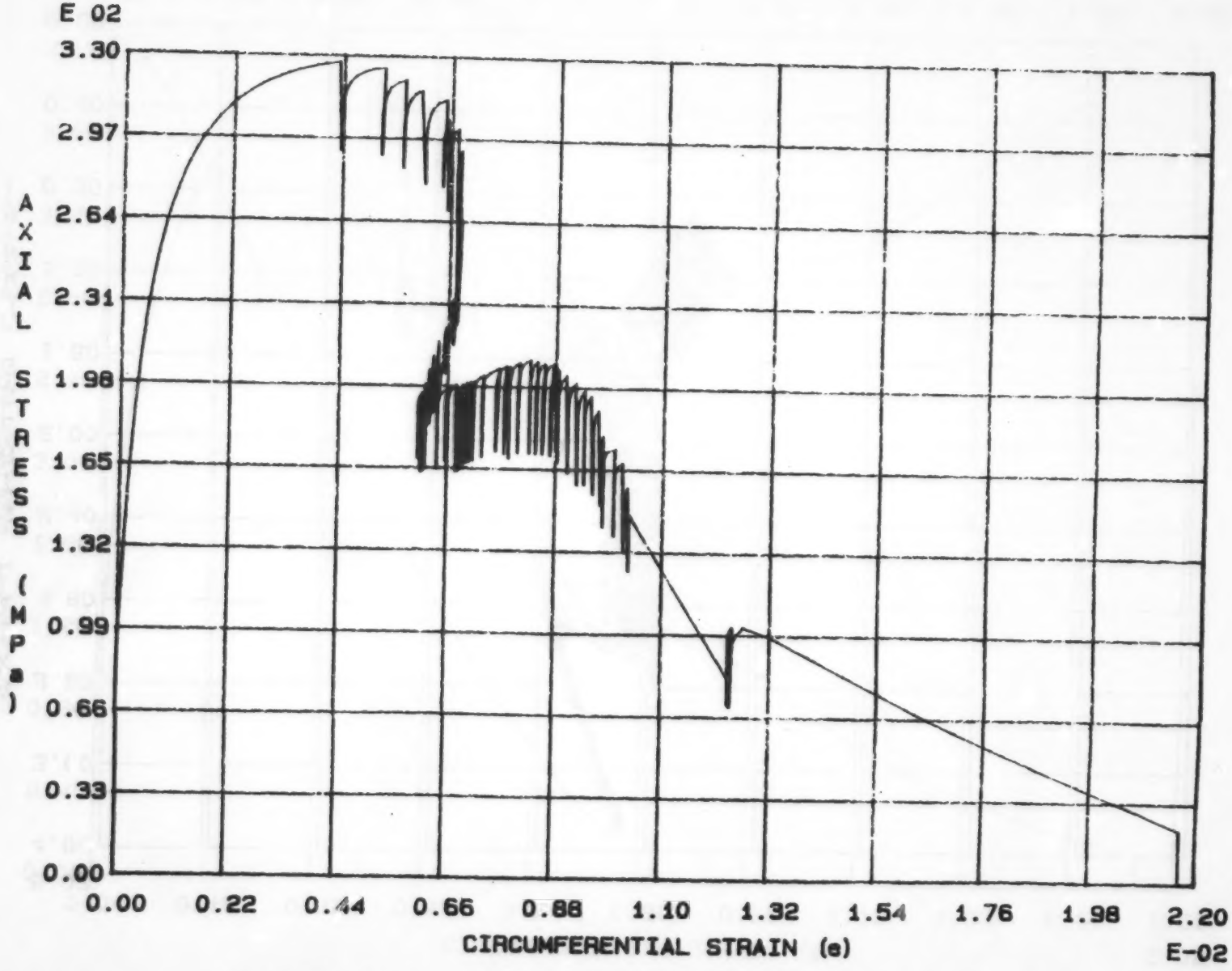

Figure A20. Loading and unloading curves (cir. strain) for Specimen HG2-37.216.

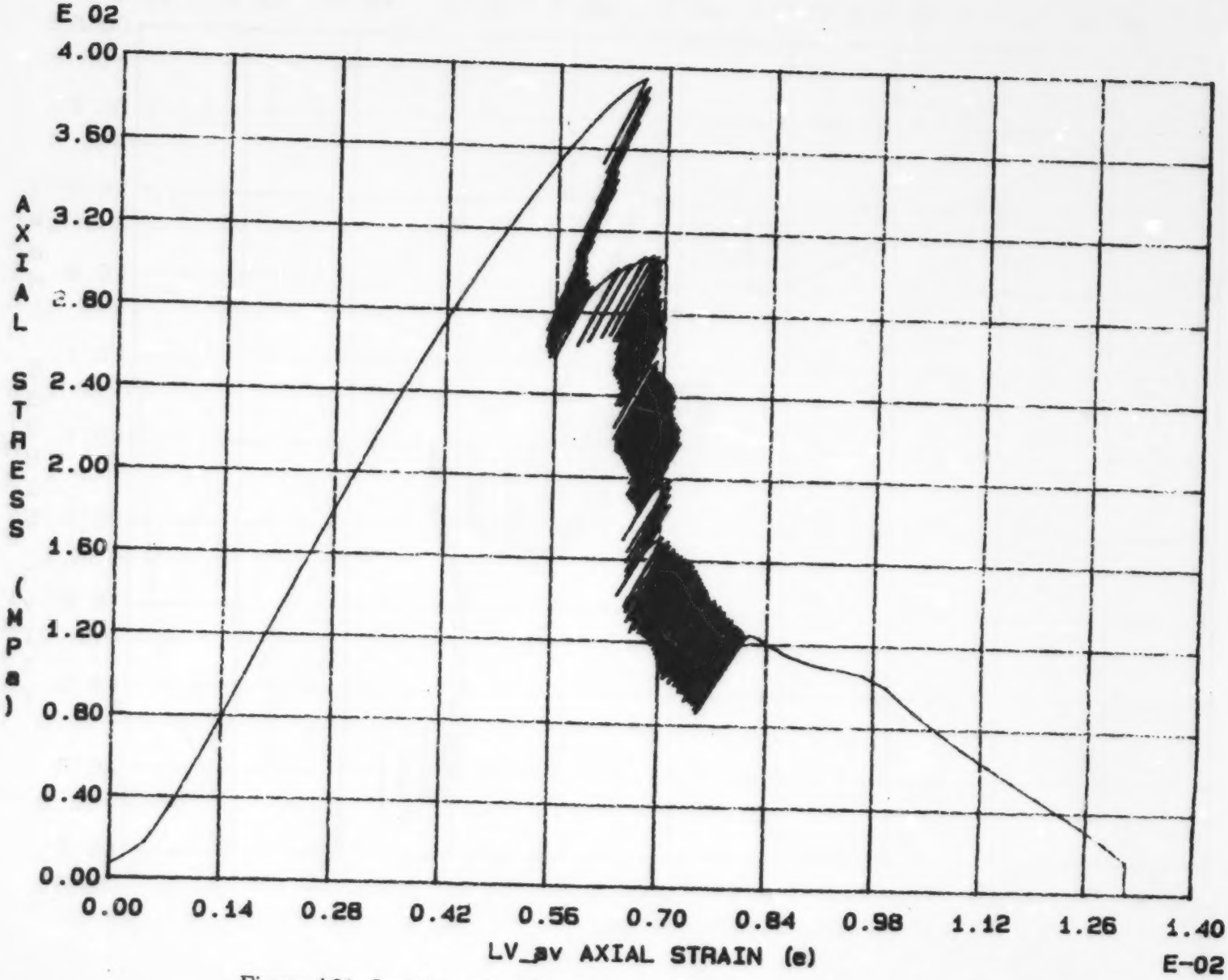

Figure A21. Loading and unloading curves (axial strain) for Specimen HG2-37.335.

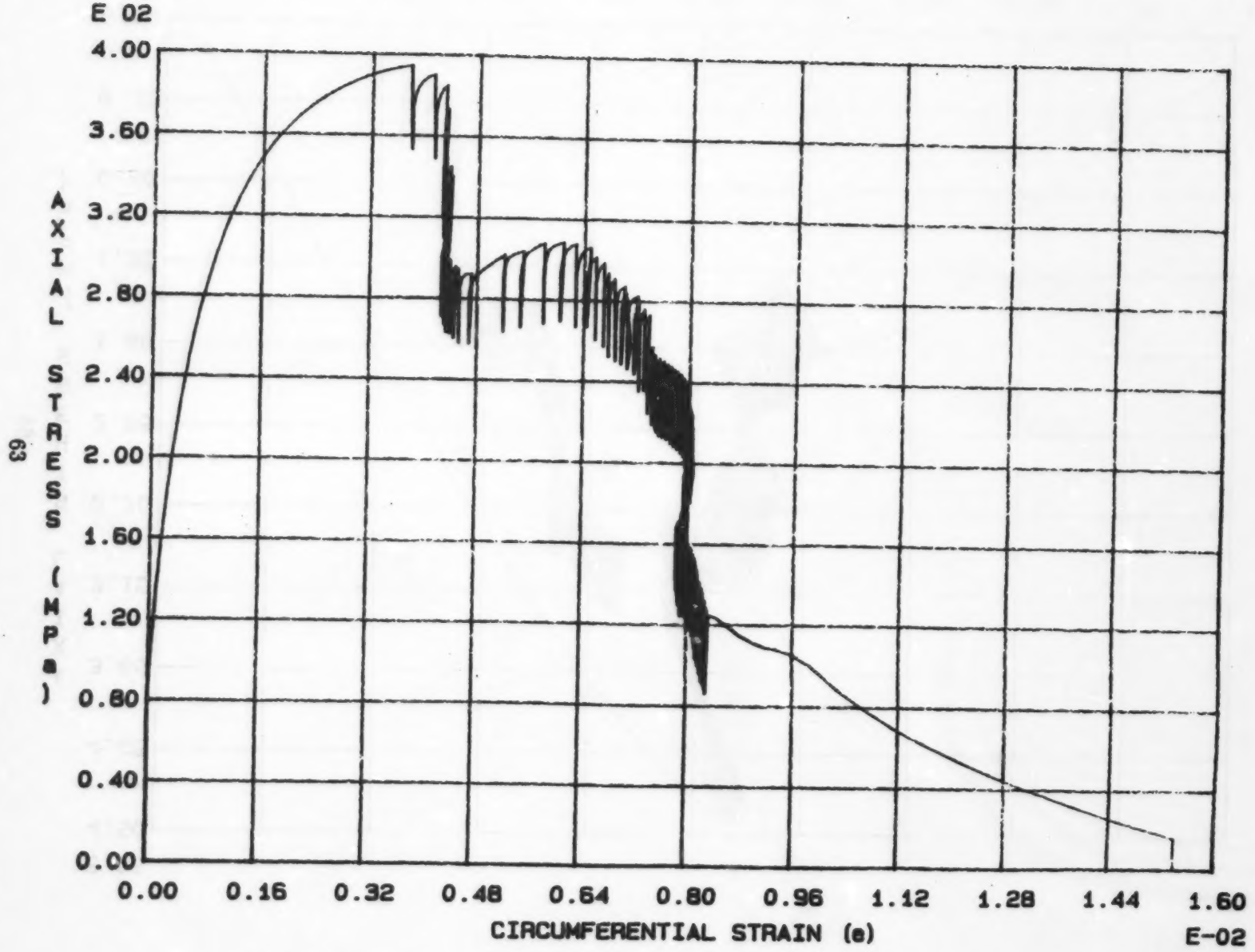

Figure A22. Loading and unloading curves (cir. strain) for Specimen HG2-37.335.

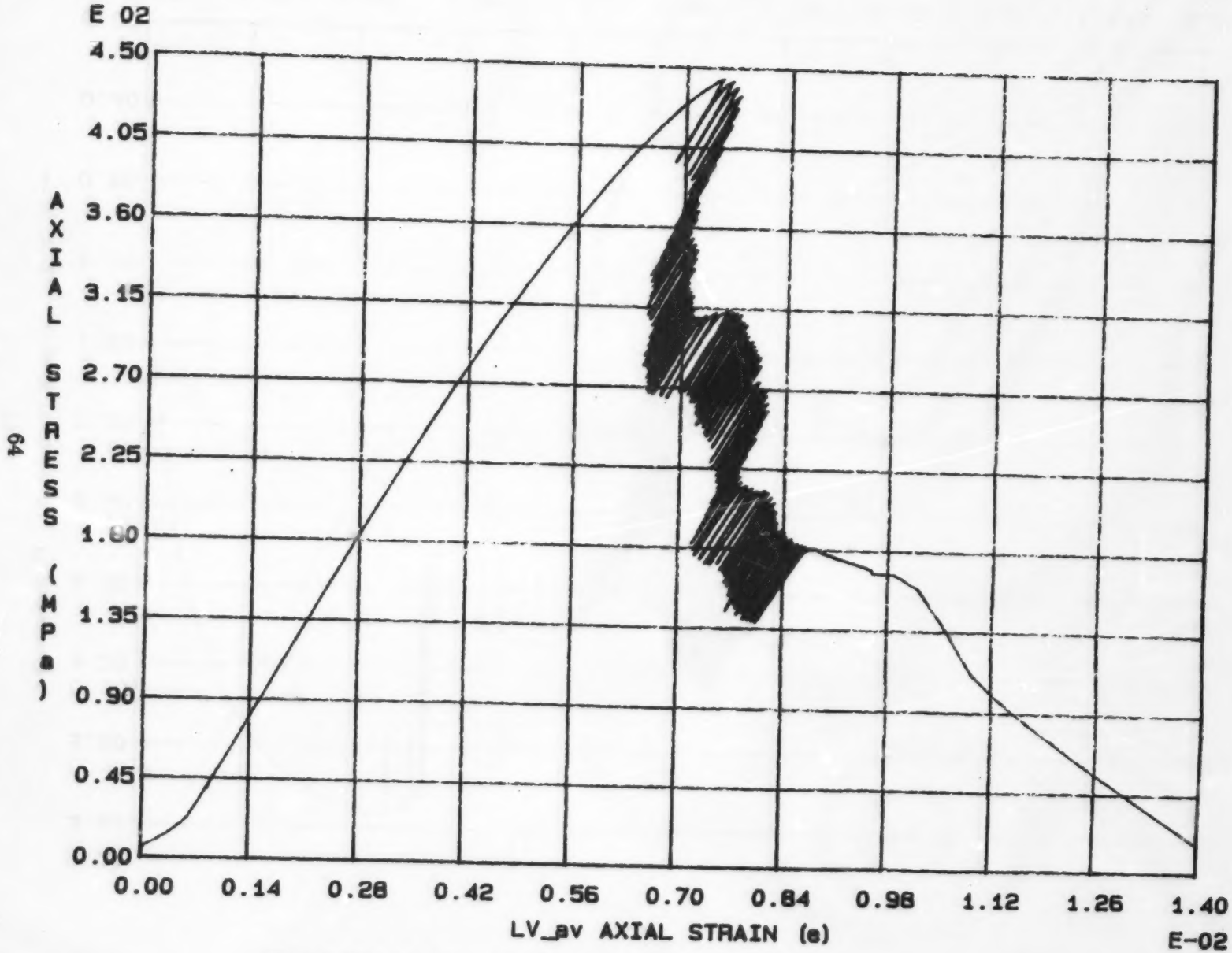

Figure A23. Loading and unloading curves (axial strain) for Specimen HG2-37.492.

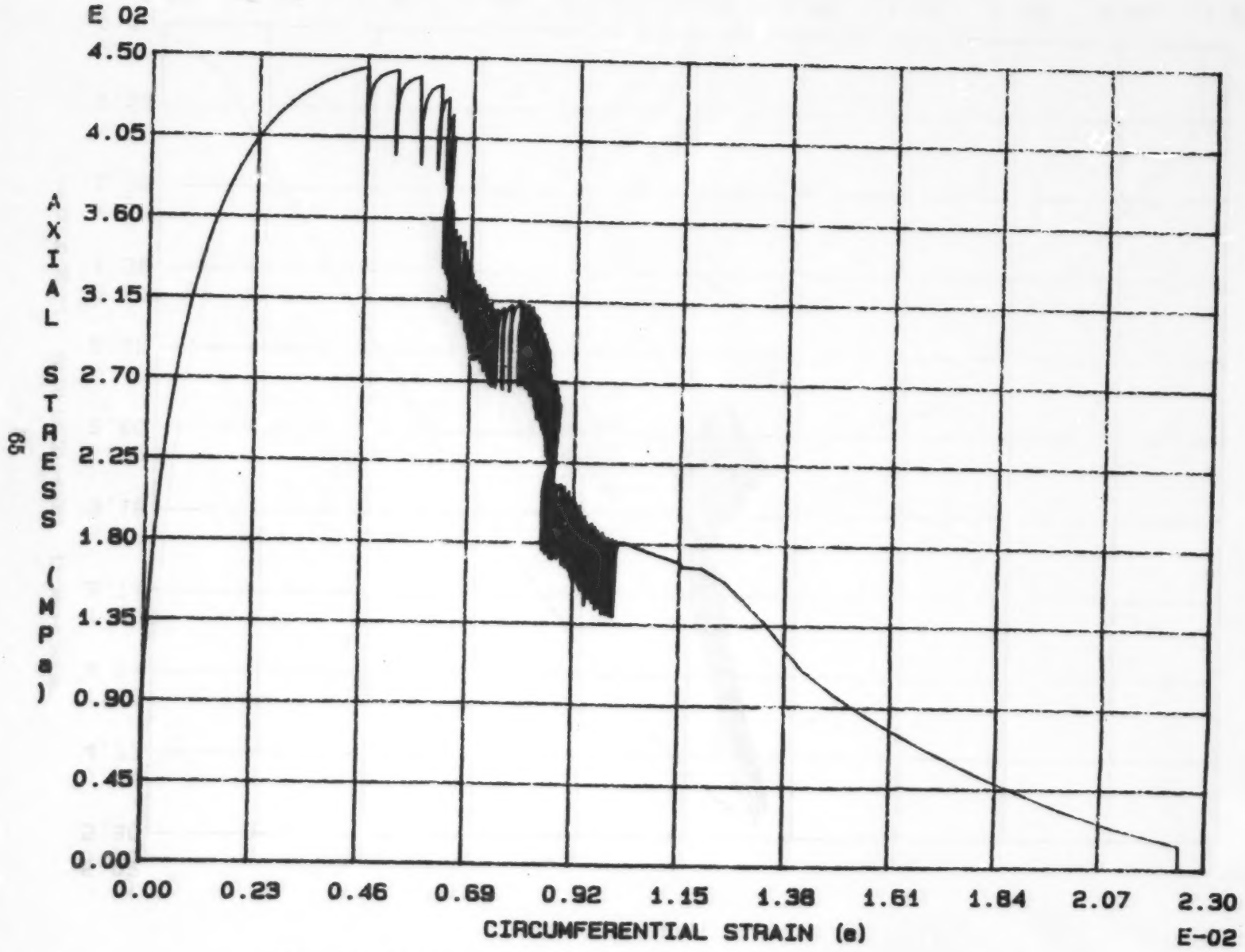

Figure A24. Loading and unloading curves (cir. strain) for Specimen HG2-37.492.

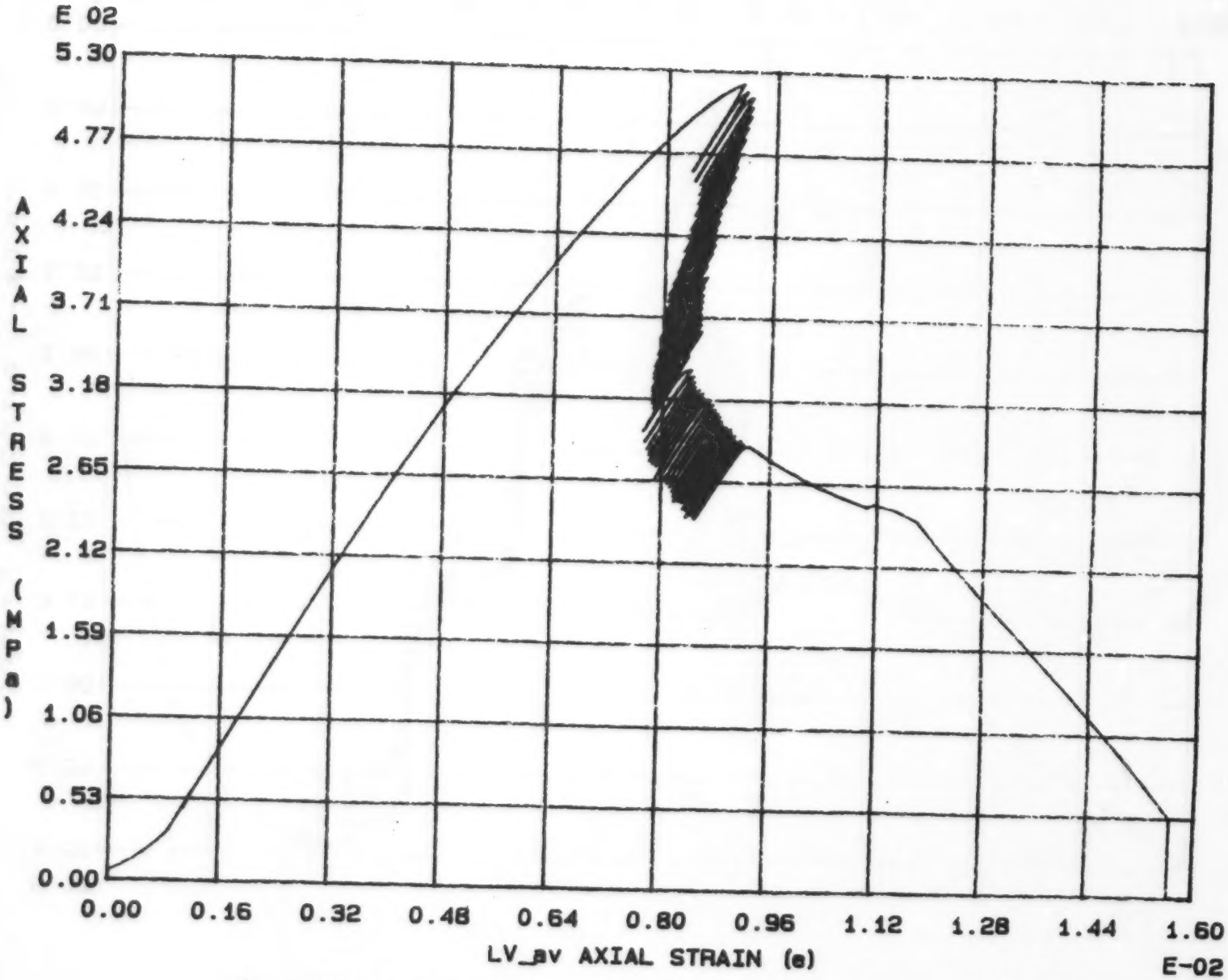

Figure A25. Loading and unloading curves (axial strain) for Specimen HG2-37.613.

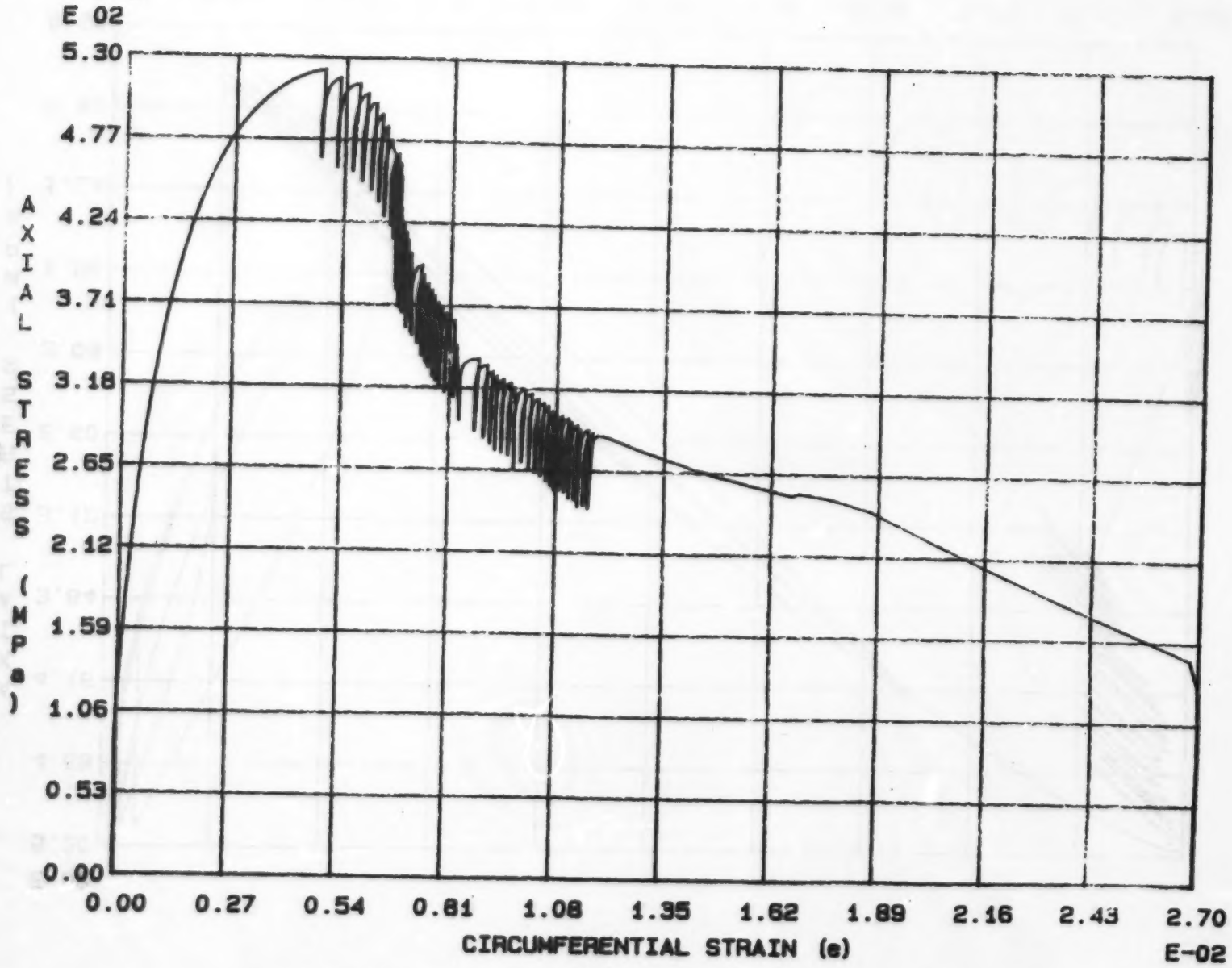

Figure A26. Loading and unloading curves (cir. strain) for Specimen HG2-37.613.

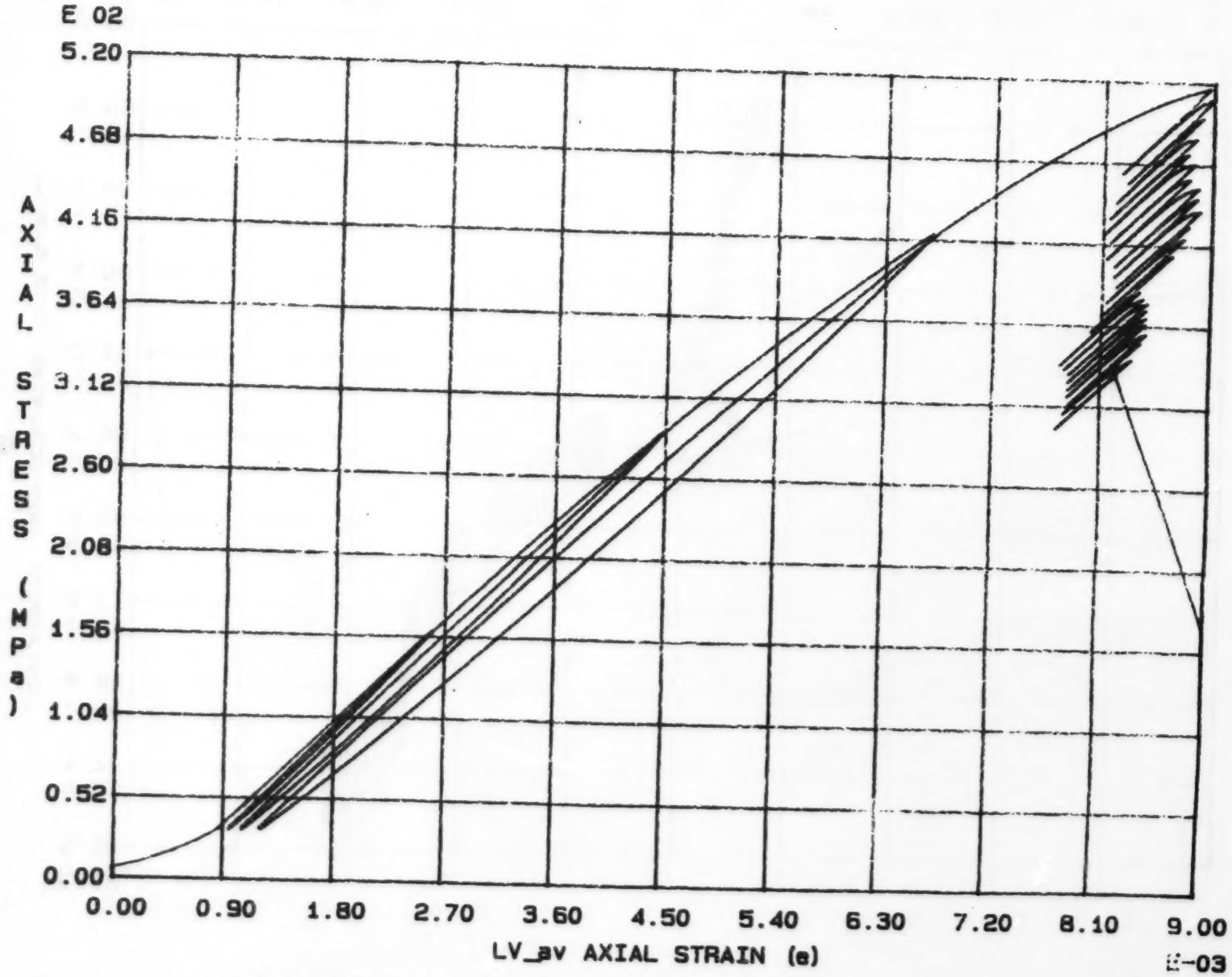

Figure A27. Loading and unloading curves (axial strain) for Specimen HG2-40.862.

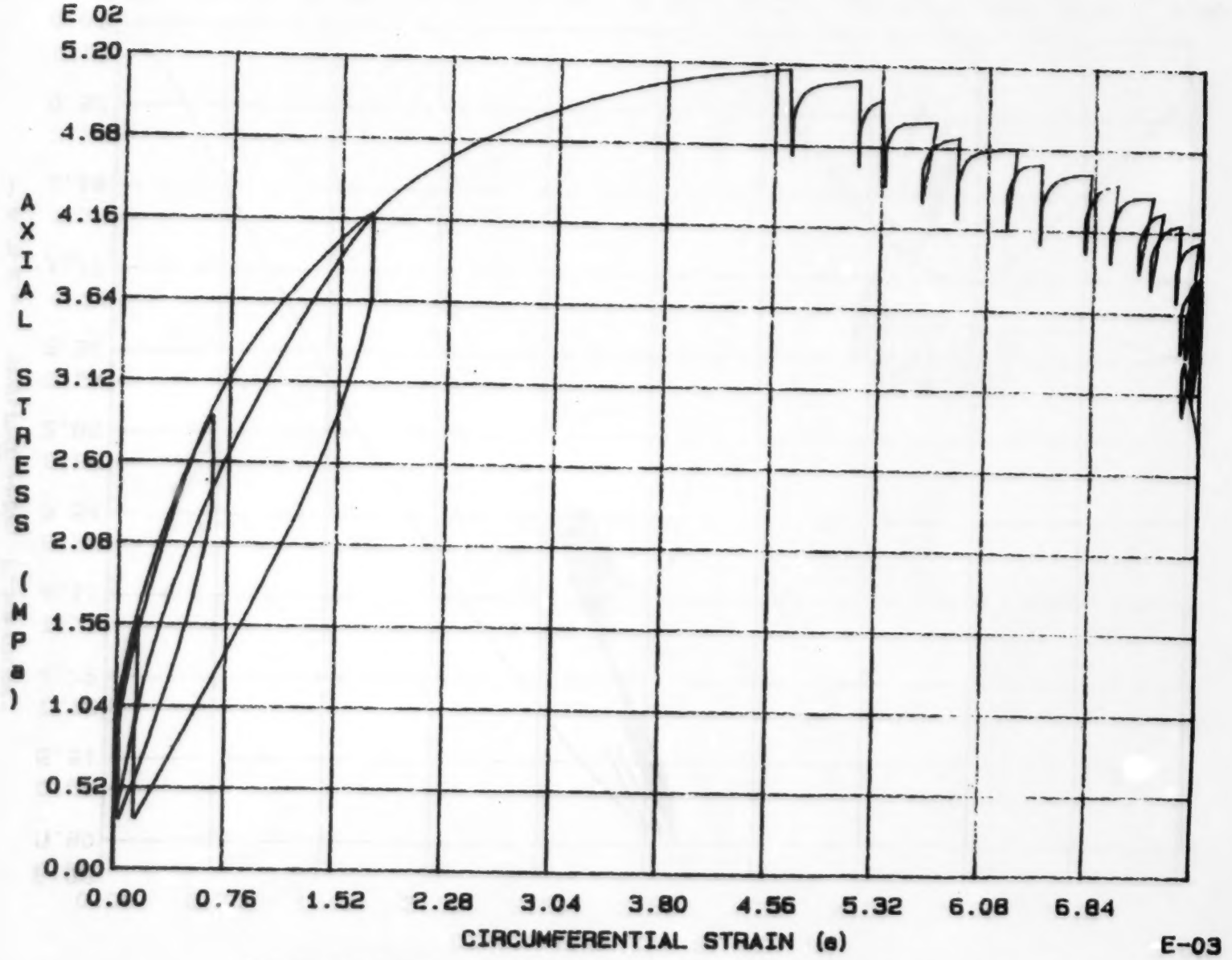

Figure A28. Loading and unloading curves (cir. strain) for Specimen HG2-40.862.

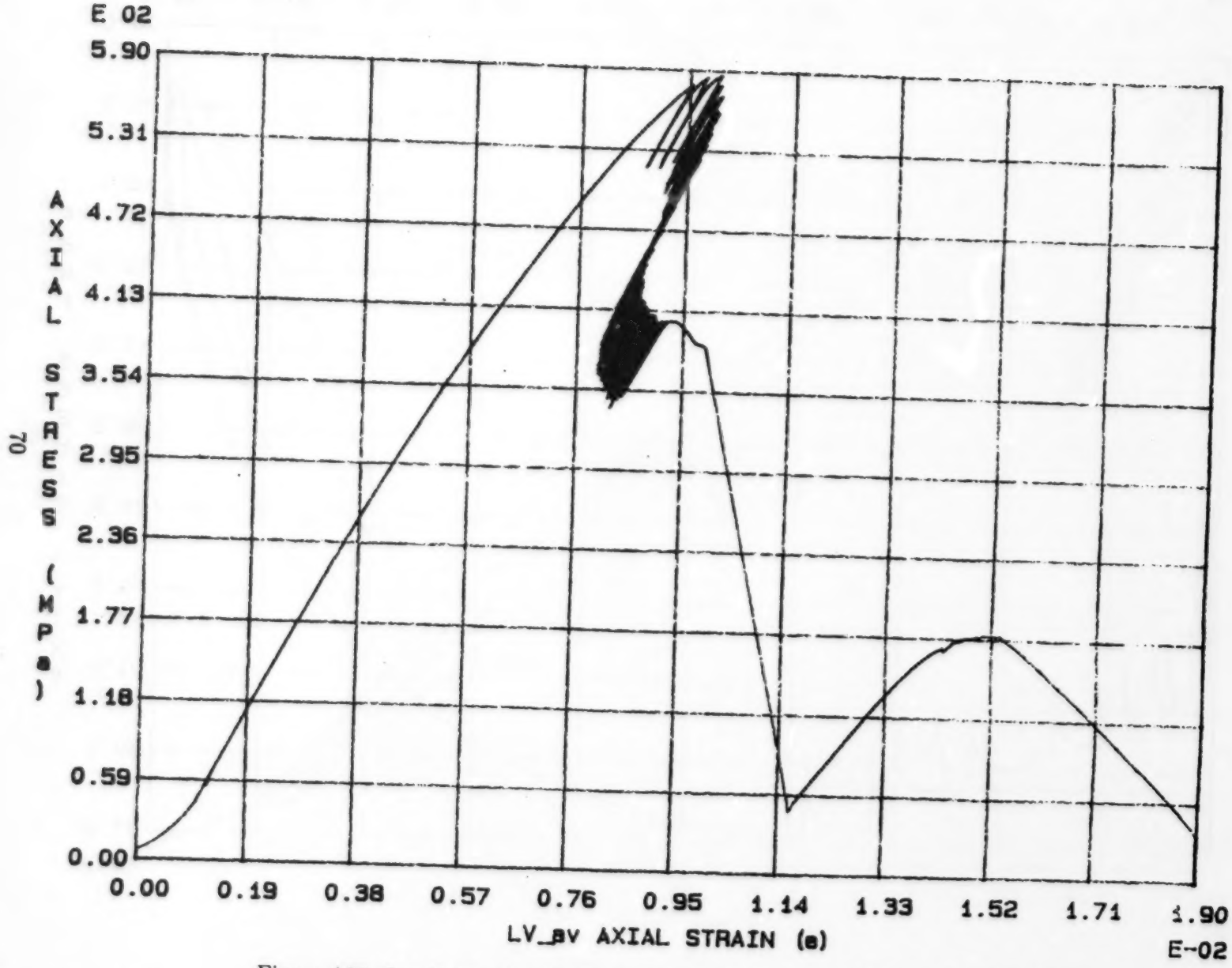

Figure A29. Loading and unloading curves (axial strain) for Specimen HG2-40.381.

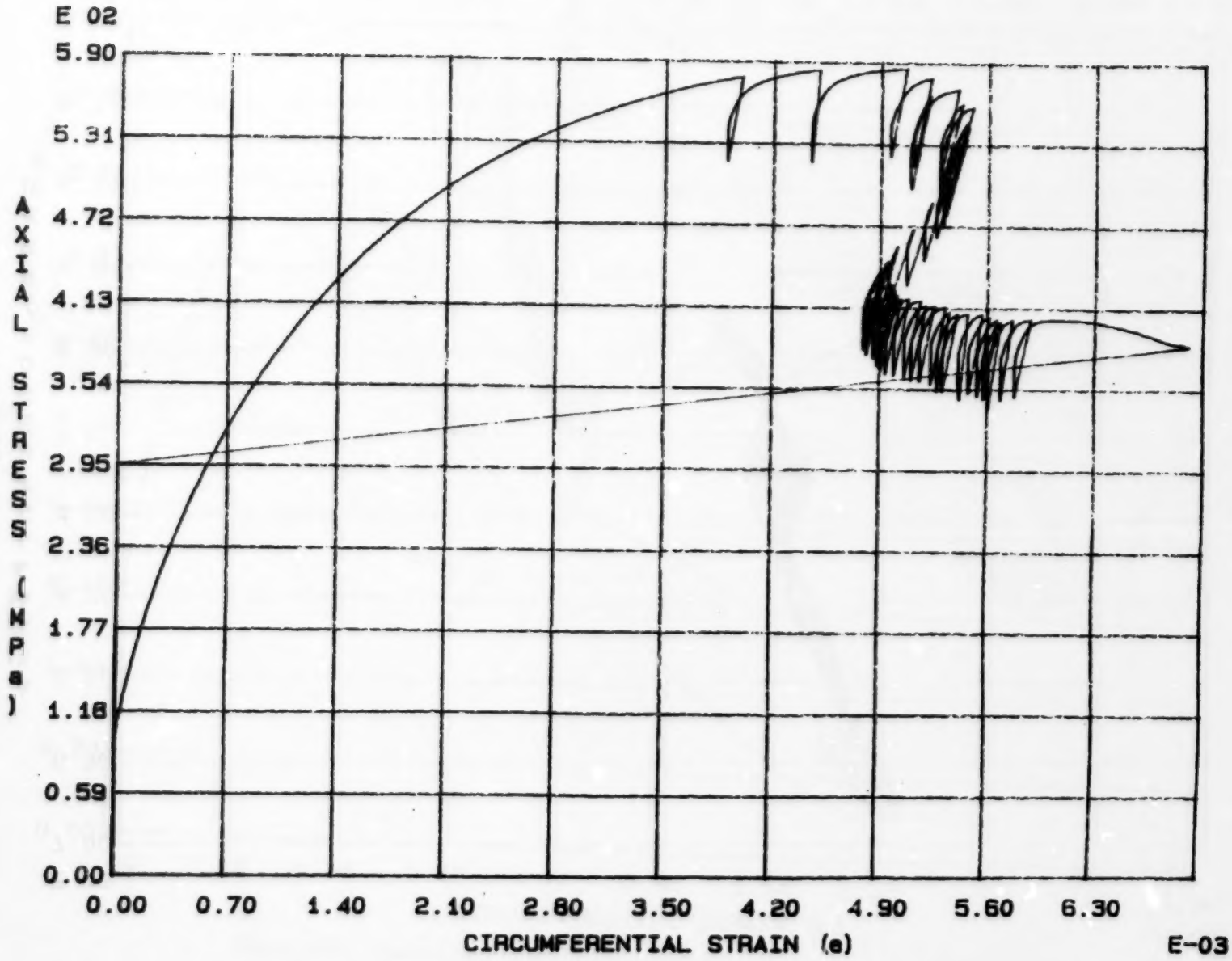

Figure A30. Loading and unloading curves (cir. strain) for Specimen HG2-40.381.

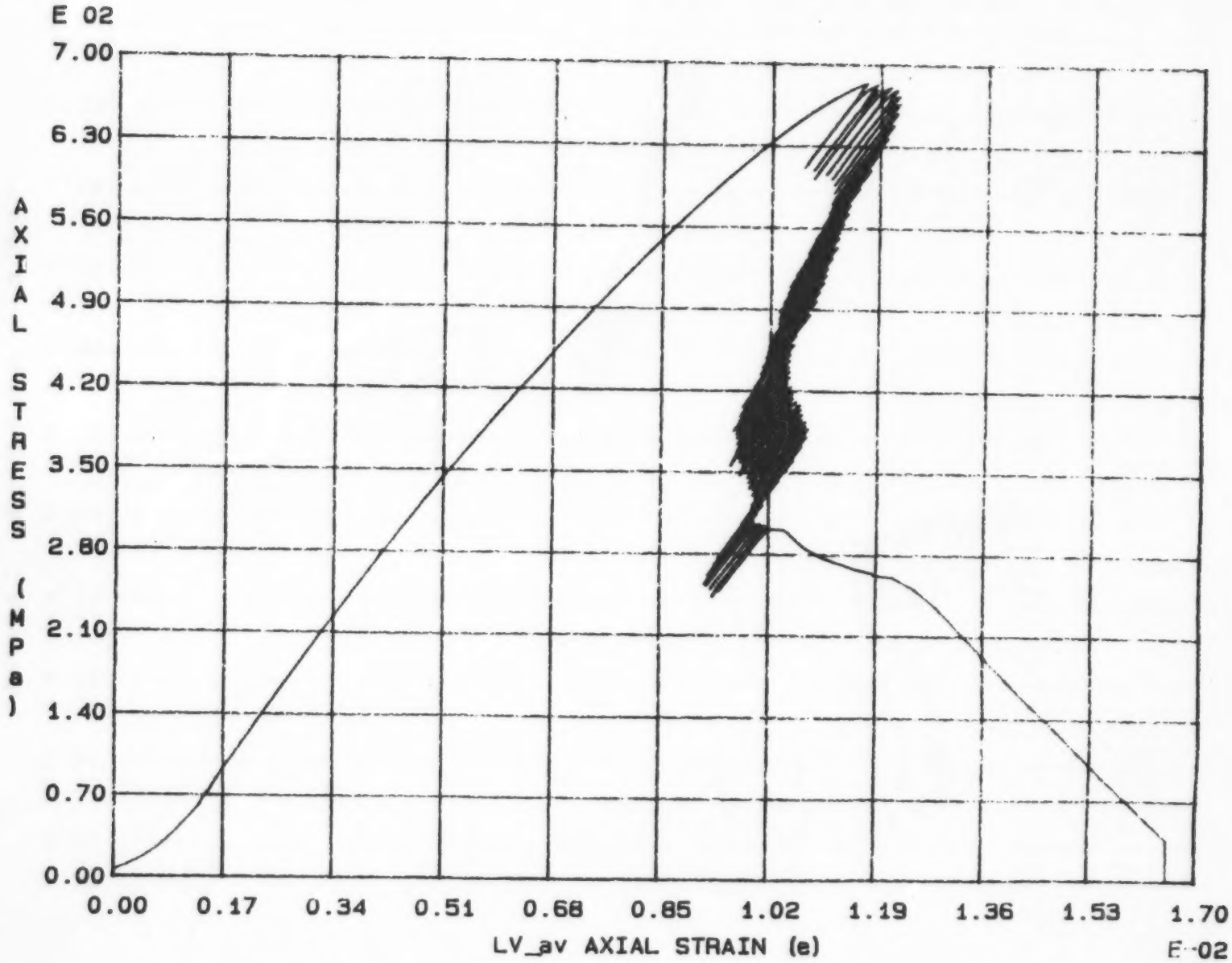

Figure A31. Loading and unloading curves (axial strain) for Specimen HG2-40.500.

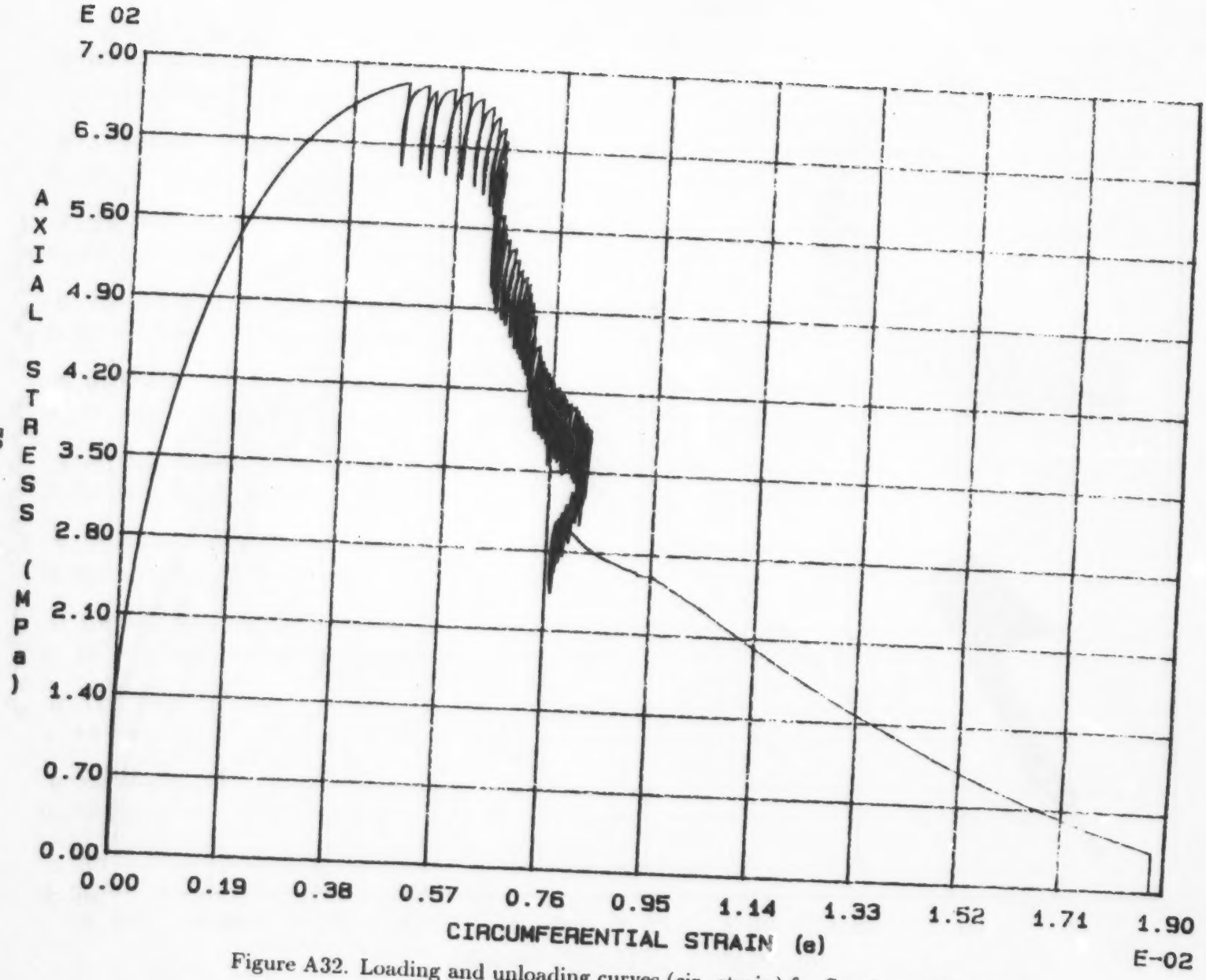

Figure A32. Loading and unloading curves (cir. strain) for Specimen HG2-40.500.

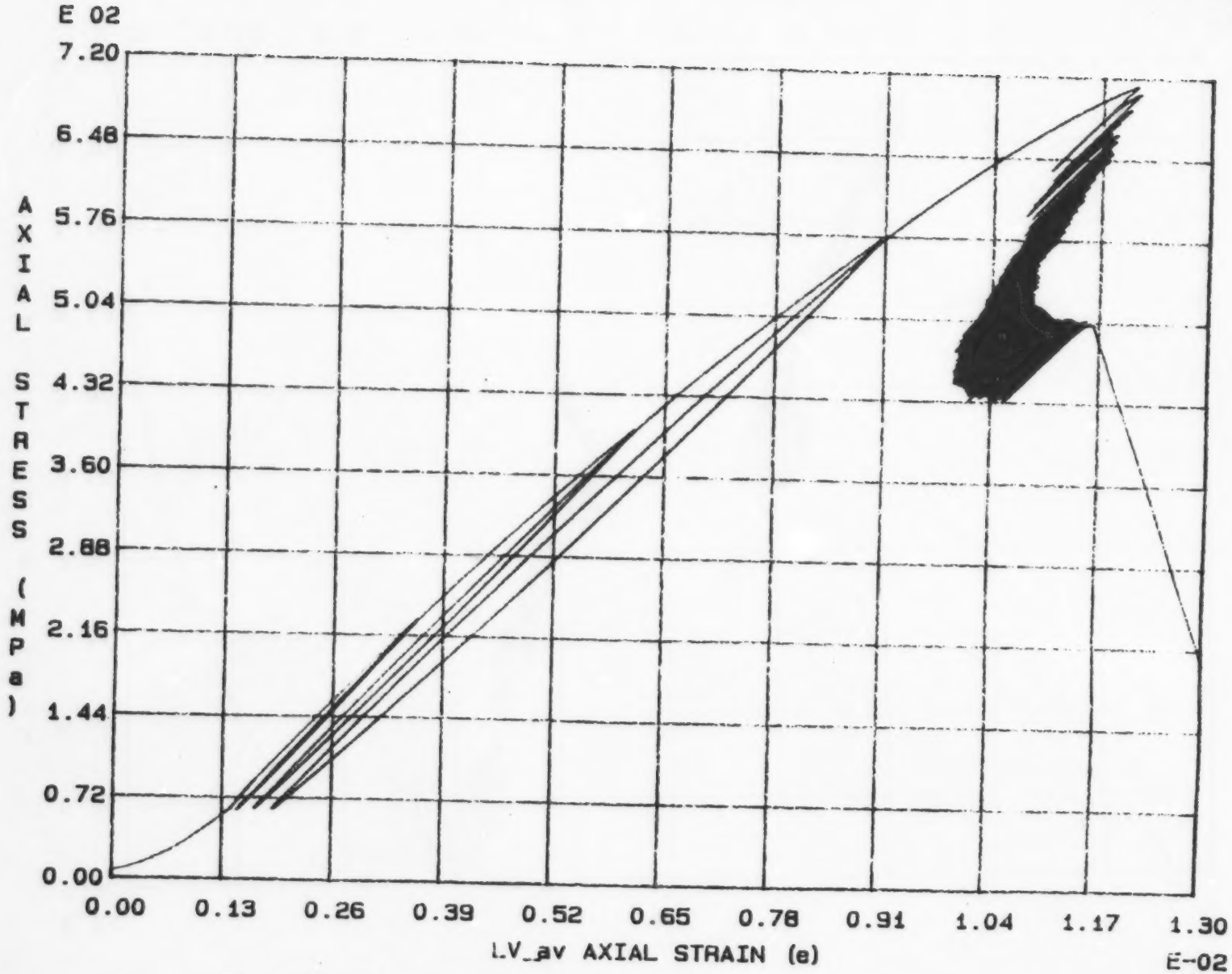

Figure A33. Loading and unloading curves (axial strain) for Specimen HG2-43.390.

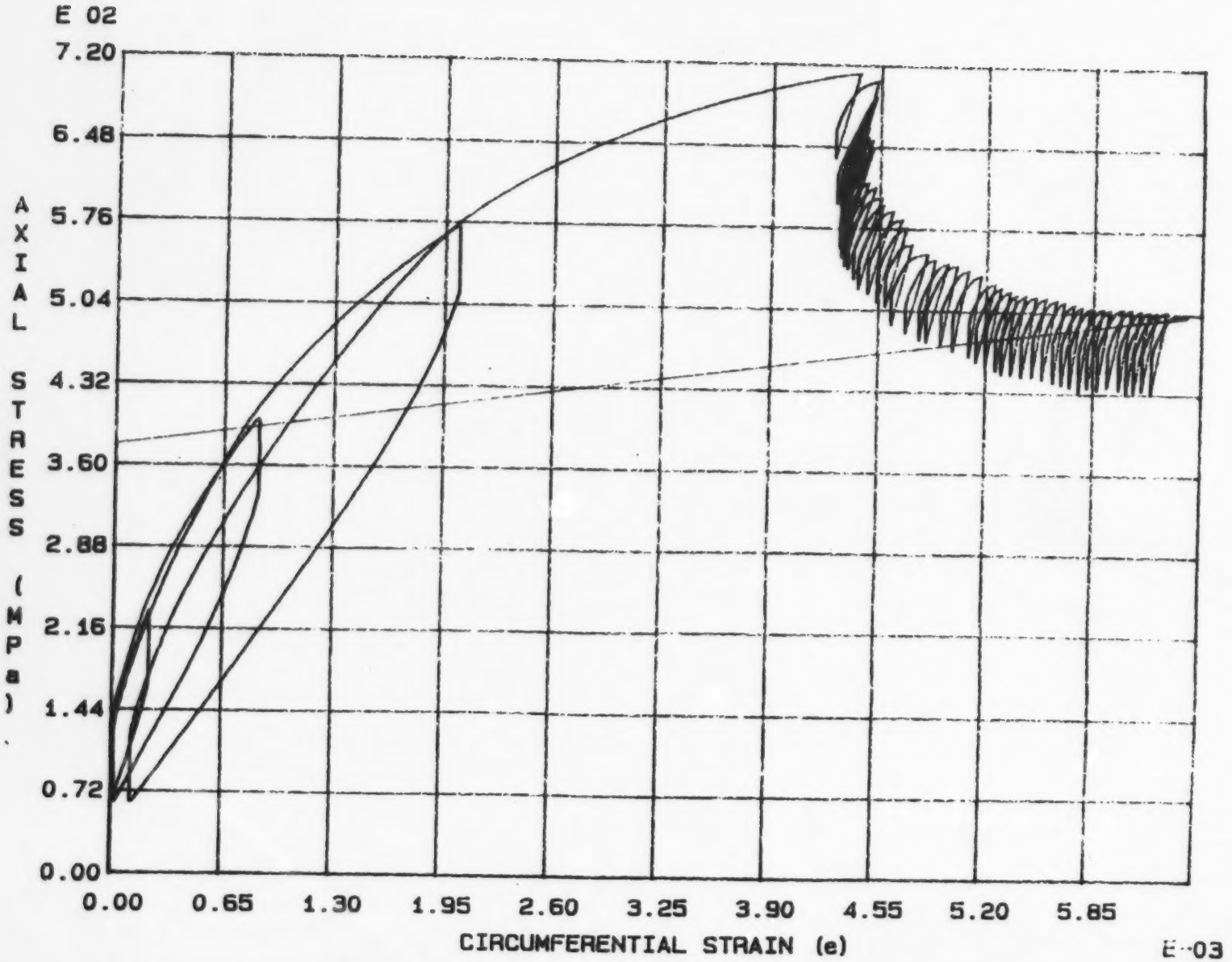

Figure A34. Loading and unloading curves (cir. strain) for Specimen HG2-43.390.